

Building a functionalizable, potent chemiluminescent agent: A rational design study on 6,8-substituted luminol derivatives

Theodoros Mikroulis,[†] M. Consuelo Cuquerella,[‡] Angelo Giussani,[§] Anna Pantelia,[†] Gemma M. Rodríguez-Muñoz,[‡] Georgios Rotas,[†] Daniel Roca-Sanjuán,^{*,§} Miguel A. Miranda,^{*,‡} and Georgios C. Vougioukalakis^{*,†}

[†] Laboratory of Organic Chemistry, Department of Chemistry, National and Kapodistrian University of Athens, Panepistimiopolis, 15771 Athens, Greece

[‡] Instituto de Tecnología Química UPV-CSIC, Universitat Politècnica de València, Camino de Vera s / n, 46022 València, Spain

[§] Instituto de Ciencia Molecular, Universitat de València, P.O. Box 22085, 46071 València, Spain

KEYWORDS Chemiluminescence, Luminescence, Luminol, Quantum chemistry computations, Imaging Agents

ABSTRACT: Luminol is a prominent chemiluminescent (CL) agent, finding applications across numerous fields, including forensics, immunoassays, and imaging. Different substitution patterns on the aromatic ring can enhance or decrease its CL efficiency. We herein report a systematic study on the synthesis and photophysics of all possible 6,8-disubstituted luminol derivatives bearing H, Ph, and/or Me substituents. Their CL responses are monitored at three pH values (8, 10, and 12), thus revealing the architecture with the optimum CL efficiency. The most efficient pattern is used for the synthesis of a strongly CL luminol derivative, bearing a functional group for further, straightforward derivatization. This adduct exhibits an unprecedented increase in chemiluminescence efficiency at pH=12, pH=10, and especially at pH=8 (closer to the biologically-relevant conditions), compared to luminol. Complementary work on the fluorescence of the emissive species, as well as quantum chemistry computations are employed for the rationalization of the observed results.

Introduction

The demand for rapid detection and testing in diverse aspects of human life has driven the invention of molecular sensors with high sensitivity and specificity. Among them, chemiluminescence (CL) based sensors comprise an exceptional category, due to their outstanding properties, including fast response and high signal-to-noise ratio. A wide range of application fields, such as forensics,¹ (immuno)assays² (including even the detection of the lately emerged SARS-CoV-2),³ bioimaging,⁴ and theranostics,⁵ benefit from their supreme sensing ability. CL agents emit light upon chemical stimuli, usually triggered by oxidation from reactive oxygen or nitrogen species.⁶ The most widely used CL probe is 5-amino-2,3-dihydro-1,4-phthalazinedione, commonly known as luminol, whose CL is triggered by oxidation. Luminol's strong CL is known for almost a century,⁷ and since its discovery numerous works have studied its properties and applications.⁸

The need for molecular probes with optimized CL performance has triggered the design of a variety of substituted luminols. To this end, 6-Me and 7-Me⁹ derivatives (**La,b**, Figure 1) exhibit weaker CL than luminol. On the contrary, 8-alkyl substituted derivatives (prepared using a cycloaddition/aromatization strategy), have been shown to enhance CL. In fact, it seems that the less bulky the substituent, the higher the CL quantum yield (Φ_{CL}) (**Lc-e**). These findings suggest that both steric and electronic effects impact luminol's CL.¹⁰ Recently, the 6,8-symmetrical alkyl

disubstituted derivatives **Lf-i**, prepared using a similar strategy, have been shown to greatly enhance CL up to 20-fold,⁹ an observation attributed to a "steric gearing" effect. Strong CL response has also been reported for **L-012**, a related, commercially available pyridopyridazine based hydrazide derivative.¹¹ Despite these impressive results, the phthalhydrazide derivatives **ABMI** and **ABEI**,¹² which are currently used as chemiluminescent probes with functional tips for the attachment on target molecules, are based on the substituted isoluminol isomer, rather than luminol itself. These derivatives show weaker CL, but are more easily accessible.

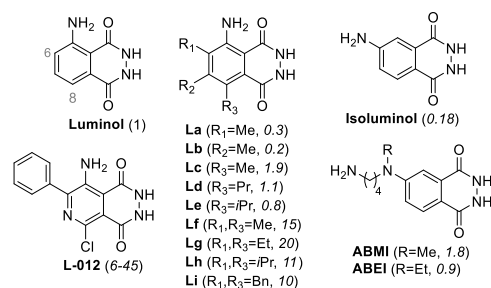


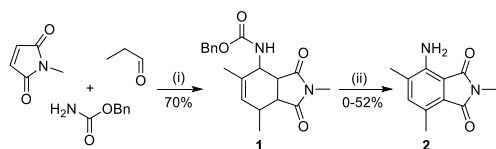
Figure 1. Phthalhydrazide derivatives and their reported relative CL efficiency.

With this knowledge in mind, we herein report the synthesis of all possible 6,8-substituted luminol derivatives, bearing methyl, phenyl, and/or hydrogen substituents, as well

as their photophysical characterization, regarding their CL properties. A novel, modular, reproducible, and highly efficient synthetic procedure, based on a Suzuki coupling reaction in its key step, is developed, both for the phthalhydrazides and their corresponding phthalic acid derivatives. The chemiluminescence properties of the former and the fluorescence properties of the latter have shed light on the CL reaction mechanism of luminol at pH 10, as well as under milder conditions (pH 8), more closely resembling the environment of biological applications. Quantum chemistry computations have also been carried out, aiming to shed light on and rationalize the observed experimental results. Equally important, our study points towards the structural characteristics for the rational design of a highly efficient chemiluminescent phthalhydrazide, also bearing an easy-to-functionalize handle, thus paving the way for the preparation of innovative, tailor-designed, luminol-based, strongly chemiluminescent probes with variable uses.

Results and discussion

The synthesis of the desired ring-substituted luminol derivatives was initially approached through a published procedure.¹³ According to that route, a 3-component condensation, followed by Pd-catalyzed aromatization with concomitant de-benzylation, affords the corresponding amino phthalimide (Scheme 1). Hydrazinolysis of the latter yields the desired phthalhydrazide. However, in our hands, phthalimide's **2** synthesis proved quite troublesome. Even though the first step proceeded smoothly and afforded precursor **1** in good yields, the aromatization step exhibited low reproducibility.

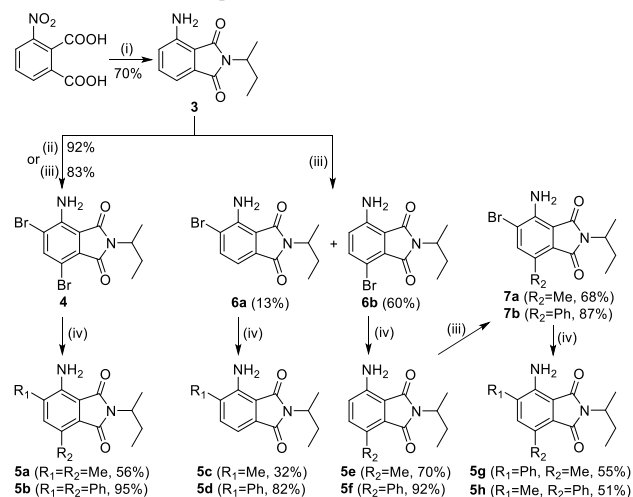


Scheme 1. Synthesis of 2. Reagents and conditions: (i) pTsOH, Ac₂O, NMP, 120°C, 24h, (ii) Pd/C, triglyme, 140°C, 2d.

We thus opted for an alternative, modular, reproducible synthetic strategy. 3-Aminophthalimide **3**, prepared easily from 3-aminophthalic acid,¹⁴ was used as the starting material. Bromination, using excess of bromine or NBS, afforded the 4,6-dibrominated derivative **4** in high yield (Scheme 2). Then, Suzuki coupling with trimethyl boroxine or phenyl boronic acid yielded the corresponding symmetrically 4,6-disubstituted 3-aminophthalimide derivatives **5a,b**. Monobromination of **3** afforded a mixture of the 4- and 6-bromophthalimides **6a,b**, which were separated using column chromatography in 13% and 60% yields respectively. Again, Suzuki methylation or phenylation of **6a,b** afforded the corresponding monosubstituted 3-aminophthalimide derivatives **5c-f**. The 6-monosubstituted derivatives **5e,f** were further brominated towards **7a,b**, followed by coupling with the appropriate boronic compound towards the non-symmetrically 4,6-disubstituted aminophthalimide derivatives **5g,h**.

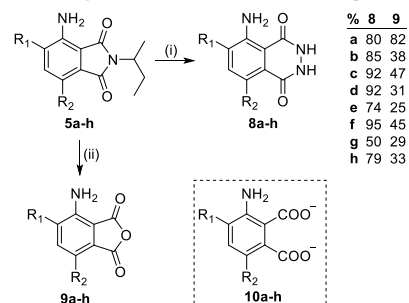
Once phthalimides **5a-h** were synthesized, the desired luminol derivatives **8a-f** were easily acquired via hydrazinolysis¹⁵ in moderate to high yields (Scheme 3). Moreover, in

order to fully assess the corresponding CL results, the fluorescence behavior of the phthalates **10**, being the light emitting species of the corresponding phthalhydrazides **8** (see below), had to be investigated. In this respect, complete hydrolysis of phthalimides **5a-h** in strongly alkaline conditions yielded, upon acidic workup of the reaction mixtures, the corresponding phthalic acid anhydrides **9a-h**. These anhydrides were readily hydrolyzable towards the phthalates **10** in aqueous alkaline media (see Figure S36) and, therefore, they were used as their precursors in the fluorescence experiments.

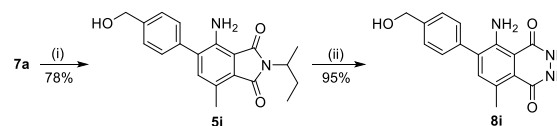


Scheme 2. Synthesis of the 3-aminophthalimide derivatives. Reagents and conditions: (i) (a) Ac₂O, Δ, (b) sec-BuNH₂, AcOH, Δ, (c) H₂, Pd/C, MeOH, (ii) Br₂, CH₃COOH/CH₃COONa, r.t. 18h, (iii) NBS, DCM, r.t. 30 mins, (iv) trimethylboroxine/phenylboronic acid, Pd(PPh₃)₄.

Finally, luminol derivative **8i**, bearing an easy to further functionalize hydroxyl moiety, was prepared from **7a** according to the above-described procedure (Scheme 4).



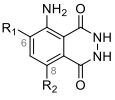
Scheme 3. Synthesis of the phthalhydrazide and phthalic anhydride derivatives. Reagents and conditions: (i) Hydrazine monohydrate, 110°C, 24-48h, (ii) 15N KOH, EtOH, Δ, 3d.



Scheme 4. Synthesis of the hydroxy functionalized luminol derivative 8i. Reagents and conditions: (i) 4-(hydroxymethyl)phenylboronic acid, Pd(PPh₃)₄, K₂CO₃,

H₂O, 1,4-dioxane, 105°C, 18h. (ii) Hydrazine monohydrate, 110°C, 24h.

Table 1. Chemiluminescence quantum yields (Φ_{CL}) of luminol derivatives **8 registered in aqueous solutions at pH=12, 10, and 8 and fluorescence quantum yield (Φ_F) of the corresponding phthalates **10** at pH = 10. The Φ_{CL} values are compared to that of luminol at pH=12.**

Entry		R ₂	R ₁	pH=12 Φ_{CL}	pH=10 Φ_{CL}	pH = 8 Φ_{CL}	pH=10 Φ_F
1	Luminol	H	H	0.012	0.003	<0.001	0.30 ^[a]
2	8c	H	Me	0.006	0.002	<0.001	0.32
3	8d	H	Ph	0.007	0.003	<0.001	0.32
4	8f	Ph	H	0.012	0.005	<0.001	- ^[b]
5	8h	Ph	Me	0.024	0.006	<0.001	0.54
6	8b	Ph	Ph	0.035	0.009	0.002	0.16
7	8e	Me	H	0.128	0.021	0.003	0.48
8	8a	Me	Me	0.170	0.037	0.004	0.30
9	8g	Me	Ph	0.118	0.034	0.004	- ^[b]
10	8i	Me	HOCH ₂ C ₆ H ₄	0.390	0.058	0.017	-

[a] Φ_F (3AP) = 0.3¹⁹. [b] Parent anhydride did not hydrolyze cleanly.

To assess the CL properties of the newly-synthesized luminol derivatives, these were dissolved in aqueous solutions at pH=10 or pH=8, to a final concentration of 7.5 μ M. Two milliliters of each solution were placed in a quartz cuvette, and the CL reaction was triggered by the addition of H₂O₂ and K₃[Fe(CN)₆], whilst under vigorous stirring. The process was monitored using a fluorometer running in the time-based mode (own lamp switched off, 425 nm as monitoring wavelength). All the synthesized luminol derivatives were screened for chemiluminescence, by registering their CL kinetic traces at pH=12, pH=10, and pH=8 (Figure 2); the absolute quantum yields (Φ_{CL}) were obtained by comparison with that of the parent luminol at pH=12 (Φ_{CL} = 0.012)¹⁶ (Table 1). The results clearly show that substitution at positions 6 and/or 8 has a direct influence on the overall process, irrespective of the pH.

At the three pH values, methyl substitution at position 8 (para to the amino group, **8e,a,g**) increases the Φ_{CL} significantly, compared to luminol. An enhanced CL effect (albeit much weaker), is also observed for the corresponding 8-phenyl derivatives (**8f,h,b**). Substitution at position 6 seems to have a smaller influence on the Φ_{CL} .

These results point towards a more or less independent substituent effect. A rough estimation shows that 8-Me yields a marked Φ_{CL} enhancement,¹⁷ followed by 8-Ph, 6-Ph, and 6-Me. The CL quantum yields decrease sharply with the pH decrease, an anticipated trend, as luminol's CL is known to occur in strongly alkaline conditions.^{8,18} At pH=8, although Φ_{CL} are by far lower than those measured at pH=12 and 10, the CL of the functional derivative **8i** is

most impressive, showing a massive Φ_{CL} increase at all pH values (12, 10, and 8), relative to luminol. In addition, the Φ_{CL} value obtained for **8a** at pH=12 (0.17) is in good agreement with that reported in the literature for the same compound at the same pH (0.18).⁹ This validates the uniqueness of **8i** as a superior luminol-derived chemiluminescent agent. It is quite remarkable that the CL of **8i** at pH=8 is even higher than that of parent luminol at pH=12 (Φ_{CL} =0.017 vs 0.012). This is highly relevant, given that the use of luminol's CL is often hampered, or at least limited, by its low CL quantum yield at near neutral conditions, e.g. in biological environments.

Mechanistically, it is well established that luminols' CL consists of several steps, grouped here in two phases: phase 1, a multi-step oxidation procedure of the luminol moiety, leading to the formation of 3-aminophthalate in its excited singlet state (¹3AP*), and phase 2, relaxation of this excited species to its ground state, in part, emitting fluorescence with a maximum at 425 nm (Scheme 5), thus producing the observed chemiluminescence (mechanism is discussed below in more detail). As a result, luminol's chemiluminescence depends on the efficiency of both phases. To gain a deeper insight into the second phase, we measured the fluorescence quantum yields of some of the phthalates corresponding to our luminol derivatives (Scheme 5).

The fluorescence of isoabsorptive samples of the phthalates (A_{max} = 0.1) were measured and compared to that of **3AP** (Φ_F (3AP) = 0.3,¹⁹ Figure S37); the results are shown in Table 1. In general, the phthalates' fluorescence quantum yields are high and of the same order of

magnitude as that of 3AP. In this range, the **8b**-phthalate exhibits decreased Φ_F (0.16), while **8h** nearly doubles the reference value. Clearly, this reveals that the oxidation phase of the chemiluminescence is the one limiting the efficiency of the overall process. In other words, the efficiency of the excited state formation in the chemiexcitation phase (rather than the fluorescence quantum yield of the emitter) determines the CL efficiency.

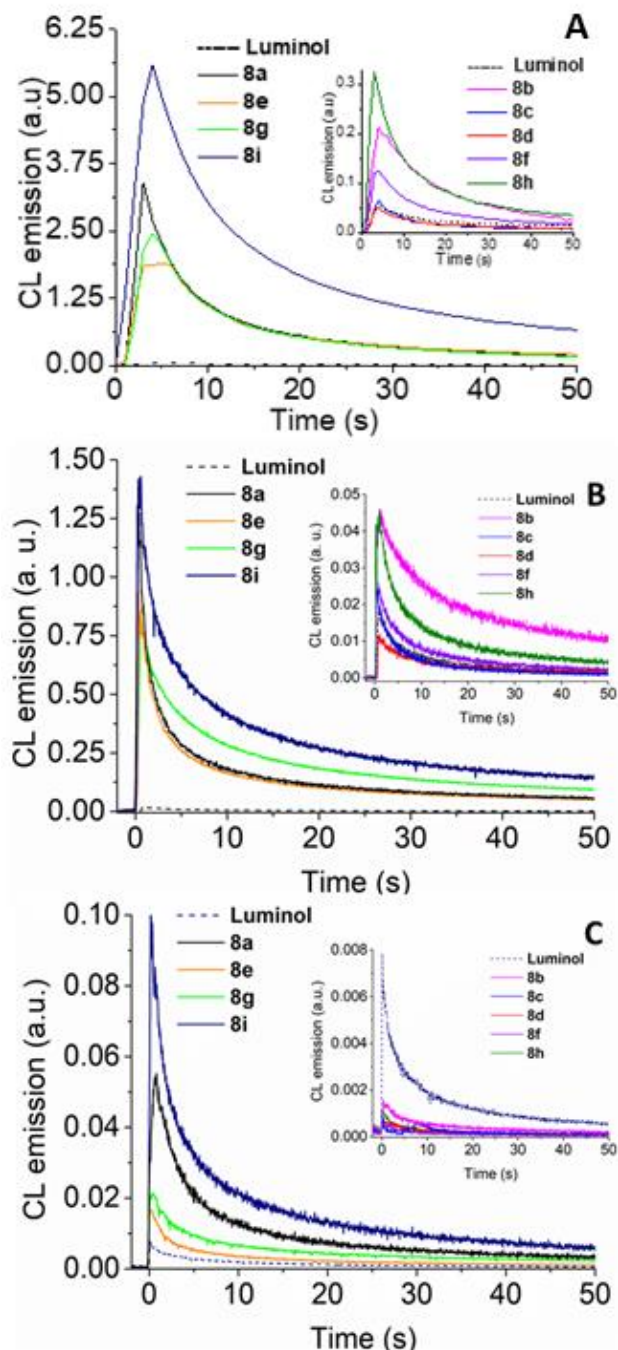
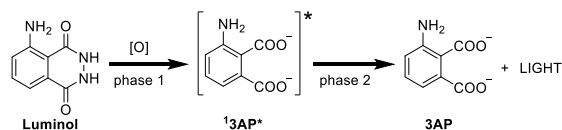


Figure 2. Typical chemiluminescence decay kinetics displayed by the luminol derivatives **8a-i** in aqueous solutions at pH=12 (A), pH=10 (B), and pH=8 (C). The insets show the traces for the less efficient compounds, with a magnified CL scale. Kinetics was followed for up to 250 s, but it is only shown until 50 s, to facilitate comparison between derivatives.



Scheme 5. Simplified mechanism for the luminol chemiluminescence reaction.

To interpret our experimental data, quantum chemistry computations were carried out focusing on the complex molecular and electronic-structure transformations which are involved in phases 1 and 2 of Scheme 5. In terms of chemical mechanisms, phase 1 depends on the media. In aprotic solvents, a strong base deprotonates luminol to a dianion which is able to react directly with molecular oxygen. In protic solvents, in which the details are less clear, the distinct proposals imply a series of oxidation and deprotonation steps and reaction with hydrogen peroxide or a superoxide radical.¹⁸ Most of the proposals involve the formation of a bicyclic endoperoxide containing two rings with O-O and N=N bonds, which upon nitrogen extrusion gives rise to a mono-cyclic peroxide (CP^{-2}). In contrast to luminol, CP^{-2} can efficiently transfer the reactivity from the ground to the excited state with low thermal energies (process so-called chemiexcitation).^{18b,20} This occurs upon O-O bond breaking, which brings the molecule to the transition state (TS) and nearby to a region of states crossing (conical intersections, CI), allowing the production of the emissive species, $3AP^*$ (see Figure 3).

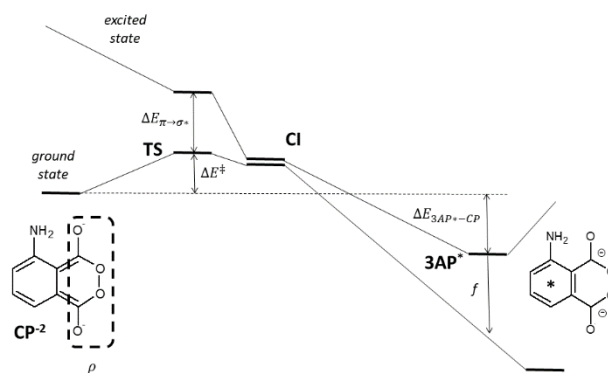


Figure 3. Scheme of the chemiexcitation of CP^{-2} in luminol illustrating theoretical quantities that are relevant for interpreting the Φ_{CL} of luminol derivatives **8**.

In aqueous solutions, such a structure is formed at high pH values (pH > 8 according to estimations by Yue and Liu).^{18a} At lower or equal values, double deprotonation is not achieved and the corresponding cyclic peroxides, neutral (CP) or monoanionic (CP^-), are much less efficient for chemiexcitation due to their dark path evolutions upon O-O bond breaking. This correlates with the lower CL yields measured in this work at pH=8. We shall focus on the theoretical analysis at pH=10, where there are less doubts that CP^{-2} is present and it is the species responsible for the chemiexcitation as in non-protic solvents.^{18b} Note also that the chemiexcitation part is expected to be mostly affected by the substitution pattern due to the large changes in the electronic structure of the molecule happening in this step. Therefore, we will theoretically analyze this part of the

complex mechanism in this work, to interpret the distinct chemiluminescence efficiencies of the luminol derivatives. Future studies on the previous oxidation steps shall be also interesting to find any possible contribution from this part.

Energy barriers between CP^{-2} and the transition state of the O-O bond breaking reaction (**TS**), ΔE^\ddagger , were computed, since this property has been previously shown to allow distinction between highly- and low-efficient CL systems, with catalyzed and non-catalyzed mechanisms respectively. A short range of values was obtained (0.14-0.24 eV) and no correlation was found between the barriers and the experimental Φ_{CL} or the combined yield of oxidation and singlet chemiexcitation (Φ_{OS}), which can be defined as the quotient between Φ_{CL} and Φ_{F} and represents the efficiency of the chemical excitation process^{20a} (see Table 2).

No significant differences were computed when changing between distinct conditions (gas phase, DMSO solution or water solution; see Table S1). For a more precise characterization, the conical intersection (**CI**) at the region of the **TS**, which mixes the ground electronic state and the excited state that corresponds to an electron promotion from a occupied π orbital delocalized over the conjugated system to the antibonding σ^* orbital of the O-O bond ($\pi \rightarrow \sigma^*$), and opens the path towards the excited electronic state,^{18b} was also computed with high-level multiconfigurational quantum chemistry for systems with the smaller size (luminol, **8c,h,a**). Accurate **CI** characterizations for the higher-size molecules are prohibitive, due to the limitations of the active space.²¹ Energy barriers to such **CI** points are also very similar (in the range 0.1-0.2 eV) and they are also unable to predict the correct trends of the Φ_{CL} . Note that a second **CI** structure is present in the chemiexcitation region.^{18b,20b} The higher Φ_{CL} of 6,8-methylated luminol (in comparison to luminol) was previously attributed to the lower position of such **CI**,⁹ facilitated by the steric gearing of the substituents. However, a more recent study improving the determination of the **CI** and the path in the excited state, has shown that the second **CI** contributes to the non-radiative decay rather than to the CL process.^{18b}

Overall, these findings indicate that the decomposition mechanism in the studied molecules is similar and the computed magnitude analyzed above (energy barriers to the **TS** and **CI**) and their associated errors (0.1-0.2 eV) might not be enough to discriminate among the experimental yields. In these conditions, analyses of other magnitudes might be helpful to disentangle distinct electronic-structure features that contribute in the trends for comparing all these rather similar systems. Based on previous knowledge,^{18a} the magnitudes shown in Figure 3 were identified as relevant candidates for the analyses of the CL process.

The energy gap between the excited and the ground state at the **TS** ($\Delta E_{\pi \rightarrow \sigma^*}$) might be linked to the accessibility of excited state, which initially carries the molecule towards **3AP***. The difference between charges of the carbonyl groups at the **TS** and at the CP^{-2} ($\Delta\rho$) shows any charge-transfer contribution that could activate the O-O bond breaking (resembling the CTIL or CIEEL mechanisms).^{20a} The energy difference between **3AP*** and CP^{-2} ($\Delta E_{3\text{AP}^*-\text{CP}}$)

represents the energy released in such process. This magnitude has been shown experimentally to correlate with Φ_{S} .²²

Note, at this point, that while in aprotic media the emissive species is a structure produced in the excited state after proton transfer from the amino to the adjacent carboxylate group, this proton transfer is not happening in aqueous solutions.²³ Finally, the oscillator strength for the electronic transition of **3AP*** from the excited to the ground state (f) correlates with the strength of the radiative decay. Note however that Φ_{F} depends on both f and the efficiency of possible non-radiative decay processes.

Table 2 compiles the computed data for the above-mentioned magnitudes together with the combined quantum yield of oxidation and chemiexcitation (Φ_{OS}). $\Delta E_{\pi \rightarrow \sigma^*}$ values have similar trends as ΔE^\ddagger and analogously their role in the Φ_{CL} is not evident. As can be seen, higher f values are obtained with phenyl substitution at position 6 (**8d,b,g**). If compared with the experimental Φ_{F} , clear disagreements are found. For example, 6-phenyl substitution is found to enhance f , whereas this is not observed in the experiments. This suggests that non-radiative decay paths are affecting each system differently. Due to this disagreement of data, f values cannot be directly compared with the Φ_{F} .

Regarding $\Delta E_{3\text{AP}^*-\text{CP}}$, it can be seen that adding a phenyl moiety at position 6 significantly releases more energy in the formation of the excited species **3AP*** than when this position is occupied by H (compare for example luminol and **8d**), while the opposite trend is obtained when the phenyl is added at position 8 (compare for example luminol and **8f**). Methylation does not affect that much this property. Based on the $\Delta\rho$ magnitude, **Table 2** shows that 8-substitution helps activating the decomposition via a partial negative charge donation to the peroxide region ($\Delta\rho$ becomes in general lower when a substituent is added at this position). On the contrary, 6-substitution decreases the activation ($\Delta\rho$ in general increases). To compensate for these properties, 6-phenyl and 8-methyl substitution (**8g**) arises as the optimal solution.

Finally, for further rationalization we would like to remind the possible contribution of the previous oxidation steps to the chemiexcitation from the luminol starting molecule to CP^{-2} (mentioned above). We would like to point also to other factors in the chemiexcitation part, such as dynamical aspects and excited-state path evolution after chemiexcitation, which are too challenging to study, due to the size and complexity of the current set of molecules. In small-size systems, in particular, 1,2-dioxetane with and without methyl substitution, dynamics simulations have shown that methylation enhances the yield of chemiexcitation.²⁴ Note, however, that 1,2-dioxetane is based on a preferential triplet chemiexcitation, and for luminol the dynamical effects might be different.

Table 2. Computed theoretical quantities of luminol derivatives 8 and combined quantum yields of oxidation and singlet chemiexcitation (Φ_{OS}).

Compound	ΔE^\ddagger [a]	$\Delta E_{\pi \rightarrow \sigma^*}$ [b]	$\Delta \rho$ [c]	$\Delta E_{3AP^* \cdot CP}$ [d]	f [e]	Φ_{OS} [f]
Luminol	0.14	0.25	0.02	-1.35	0.17	0.017
8c	0.14	0.25	0.04	-1.4	0.22	0.013
8d	0.16	0.15	0.13	-1.55	0.53	0.018
8f	0.22	0.56	-0.06	-1.19	0.22	-
8h	0.23	0.58	-0.06	-1.23	0.23	0.020
8b	0.24	0.42	0.05	-1.4	0.42	0.175
8e	0.17	0.37	-0.08	-1.39	0.22	0.273
8a	0.18	0.36	-0.1	-1.46	0.24	0.577
8g	0.2	0.38	0.1	-1.61	0.54	-

[a] ΔE^\ddagger (in eV): the energy barrier between CP^{2-} and **TS**. [b] $\Delta E_{\pi \rightarrow \sigma^*}$ (in eV): the energy gap between the ground and excited states at the **TS**. [c] $\Delta \rho$: the charge difference of the carboxylate groups between the **TS** and CP^{2-} . [d] $\Delta E_{3AP^* \cdot CP}$ (in eV): the energy difference between CP^{2-} and $3AP^*$. [e] f : the oscillator strength of the $3AP^*$ for the electronic transition from the excited to the ground state. [f] Φ_{OS} : combined quantum yield of oxidation and singlet chemiexcitation ($\Phi_{OS} = \frac{\Phi_{CL}}{\Phi_F}$).

Conclusion

We have synthesized the complete series of 6,8-disubstituted luminol derivatives, having hydrogen, methyl, and/or phenyl moieties. Their synthesis has been accomplished through a new, modular and reproducible, consecutive bromination/Suzuki coupling protocol of the parent aminophthalimide, followed by hydrazinolysis. The corresponding aminophthalates have also been prepared, starting from their anhydrides. The CL quantum yields of the full series of compounds Φ_{CL} were measured at pH=12, 10, and 8, revealing a relatively independent contribution of each substituent. 8-Me was found to greatly enhance Φ_{CL} , whereas Ph has a less marked effect. This could be attributed to the fact that 8-substitution donates negative charge to the cyclic peroxide moiety, thus assisting the cleavage of the O-O bond. Substitution at position 6 contributes less, with the 6-phenyl yielding somewhat better results, probably due to the higher release of energy required to generate the emissive species from the peroxide intermediate. Determination of energy barriers related to the O-O bond breaking of this species or the relative energetic location of the conical intersection related to the chemiexcitation step do not allow further rationalization of the Φ_{CL} trends. Based on the experimental and theoretical analyses for **8a-g**, the 6-aryl-8-methyl luminol derivative **8i** has been prepared, bearing a hydroxyl function for straightforward further functionalization. This derivative shows an absolute Φ_{CL} value of 0.017 at pH=8, which is higher even to that of luminol at pH=12 (0.012). Hence, **8i** appears as an ideal CL reagent for sensing, tracking, and other possible biologically-related applications.

Experimental Section

Materials, instrumentation and methods

All chemicals were obtained from commercial sources and were used without further purification. Solvents were dried according to published procedures.²⁵ The course of the reactions was monitored with thin-layer chromatography (TLC), using aluminum sheets (0.2 mm) coated with silica gel 60 with fluorescence indicator (silica gel 60 F254). Purification of the products was carried out by flash column chromatography, using silica gel 60 (230–400 mesh). Nuclear Magnetic Resonance (NMR) spectra were obtained with a Bruker Avance 400MHz or a Varian Mercury 200MHz spectrometer. Chemical shifts are reported in ppm. HRMS spectra were recorded in a QTOF maXis impact (Bruker) spectrometer under electron spray ionization conditions.

Fluorescence spectra were registered with a Photon Technology International (PTI) spectrofluorometer (Photon Technology International, Inc. NJ, USA), model LPS-220B equipped with a 75 W Xe lamp as a light source and with a monochromator, or with a FLS1000 spectrofluorometer (Edinburgh instruments), equipped with a N-DMM double-emission monochromator and a N-G11 PMT-980 detector. Monitoring of the CL was performed using the same spectrofluorometer with its own lamp switched off. The set was run in the time-based mode with the detection dialed at 425 nm.²⁶ Each experiment was performed at least 5 times. To trigger the chemiluminescence: luminols were dissolved in aqueous basic solutions at pH 12 or 10 or phosphate buffer aqueous solutions at pH 8, giving a final concentration of 7.5 μ M. Then, 2 mL of each sample were introduced in a quartz cuvette, and the CL was prompted by addition of 2.5 μ L of H₂O₂ (50% w/w) and 8 μ L of 75 mM K₃[Fe(CN)₆] while vigorously stirring. To do so, the total area under the decay curve for each compound was measured 5 times, in separate experiments, and the average value was used to determine the absolute chemiluminescence quantum yields (Φ_{CL}) by comparison with luminol at

pH=12, whose absolute Φ_{CL} is 0.012.¹⁶ The Φ_{CL} values were calculated as $\Phi_{\text{CL}} = A/A_L \times \Phi_{\text{CL}}^0$, where A corresponds to the average area of each compound and A_L the value of the reference compound luminol at pH=12.

The fluorescence quantum yields (Φ_{F}) were measured with the same set up running in the spectral mode and by comparing the area of the fluorescence of each sample with the one obtained for the reference compound 3AP under the same conditions (Φ_{F} (3AP) = 0.3¹⁹). For that, isoabsorptive samples of 0.1 were prepared at their UV absorption maximum (ca 300 nm) to ensure that all absorb the same number of photons. The samples were prepared dissolving the corresponding phthalic anhydrides in pH 10 aqueous solutions and allowing them to hydrolyze to give the final phthalate. This reaction was monitored by UV spectroscopy as anhydrides' absorption spectrum present a maximum around 400 nm that disappears as the phthalate is formed. Moreover, phthalates display a maximum at 300 nm (Figure S36).

TD/DFT and CASPT2^{21,27} methods were used herein as implemented in the Gaussian 16²⁸ and OpenMolcas²⁹ programs, respectively. All computations were carried out by imposing no restrictions on the symmetry of the molecule (C1 symmetry). The CAM-B3LYP functional³⁰ was used with the 6-31G* basis set, hereafter CAM-B3LYP/6-31G*, to determine minima and the **TS**. The open-shell approach, as established in previous studies,³¹ was used to correctly determine the geometries and energies. The CASPT2 method was used to optimize the **CP**² geometries and to obtain the **CI** for selected molecules (see main text). Since no analytical CASPT2 gradients are available at the moment in the OpenMolcas code, all CASPT2 optimizations were performed numerically. A basis set of atomic natural orbitals (ANO) of S-type³² contracted to C,N,O[3s,2p,1d]/H[2s,1p], hereafter ANO-S-VDZP, was used for all CASPT2 calculations. An active space of 12 electrons in 10 orbitals was employed. Within the CASPT2 calculations, an imaginary level-shift correction of 0.2 au was used to minimize the effects of possible intruder states. The CASPT2 standard zeroth-order Hamiltonian was used as originally implemented.³³ The core orbitals were frozen in the CASPT2 calculations. Such a CASPT2 approach has been validated in many different studies on organic molecules.^{21,34} The nature of all minima and transition states was confirmed computing the corresponding frequencies. All TD/DFT calculations were performed either in gas-phase or simulating the solvent (either water or DMSO) using the PCM model.³⁵ All CASPT2 calculations were performed in gas-phase. ΔE^{\ddagger} was calculated at the CAM-B3LYP/6-31G* simulating the solvent (water) with PCM. $\Delta E_{\pi \rightarrow \sigma^*}$ was obtained at the **TS** computed with the CAM-B3LYP/6-31G* level and as the energy difference between the ground and excited states computed at the CASPT2(12,10) level of theory in the gas-phase. $\Delta E_{3\text{AP}^* \rightarrow \text{CP}}$ was computed at the CAM-B3LYP/6-31G*-PCM(water) level. The f associated with the fluorescence emission at the 3AP* minimum was evaluated by performing a TDDFT-B3LYP/6-31G*-PCM(water) calculation at the 3AP* minimum. For $\Delta\rho$, Mulliken charges computed at the DFT-B3LYP/6-31G*-PCM(water) level were used.

Synthesis

Synthesis of benzyl (2,5,7-trimethyl-1,3-dioxo-2,3,3a,4,7,7a-hexahydro-1H-isoindol-4-yl)carbamate

(1). According to a previously published procedure:^{13a} In a pressure tube was added benzyl carbamate (1 g, 6.6 mmol, 1.4 equiv.) in NMP (1.65 mL) followed by *N*-methylmaleimide (535 mg, 4.8 mmol), propionaldehyde (0.48 mL, 6.6 mmol, 1.4 equiv.), acetic anhydride (0.62 mL, 6.6 mmol, 1.4 equiv.) and *p*-toluenesulfonic acid monohydrate (catalytic, 19.2 mg, 0.1 mmol). The tube was sealed, submerged in an oil bath, and the mixture was stirred at 120°C for 48 hours. The mixture was then quenched with H₂O and extracted with ethyl acetate. The combined organic phase was dried over anhydrous Na₂SO₄, filtered and concentrated *in vacuo*. Purification by column chromatography, using a gradient of petroleum ether/EtOAc 70:30 to 60:40, afforded **1** as an orange oil. (792 mg, 70%). ¹H NMR (DMSO-*d*₆, 200 MHz): δ 7.46-7.28 (m, 5H, Ph), 6.93 (d, J = 9.2 Hz, 1H, NH), 5.34 (s, 1H, CH=), 5.11 (s, 2H, CH₂), 4.40-4.23 (m, 1H, NHCH), 3.28 (d, J = 6.1 Hz, 1H, NHCHCHCO), 3.08 (t, J = 7.5 Hz, 1H, CH₃CHCHCO), 2.75 (s, 3H, NCH₃), 2.49-2.37 (m, 1H, CH₃CH), 1.58 (s, 3H, CH₃C=), 1.25 (d, J = 7.1 Hz, 3H, CH₃CH).

Synthesis of 4-amino-2,5,7-trimethylisoindoline-1,3-dione

(2). According to a modified published procedure:^{13a} A round bottom flask was charged with carbamate **1** (200 mg, 0.58 mmol) in triglyme (2.5 mL) and then 10% Pd/C was added (10mol%). A CaCl₂ tube was attached and the mixture was submerged in an oil bath and was stirred at 140°C for 24 hours. Palladium was removed via filtration through a Celite pad with EtOAc, and the filtrate was washed with H₂O and brine. The organic phase was dried over anhydrous Na₂SO₄, filtered and concentrated *in vacuo* and the residue was subjected to column chromatography. The product was eluted with P.E./EtOAc 90:10 and was acquired as a yellow solid after condensation (62 mg, 52% max. - large yield variations). ¹H NMR (CDCl₃, 200 MHz): δ 7.01 (s, 1H, ArH), 5.11 (bs, 2H, NH₂), 3.06 (s, 1H, NCH₃), 2.46 (s, 3H, CH₃), 2.17 (s, 3H, CH₃).

Synthesis of 4-amino-5,7-dibromo-2-(*sec*-butyl)isoindoline-1,3-dione

(4). *Procedure A*. A mixture of phthalimide **3** (1.5 g, 6.88 mmol), sodium acetate (1.13 g, 13.76 mmol) and acetic acid (17 mL) was stirred for 30 minutes. Then, a solution of bromine (0.71 mL, 13.76 mmol, 2 equiv.) in acetic acid (6 mL) was added dropwise and the resulting solution was stirred for 18 hours. The mixture was poured into ice/water mixture (100 mL) and the precipitate was filtered, washed with water and dried *in vacuo*, leaving **4** as yellow powder (2.39 g, 92%). *Procedure B*. Phthalimide **3** (300 mg, 1.38 mmol) was added in a solution of *N*-bromosuccinimide (510 mg, 2.89 mmol, 2.1 equiv.) in DMF (4 mL) and the whole was stirred in the dark o/n. Water (80 mL) was added, the mixture was stirred, left for 1 hour, filtered and washed with water. The filter cake was suspended in methanol (30 mL) and re-precipitated with the addition of water (30 mL). The solid was dried *in vacuo*, affording **4** as yellow powder (430 mg, 83%). ¹H NMR (CDCl₃, 200 MHz): δ = 7.79 (s, 1H, ArH), 5.76 (bs, 1H, NH), 4.34 - 4.06 (m, 1H, NCH), 2.19 - 1.61 (m, 2H, CH₂), 1.44 (d, J = 6.9 Hz, 3H, CHCH₃), 0.87 (t, J = 7.4 Hz, 3H, CH₃). ¹³C{¹H} NMR (CDCl₃, 50 MHz): δ 168.4, 166.0, 142.2, 141.0, 128.4, 115.6, 113.0, 103.9, 49.2, 26.7, 18.3, 11.3. Molecular Ion could not be detected on ES-MS nor ES-HRMS.

Monobromination of 3-aminophthalimide 3. Phthalimide **3** (5.33 g, 24.43 mmol) was added in a solution of *N*-bromosuccinimide (3.9 g, 21.91 mmol, 0.9 equiv.) in dichloromethane (20 mL) and the resulting mixture was stirred in the dark for 30 minutes. Then, the solvent was evaporated and the residue was subjected to column chromatography (5-10% EtOAc/PE), where the two mono-brominated isomers **6a** and **6b** were successively eluted.

4-amino-5-bromo-2-(sec-butyl)isoindoline-1,3-dione (6a). Yellow solid (846 mg, 13%). ¹H NMR (CDCl₃, 400 MHz): δ 7.64 (d, *J* = 7.7 Hz, 1H, H-6), 6.97 (d, *J* = 7.6 Hz, 1H, H-7), 5.67 (bs, 2H, NH₂), 4.21 – 4.12 (m, 1H, CH), 2.05 – 1.68 (m, 2H, CH₂), 1.42 (d, *J* = 6.9 Hz, 3H, CHCH₃), 0.85 (t, *J* = 7.4 Hz, 3H, CH₂CH₃). ¹³C{¹H} NMR (CDCl₃, 100 MHz): δ 170.0 (C-3), 168.2 (C-1), 142.8 (C-4), 137.8 (C-6), 131.9 (C-7a), 115.2 (C-3a), 112.8 (C-7), 112.2 (C-5), 49.0 (CH), 27.0 (CH₂), 18.5 (CHCH₃), 11.4 (CH₂CH₃). ESI-HRMS *m/z* for C₁₂H₁₄BrN₂O₂ [M+H]⁺: calcd. 297.0233, found 297.0242.

4-amino-7-bromo-2-(sec-butyl)isoindoline-1,3-dione (6b). Yellow solid (3.9 g, 60%). ¹H NMR (CDCl₃, 200 MHz): δ 7.42 (d, *J* = 8.7 Hz, 1H, H-6), 6.73 (d, *J* = 8.7 Hz, 1H, H-5), 5.36 (s, 2H, NH₂), 4.29 – 4.08 (m, 1H, CH), 2.14 – 1.62 (m, 2H, CH₂), 1.42 (d, *J* = 6.9 Hz, 3H, CHCH₃), 0.85 (t, *J* = 7.3 Hz, 3H, CH₂CH₃). ¹³C{¹H} NMR (CDCl₃, 50 MHz): δ 169.2, 166.8, 144.7, 139.5, 129.3, 122.5, 112.9, 104.6, 49.1, 26.9, 18.5, 11.4. ESI-HRMS *m/z* for C₁₂H₁₄BrN₂O₂ [M+H]⁺: calcd. 297.0233, found 297.0233.

General procedure for the bromination of the 7-substituted aminophthalimides 5e and 5f. The phthalimide (2.8 mmol, 1 equiv.) was added in a solution of *N*-bromosuccinimide (500 mg, 2.8 mmol, 1 equiv.) in dichloromethane (6 mL) and the resulting mixture was stirred in the dark for 2 hours. Then, the solvent was evaporated and the residue was subjected to column chromatography yielding the corresponding phthalimide.

4-amino-5-bromo-2-(sec-butyl)-7-methylisoindoline-1,3-dione (7a). From phthalimide **5e** (650 mg). Purification by column chromatography (0-10% EtOAc, PE). Yellow solid (592 mg, 68%). ¹H NMR (CDCl₃, 200 MHz): δ 7.47 (s, 1H, H-6), 5.56 (s, 2H, NH₂), 4.27 – 4.09 (m, 1H, CH), 2.50 (s, 3H, ArCH₃), 2.14 – 1.64 (m, 2H, CH₂), 1.44 (d, *J* = 7.0 Hz, 3H, CHCH₃), 0.87 (t, *J* = 7.4 Hz, 3H, CH₂CH₃). ¹³C{¹H} NMR (CDCl₃, 100 MHz): δ 170.0, 168.9, 141.2, 140.2, 128.0, 127.3, 115.3, 112.2, 48.9, 27.1, 18.6, 16.4, 11.5. GC-MS (EI): 312 (M⁺+2, 33), 310 (M⁺, 36), 283 (98), 281 (100), 266 (22), 264 (23%). Molecular Ion could not be detected on ESI-MS or HRMS.

4-amino-5-bromo-2-(sec-butyl)-7-phenylisoindoline-1,3-dione (7b). From phthalimide **5f** (824 mg). Purification by column chromatography (0-10% EtOAc, PE). Yellow solid (909 mg, 87%). ¹H NMR (CDCl₃, 200 MHz): δ 7.66 (s, 1H, H-6), 7.58 – 7.33 (m, 5H, PhH), 5.82 (bs, 2H, NH₂), 4.33 – 4.03 (m, 1H, CH), 2.19 – 1.60 (m, 2H, CH₂), 1.45 (d, *J* = 7.0 Hz, 3H, CHCH₃), 0.88 (t, *J* = 7.3 Hz, 3H, CH₂CH₃). ¹³C{¹H} NMR (CDCl₃, 50 MHz): δ 169.7, 167.5, 142.1, 139.6, 135.6, 130.6, 129.3, 128.2, 128.0, 126.7, 115.2, 112.3, 48.9, 26.8, 18.4, 11.4. ESI-HRMS *m/z* for C₁₈H₁₈BrN₂O₂ [M+H]⁺: calcd. 373.0546, found 373.0541.

General procedure for the Suzuki-Miyaura coupling. A mixture of the brominated phthalimide (4 mmol, 1 equiv.),

the boronic acid derivative (4.5 mmol, 1.1 equiv. for mono- or 9 mmol, 2.3 equiv. for di-brominated phthalimides), potassium carbonate (2.5 g, 18 mmol, 4.5 equiv.), water (6 mL) and 1,4-dioxane (6 mL) was bubbled with argon for 30 minutes. Tetrakis(triphenylphosphine)-palladium(0) (69 mg, 0.06 mmol, 0.015 equiv.) was added and bubbling continued for another 15 minutes. Then, the mixture was stirred under an inert atmosphere, in an oil bath at 105°C for 18 hours. After cooling, the solvent was partially evaporated, water (60 mL) and EtOAc (150 mL) were added, the phases were separated, the organic phase was washed with 1N HCl (40 mL) and brine (40 mL), dried (MgSO₄) and the solvent was evaporated. The residue was further treated as indicated in each case, affording the corresponding substituted derivative.

4-amino-2-(sec-butyl)-5,7-dimethylisoindoline-1,3-dione (5a). From dibromophthalimide **4** (1.5 g) and trimethylboroxine (3.5 M in THF, 2.6 mL). Purification with column chromatography (10-30% EtOAc/P.E.). Yellow solid (552 mg, 56%). ¹H NMR (CDCl₃, 200 MHz): δ 7.01 (s, 1H, H-6), 5.15 (bs, 2H, NH₂), 4.26 – 3.94 (m, 1H, CH), 2.46 (s, 3H, 7-CH₃), 2.17 (s, 3H, 5-CH₃), 2.10 – 1.61 (m, 2H, CH₂) 1.41 (d, *J* = 7.0 Hz, 3H, CH₂CH₃), 0.85 (t, *J* = 7.4 Hz, 3H, CHCH₃). ¹³C{¹H} NMR (CDCl₃, 50 MHz): δ 170.9, 169.5, 142.3, 138.0, 129.5, 126.4, 126.3, 111.0, 48.3, 27.0, 18.6, 16.8, 16.4, 11.4. ESI-HRMS *m/z* for C₁₄H₁₉N₂O₂⁺ [M+H]⁺: calcd. 247.1447, found 247.1429.

4-amino-2-(sec-butyl)-5,7-diphenylisoindoline-1,3-dione (5b). From dibromophthalimide **4** (1.5 g) and phenylboronic acid (1.1 g). No further treatment needed. Yellow solid (1.4 g, 95%). ¹H NMR (CDCl₃, 200 MHz): δ 7.65 – 7.31 (m, 11H, ArH), 5.59 (bs, 2H, NH₂), 4.37 – 4.10 (m, 1H, CH), 2.24 – 1.65 (m, 2H, CH₂), 1.48 (d, *J* = 7.0 Hz, 3H, CHCH₃) 0.92 (t, *J* = 7.4 Hz, 3H, CH₂CH₃). ¹³C{¹H} NMR (CDCl₃, 50 MHz): δ 170.7, 168.1, 142.4, 138.1, 136.8, 136.7, 134.0, 130.1, 129.4, 129.4, 128.8, 128.6, 128.1, 127.9, 126.6, 111.9, 48.8, 26.9, 18.6, 11.5. ESI-HRMS *m/z* for C₂₄H₂₂NaN₂O₂⁺ [M+Na]⁺: calcd. 393.1573, found 393.1572.

4-amino-2-(sec-butyl)-5-methylisoindoline-1,3-dione (5c). From bromophthalimide **6a** (1.2 g) and trimethylboroxine (3.5 M in THF, 1.3 mL). Purification with column chromatography (20% EtOAc/P.E.). Yellow solid (297 mg, 32%). ¹H NMR (CDCl₃, 200 MHz): δ 7.27 (d, *J* = 7.4 Hz, 1H H-7), 7.06 (d, *J* = 7.3 Hz, 1H, H-5), 5.23 (bs, 2H, NH₂), 4.37 – 3.97 (m, 1H, CH), 2.23 (s, 3H, ArCH₃), 2.15 – 1.66 (m, 2H, -CH₂), 1.44 (d, *J* = 6.9 Hz, 3H, CHCH₃) 0.88 (t, *J* = 7.4 Hz, 3H, CH₂CH₃). ¹³C{¹H} NMR (CDCl₃, 50 MHz): δ 171.1, 169.0, 143.9, 135.2, 130.6, 129.3, 112.4, 111.1, 48.6, 27.0, 18.6, 17.1, 11.4. ESI-HRMS *m/z* for C₁₃H₁₆NaN₂O₂⁺ [M+Na]⁺: calcd. 255.1104, found 255.1104.

4-amino-2-(sec-butyl)-5-phenylisoindoline-1,3-dione (5d). From bromophthalimide **6a** (1.2 g) and phenylboronic acid (553 mg). No further treatment needed. Yellow solid (965 mg, 82%). ¹H NMR (CDCl₃, 200 MHz): δ 7.55 – 7.37 (m, 5H, PhH), 7.34 (d, *J* = 7.3 Hz, 1H, H-6), 7.16 (d, *J* = 7.3 Hz, 1H, H-7), 5.42 (bs, 2H, NH₂), 4.34 – 4.02 (m, 1H, CH), 2.20 – 1.59 (m, 2H, CH₂), 1.45 (d, *J* = 7.0 Hz, 3H, CHCH₃), 0.89 (t, *J* = 7.5 Hz, 3H, CH₂CH₃). ¹³C{¹H} NMR (CDCl₃, 50 MHz): δ 170.9, 168.7, 142.9, 136.9, 135.7, 133.7, 131.8, 129.3, 128.7, 128.4, 112.4, 111.5, 48.7, 27.0, 18.6, 11.4. ESI-HRMS *m/z*

for $C_{18}H_{18}N_2NaO_2^+$ $[M+Na]^+$: calcd. 317.1260, found 317.1259.

4-amino-2-(sec-butyl)-7-methylisoindoline-1,3-dione (5e). From bromophthalimide **6b** (1.2 g) and trimethylboroxine (3.5 M in THF, 1.3 mL). Purification with column chromatography (10% EtOAc/P.E.). Yellow solid (650 mg, 70%). 1H NMR ($CDCl_3$, 400 MHz): δ 7.13 (dq, $J = 8.4, 0.6$ Hz, 1H, H-6), 6.73 (dd, $J = 8.4, 0.3$ Hz, 1H, H-5), 5.13 (s, 2H, NH_2), 4.22 – 4.13 (m, 1H, CH), 2.50 (s, 3H, $ArCH_3$), 2.02 (ddq, $J = 7.4, 9.3, 13.8$ Hz, 1H, CH_2), 1.74 (ddq, $J = 6.1, 7.4, 13.5$ Hz, 1H, CH_2), 1.43 (d, $J = 7.0$ Hz, 3H, $CHCH_3$), 0.87 (t, $J = 7.4$ Hz, 3H, CH_2CH_3). $^{13}C\{^1H\}$ NMR ($CDCl_3$, 100 MHz): δ 170.6 (C-3), 169.6 (C-1), 143.5 (C-4), 137.9 (C-6), 128.5 (C-7a), 126.8 (C-7), 121.2 (C-5), 111.4 (C-3a), 48.5 (C-2'), 27.03 (C-3'), 18.6 (C-1'), 16.6 ($ArCH_3$), 11.5 (C-4'). ESI-HRMS m/z for $C_{13}H_{16}N_2NaO_2^+$ $[M+Na]^+$: calcd. 255.1104, found 255.1103.

4-amino-2-(sec-butyl)-7-phenylisoindoline-1,3-dione (5f). From bromophthalimide **6b** (1.2 g) and phenylboronic acid (553 mg). Purification with column chromatography (20% EtOAc/P.E.). Yellow solid (1.1 g, 92%). 1H NMR ($CDCl_3$, 200 MHz): δ 7.61 – 7.38 (m, 5H, PhH), 7.34 (d, $J = 8.6$ Hz, 1H, H-6), 6.85 (d, $J = 8.5$ Hz, 1H, H-5), 5.47 (bs, 2H, NH_2), 4.37 – 4.06 (m, 1H, CH), 2.21 – 1.64 (m, 2H, CH_2), 1.47 (d, $J = 6.9$ Hz, 3H, $CHCH_3$), 0.91 (t, $J = 7.4$ Hz, 3H, CH_2CH_3). $^{13}C\{^1H\}$ NMR ($CDCl_3$, 50 MHz): δ 170.3, 168.2, 144.7, 137.4, 136.8, 129.9, 129.2, 127.9, 127.7, 127.2, 121.3, 111.1, 48.5, 26.8, 18.4, 11.3. ESI-HRMS m/z for $C_{18}H_{19}N_2O_2$ $[M+H]^+$: calcd. 295.1441, found 295.1442.

4-amino-2-(sec-butyl)-7-methyl-5-phenylisoindoline-1,3-dione (5g). From bromophthalimide **7a** (1.2 g) and phenylboronic acid (553 mg). Purification with column chromatography (10% EtOAc/P.E.). Yellow solid (679 mg, 55%). 1H NMR ($CDCl_3$, 400 MHz): δ 7.50 – 7.35 (m, 5H, PhH), 7.12 (s, 1H, H-6), 5.30 (bs, 2H, NH_2), 4.31 – 4.13 (m, 1H, CH), 2.54 (s, 3H, $ArCH_3$), 2.06 (ddq, $J = 14.7, 9.4, 7.4$ Hz, 1H, CH_2), 1.84 – 1.69 (m, 1H, CH_2), 1.45 (d, $J = 7.0$ Hz, 3H, $CHCH_3$), 0.90 (t, $J = 7.4$ Hz, 3H, CH_2CH_3). $^{13}C\{^1H\}$ NMR ($CDCl_3$, 100 MHz): δ 170.7, 169.3, 141.3, 138.5, 137.0, 134.0, 129.2, 128.7, 128.3, 127.7, 126.4, 111.6, 48.5, 27.0, 18.6, 16.5, 11.4. ESI-HRMS m/z for $C_{19}H_{21}N_2O_2$ $[M+H]^+$: calcd. 309.1598, found 309.1599.

4-amino-2-(sec-butyl)-5-methyl-7-phenylisoindoline-1,3-dione (5h). From bromophthalimide **7b** (1.5 g) and trimethylboroxine (3.5 M in THF, 1.3 mL). Purification with column chromatography (10% EtOAc/P.E.). Yellow solid (629 mg, 51%). 1H NMR ($CDCl_3$, 200 MHz): δ 7.58 – 7.34 (m, 5H, PhH), 7.26 (s, 1H, H-6), 5.27 (bs, 2H, NH_2), 4.33 – 3.99 (m, 1H, CH), 2.26 (s, 3H, $ArCH_3$), 2.17 – 1.62 (m, 2H, CH_2), 1.44 (d, $J = 7.0$ Hz, 3H, $CHCH_3$), 0.88 (t, $J = 7.4$ Hz, 3H, CH_2CH_3). $^{13}C\{^1H\}$ NMR ($CDCl_3$, 50 MHz): δ 170.9, 168.2, 143.4, 137.7, 137.0, 130.1, 129.6, 129.4, 128.0, 127.8, 125.4, 111.4, 48.6, 26.9, 18.6, 17.0, 11.5. ESI-HRMS m/z for $C_{19}H_{20}N_2NaO_2$ $[M+Na]^+$: calcd. 331.1417, found 331.1417.

4-amino-2-(sec-butyl)-5-(4-(hydroxymethyl)phenyl)-7-methylisoindoline-1,3-dione (5i). From bromophthalimide **7a** (1.2 g) and 4-(hydroxymethyl)phenylboronic acid (684 mg). Purification with column chromatography (10% EtOAc/P.E.). Yellow solid (1.06 g, 78%). 1H NMR ($CDCl_3$, 400 MHz): δ 7.50 (app d, $J = 8.3$ Hz, 2H, H-3'), 7.43 (app d, $J = 8.3$ Hz, 2H, H-2'), 7.12 (s, 1H, H-6), 5.30 (bs, 2H, NH_2), 4.77 (s, 2H, OCH_2), 4.27 – 4.16 (m, 1H, CH), 2.55 (s, 3H, $ArCH_3$),

2.14 – 1.99 (m, 1H, $CHCH_2$), 1.84 – 1.69 (m, 2H, OH, $CHCH_2$), 1.46 (d, $J = 7.0$ Hz, 3H, $CHCH_3$), 0.90 (t, $J = 7.4$ Hz, 3H, CH_2CH_3). $^{13}C\{^1H\}$ NMR ($CDCl_3$, 50 MHz): δ 170.8, 169.4, 141.3, 141.2, 138.5, 136.3, 133.8, 129.0, 127.8, 127.7, 126.5, 111.6, 64.9, 48.6, 27.1, 18.7, 16.6, 11.5. ESI-HRMS m/z for $C_{20}H_{22}N_2NaO_3$ $[M+Na]^+$: calcd. 361.1522, found 361.1520.

General procedure for the synthesis of phthalhydrazides (8). A suspension of phthalimide (0.4 mmol) in a large excess of hydrazine monohydrate (5mL) was heated in an oil bath at 110°C under Ar for 18h. After cooling, the pH was adjusted to 2 using concentrated hydrochloric acid and the precipitate was filtered and washed with water, affording the corresponding phthalhydrazide.

5-amino-6,8-dimethyl-2,3-dihydrophthalazine-1,4-dione (8a). From phthalimide **5a** (99 mg). Yellow solid (66 mg, 80%).^{13a} 1H NMR (DMSO- d_6 , 200 MHz): δ 11.08 (bs, 2H, $NHNH$), 7.21 (s, 1H, H-7), 6.89 (bs, 2H, NH_2), 2.48 (s, 3H, $8-CH_3$), 2.12 (s, 3H, 6- CH_3).

5-amino-6,8-diphenyl-2,3-dihydrophthalazine-1,4-dione (8b). From phthalimide **5b** (148 mg). Yellow solid (112 mg, 85%).^{13a} 1H NMR (DMSO- d_6 , 400 MHz): δ 9.67 (bs, 2H, $NHNH$), 8.11 – 6.64 (m, 13H, PhH, H-7, NH_2). $^{13}C\{^1H\}$ NMR (DMSO- d_6 , 100 MHz): δ 162.0, 151.3, 147.1, 142.7, 138.4, 137.5, 129.3, 129.1, 128.8, 127.8, 127.2, 126.8, 125.9, 125.8, 122.5, 111.6. ESI-HRMS m/z for $C_{20}H_{16}N_3O_2$ $[M+H]^+$: calcd. 330.1237, found 330.1239.

5-amino-6-methyl-2,3-dihydrophthalazine-1,4-dione (8c). From phthalimide **5c** (93 mg). Pale yellow solid (70 mg, 92%).^{13b} 1H NMR (DMSO- d_6 , 200 MHz): δ 11.25 (br 2H, $NHNH$), 7.41 (d, $J = 7.9$ Hz, 1H, H-8), 6.95 (d, $J = 7.7$ Hz, 1H, H-7), 4.00 (bs, 2H, NH_2), 2.16 (s, 3H, CH_3). $^{13}C\{^1H\}$ NMR (DMSO- d_6 , 50 MHz): δ 161.8, 151.7, 148.6, 134.9, 124.5, 124.2, 110.1, 109.5, 17.7. ESI-HRMS, m/z for $C_9H_{10}N_3O_2$ $[M+H]^+$: calcd. 192.0768, found 192.0756.

5-amino-6-phenyl-2,3-dihydrophthalazine-1,4-dione (8d). From phthalimide **5d** (118 mg). Pale yellow solid (93 mg, 92%). 1H NMR (DMSO- d_6 , 400 MHz): δ 7.63 – 7.29 (m, 6H, H-6, PhH), 7.09 (d, $J = 7.9$ Hz, 1H, H-8), 7.30 – 6.98 (bs, 2H, NH_2). $^{13}C\{^1H\}$ NMR (DMSO- d_6 , 100 MHz): δ 161.7, 151.6, 147.3, 138.0, 135.1, 129.1, 128.8, 127.9, 127.7, 126.0, 111.2, 110.0. ESI-HRMS, m/z for $C_{14}H_{12}N_3O_2$ $[M+H]^+$: calcd. 254.0924, found 254.0923.

5-amino-8-methyl-2,3-dihydrophthalazine-1,4-dione (8e). From phthalimide **5e** (93 mg). Pale-yellow solid (57 mg, 74%).^{13b} 1H NMR (DMSO- d_6 , 400 MHz): δ 11.03 (bs, 2H, $NHNH$), 7.24 (d, $J = 8.4$ Hz, 1H, H-6), 6.80 (d, $J = 8.4$ Hz, 1H, H-7), 2.52 (s, 3H, CH_3). $^{13}C\{^1H\}$ NMR (DMSO- d_6 , 100 MHz): δ 161.3, 153.3, 149.2, 137.5, 124.7, 121.4, 116.9, 111.2, 22.0. ESI-HRMS, m/z for $C_9H_{10}N_3O_2$ $[M+H]^+$: calcd. 192.0768, found 192.0758.

5-amino-8-phenyl-2,3-dihydrophthalazine-1,4-dione (8f). From phthalimide **5f** (118 mg). Yellow solid (96 mg, 95%). 1H -NMR (DMSO- d_6 , 400 MHz): δ 11.28 (bs, 2H, $NHNH$), 7.32 – 7.13 (m, 6H, PhH, H-6), 6.95 (d, $J = 8.6$ Hz, 1H, H-7). $^{13}C\{^1H\}$ NMR (DMSO- d_6 , 100 MHz): δ 161.5, 151.4, 149.8, 143.0, 137.4, 129.3, 126.8, 126.2, 125.7, 123.1, 116.4, 111.1. ESI-HRMS, m/z for $C_{14}H_{10}N_3O_2$ $[M-H]^+$: calcd. 252.0778, found 252.0762

5-amino-8-methyl-6-phenyl-2,3-dihydrophthalazine-1,4-dione (8g). From phthalimide **5g** (123 mg). Yellow solid (53 mg, 50%). ¹H NMR (DMSO-d₆, 400 MHz): δ 11.25 (bs, 2H, NHNH), 7.52 – 7.39 (m, 5H, PhH), 7.22 (s, 1H, H-7), 7.02 (bs, 2H, NH₂), 2.57 (s, 3H, CH₃). ¹³C{¹H} NMR (DMSO-d₆, 101 MHz): δ 162.2, 153.5, 146.3, 139.2, 138.3, 129.5, 129.3, 128.6, 128.2, 124.6, 122.2, 112.5, 22.5. ESI-HRMS, m/z for C₁₅H₁₄N₃O₂ [M+H]⁺: calcd. 268.1081, found 268.1066.

5-amino-6-methyl-8-phenyl-2,3-dihydrophthalazine-1,4-dione (8h). From phthalimide **5h** (123 mg). Yellow solid (84 mg, 79%). ¹H NMR (DMSO-d₆, 400 MHz): δ 11.31 (bs, 2H, NHNH), 7.29 – 7.17 (m, 6H, PhH, H-7), 2.18 (s, 3H, CH₃). ¹³C{¹H} NMR (DMSO-d₆, 101 MHz): δ 162.0, 151.5, 148.3, 143.1, 138.4, 129.3, 126.8, 125.7, 125.6, 123.7, 121.0. ESI-HRMS, m/z for C₁₅H₁₄N₃O₂ [M+H]⁺: calcd. 268.1081, found 268.1080.

5-amino-6-(4-(hydroxymethyl)phenyl)-8-methyl-2,3-dihydrophthalazine-1,4-dione (8i). From phthalimide **5i** (135 mg). Yellow solid (113 mg, 95%). ¹H NMR (400 MHz, MeOD-d₄): δ 7.77 (s, 1H, H-7), 7.59 (app d, J = 8.5 Hz, 2H, H-3'), 7.52 (app d, J = 8.4 Hz, 2H, H-2'), 4.72 (s, 2H, OCH₂), 2.89 (s, 3H, ArCH₃). ¹H NMR (200 MHz, DMSO-d₆) δ 7.43 (app s, 4H, H-2',3'), 7.28 (s, 1H, H-7), 4.55 (s, 2H, OCH₂), 2.59 (s, 3H, ArCH₃). ¹³C{¹H} NMR (50 MHz, DMSO-d₆): δ 161.7, 153.1, 148.5, 145.3, 142.1, 138.7, 136.0, 128.5, 127.1, 124.1, 122.2, 112.3, 62.6, 22.0. ESI-HRMS m/z for C₁₆H₁₅N₃NaO₃ [M+Na]⁺: calcd. 320.1006, found 320.1003.

General procedure for the synthesis of phthalic acid anhydrides (9). Large excess aqueous potassium hydroxide (15 N, 3 mL) was added to a solution of the phthalimide (0.3 mmol) in ethanol (3 mL) and the mixture was heated in an oil bath to reflux and stirred at that temperature for 3 days. Subsequently, ethanol was removed under reduced pressure, water (10 mL) was added, and the resulting solution was extracted with DCM (3 x 15 mL). The aqueous phase was collected and acidified with 1 N hydrochloric acid until pH=3. Immediately after acidification, the aqueous phase turned fluorescent green, indicative of the anhydride formation. The solution was extracted with ethyl acetate (3 x 20 mL) and the combined organic phase was dried (MgSO₄) and concentrated in vacuo. The residue was further treated as indicated in each case below, affording the corresponding anhydride.

4-amino-5,7-dimethylisobenzofuran-1,3-dione (9a). From phthalimide **5a** (74 mg). No further treatment needed. Yellow solid (47 mg, 82%). ¹H NMR (DMSO-d₆, 200 MHz): δ 7.34 (s, 1H, H-6), 6.38 (s, 2H, NH₂), 2.39 (s, 3H, 7-CH₃), 2.21 (s, 3H, 5-CH₃). ¹³C{¹H} NMR (DMSO-d₆, 50 MHz): δ 164.4, 163.5, 145.2, 139.8, 131.9, 126.4, 124.8, 107.7, 17.3, 15.9. ESI-HRMS, m/z for C₁₀H₈NO₃ [M-H]⁻: calcd. 190.0509, found 190.0497.

4-amino-5,6-diphenylisobenzofuran-1,3-dione (9b). From phthalimide **5b** (111 mg). Purification with column chromatography (20% EtOAc/P.E.). Yellow solid (36 mg, 38%). ¹H NMR (CDCl₃, 400 MHz): δ 7.58 – 7.38 (m, 11H, PhH, H-6), 5.61 (s, 2H, NH₂). ¹³C{¹H} NMR (CDCl₃, 101 MHz): δ 165.1, 162.3, 144.1, 140.1, 135.7, 135.5, 135.4, 132.2, 129.7, 129.2, 129.2, 128.7, 128.5, 125.6, 111.3. ESI-HRMS, m/z for C₂₀H₁₄NO₃ [M+H]⁺: calcd. 316.0968, found 316.0942.

4-amino-5-methylisobenzofuran-1,3-dione (9c). From phthalimide **5c** (70 mg). Purification with column chromatography (10% EtOAc/P.E.). Yellow solid (25 mg, 47%). ¹H NMR (CDCl₃, 200 MHz): δ 7.45 (d, J = 7.3 Hz, 1H, H-6), 7.19 (d, J = 7.3 Hz, 1H, H-7), 5.33 (bs, 2H, NH₂), 2.29 (s, 3H, CH₃). ¹³C{¹H} NMR (CDCl₃, 50 MHz): δ 165.1, 163.4, 145.6, 137.8, 130.7, 129.5, 114.7, 110.4, 17.2. ESI-HRMS m/z for C₉H₈NO₃ [M+H]⁺: calcd. 178.0499, found 178.0500.

4-amino-5-phenylisobenzofuran-1,3-dione (9d). From phthalimide **5d** (88 mg). Purification with column chromatography (10% EtOAc/P.E.). Yellow solid (22 mg, 31%). ¹H NMR (CDCl₃, 400 MHz): δ 7.58 – 7.39 (m, 6H, 5-PhH, H-6), 7.31 (d, J = 7.3 Hz, 1H, H-7), 5.50 (s, 2H, NH₂). ¹³C{¹H} NMR (CDCl₃, 101 MHz): δ 165.0, 163.2, 144.8, 138.1, 135.9, 135.0, 130.7, 129.7, 129.1, 128.7, 114.7, 111.0. ESI-HRMS m/z for C₁₅H₁₂NO₄ [M+MeOH-H]⁻: calcd. 270.0772, found 270.0778.

4-amino-7-methylisobenzofuran-1,3-dione (9e). From phthalimide **5e** (70 mg). Purification with column chromatography (20% EtOAc/P.E.). Yellow solid (13 mg, 25%). ¹H-NMR (CDCl₃, 400 MHz), δ = 7.34 (d, J = 8.4 Hz, 1H, H-6), 6.89 (d, J = 8.4 Hz, 1H, H-5), 5.21 (s, 2H, NH₂), 2.54 (s, 3H, CH₃). ¹³C{¹H} NMR (CDCl₃, 101 MHz), δ = 164.8, 163.6, 145.3, 140.0, 129.1, 128.0, 122.3, 110.5, 16.7. ESI-HRMS m/z for C₉H₈NO₃ [M+H]⁺: calcd. 178.0499, found 178.0504.

4-amino-7-phenylisobenzofuran-1,3-dione (9f). From phthalimide **5f** (88 mg). Purification with column chromatography (20% EtOAc/P.E.). Yellow solid (32 mg, 45%). ¹H-NMR (CDCl₃, 400 MHz), δ = 7.57 – 7.06 (m, 6H, PhH, H-6), 7.04 (d, J = 8.5 Hz, 1H, H-5), 5.43 (s, 2H, NH₂). ¹³C{¹H} NMR (CDCl₃, 101 MHz), δ = 164.8, 162.5, 146.2, 139.6, 135.6, 132.5, 129.2, 128.7, 128.5, 126.7, 122.3, 111.0. ESI-HRMS m/z for C₁₄H₁₀NO₃ [M+H]⁺: calcd. 240.0655, found 240.0638.

4-amino-7-methyl-5-phenylisobenzofuran-1,3-dione (9g). From phthalimide **5g** (93 mg). Purification with column chromatography (20% EtOAc/P.E.). Yellow solid (22 mg, 29%). ¹H-NMR (CDCl₃, 400 MHz) δ = 7.53 – 7.37 (m, 6H, PhH, H-6), 5.43 (bs, 2H, NH₂), 2.32 (s, 3H, CH₃). ¹³C{¹H} NMR (CDCl₃, 101 MHz) δ = 165.3, 162.5, 145.0, 139.8, 135.7, 132.2, 129.2, 128.5, 128.4, 124.4, 110.7, 17.1. ESI-HRMS, m/z for C₁₅H₁₂NO₄ [M+H₂O-H]⁻: calcd. 270.0772, found 270.0770.

4-amino-5-methyl-7-phenylisobenzofuran-1,3-dione (9h). From phthalimide **5h** (93 mg). Purification with column chromatography (20% EtOAc/P.E.). Yellow solid (25 mg, 33%). ¹H-NMR (CDCl₃, 400 MHz) δ = 7.54 – 7.41 (m, 5H, PhH), 7.30 (s, 1H, H-6), 5.37 (bs, 2H, NH₂), 2.56 (s, 3H, CH₃). ¹³C{¹H} NMR (CDCl₃, 101 MHz) δ = 165.0, 163.4, 143.2, 140.5, 136.0, 135.4, 129.6, 129.0, 128.7, 128.7, 127.0, 110.7, 16.6. ESI-HRMS, m/z for C₁₅H₁₂NO₃ [M+H]⁺: calcd. 254.0812, found 254.0811.

ASSOCIATED CONTENT

Supporting Information. ¹H and ¹³C NMR spectra for all the synthesized compounds, as well as UV spectra from the hydrolysis of anhydrides **9a-h**. Fluorescence spectra of phthalates **10a-e**, **10h** and **3AP**. Comparative CL kinetics of luminol, **8a**, **8i** at given pH. Energy barrier calculations between **CP-2** and **TS** of **8a-h**. This material is available free of charge via the Internet at <http://pubs.acs.org>.

AUTHOR INFORMATION

Corresponding Authors

*E-mail for G. C. Vougioukalakis: vougiouk@chem.uoa.gr

*E-mail for M. A. Miranda: mmiranda@qim.upv.es

*E-mail for D. Roca-Sanjuán: daniel.roca@uv.es

Author Contributions

The manuscript was written through contributions of all authors. All authors have given approval to the final version of the manuscript.

Notes

The Foundation takes no responsibility for the opinions, statements, and contents of this project, which are entirely the responsibility of its authors.

ACKNOWLEDGMENTS

We would like to thank Ekaterini Bouga and Christina-Ioanna Vrettou for assisting with certain synthetic steps. This project was financially supported by the European Union's Horizon 2020 framework program for research and innovation under grant agreement no. 712921. T.M. and A.P. would like to thank the State Scholarships Foundation (IKY) for financial support through PhD fellowships through the "Strengthening of Human Resources through Doctoral Research" program of the Operational Program "Human Resource Development, Education and Lifelong Learning" 2014-2020, co-financed by the European Union (European Social Fund ESF) and Greek national funds. We would also like to thank prof. N. Thomaidis and Dr. Maria-Christina for the HRMS analyses. M.A.M. and G.M.R.-M. thank the Generalitat Valenciana (Prometeo Program/2017/075) for financial support. A.G. and D.R.-S. acknowledge Spanish "Ministerio de Ciencia e Innovación (MICINN)" (Project Ref. CTQ2017-87054-C2-2-P). A. G. is also thankful to the MICINN for a "Juan de la Cierva" grant (Ref. IJC2018-035123-I). D.R.-S. is also thankful to the MICINN for a "Ramón y Cajal" grant (Ref. RYC-2015-19234) and to the BBVA Foundation for a 2019 Leonardo Grant for Researchers and Cultural Creators.

REFERENCES

(1) Barni, F.; Lewis, S. W.; Berti, A.; Miskelly, G. M.; Lago, G. Forensic application of the luminol reaction as a presumptive test for latent blood detection. *Talanta* **2007**, *72*, 896.

(2) a) Yan, X.; Li, H.; Su, X. Review of optical sensors for pesticides. *TrAC-Trend. Anal. Chem.* **2018**, *103*, 1; b) Dodeigne, C.; Thunus, L.; Lejeune, R. Chemiluminescence as a diagnostic tool. A review. *Talanta* **2000**, *51*, 415.

(3) Padoan, A.; Cosma, C.; Sciacovelli, L.; Faggian, D.; Plebani, M. Analytical performances of a chemiluminescence immunoassay for SARS-CoV-2 IgM/IgG and antibody. *Clin. Chem. Lab. Med. (CCLM)* **2020**, *58*, 1081.

(4) a) Hananya, N.; Shabat, D. A Glowing Trajectory between Bio- and Chemiluminescence: From Luciferin-Based Probes to Triggerable Dioxetanes. *Angew. Chem. Int. Ed.* **2017**, *56*, 16454; b) Green, O.; Eilon, T.; Hananya, N.; Gutkin, S.; Bauer, C. R.; Shabat, D. Opening a Gateway for Chemiluminescence Cell Imaging: Distinctive Methodology for Design of Bright Chemiluminescent Dioxetane Probes. *ACS Cent. Sci.* **2017**, *3*, 349.

(5) a) Yang, M.; Huang, J.; Fan, J.; Du, J.; Pu, K.; Peng, X. Chemiluminescence for bioimaging and therapeutics: recent advances and challenges. *Chem. Soc. Rev.* **2020**, *49*, 6800-6815; b) Gnaïm, S.; Scomparin, A.; Das, S.; Blau, R.; Satchi-Fainaro, R.; Shabat, D. Direct Real-Time Monitoring of Prodrug Activation by

Chemiluminescence. *Angew. Chem. Int. Ed.* **2018**, *57*, 9033; c) Mao, D.; Wu, M.; Ji, S.; Chen, C.; Hu, F.; Kong, D.; Ding, D.; Liu, B. Chemiluminescence-Guided Cancer Therapy Using a Chemiexcited Photosensitizer. *Chem.* **2017**, *3*, 991.

(6) a) Yamaguchi, S.; Kishikawa, N.; Ohyama, K.; Ohba, Y.; Kohno, M.; Masuda, T.; Takadate, A.; Nakashima, K.; Kuroda, N. Evaluation of chemiluminescence reagents for selective detection of reactive oxygen species. *Anal. Chim. Acta* **2010**, *665*, 74; b) Barnett, W. N.; Francis, P. S. in *Encyclopedia of Analytical Science (Second Edition)* (Eds.: P. Worsfold, A. Townshend, C. Poole), Elsevier, Oxford, **2005**, pp. 511-521.

(7) Albrecht, H. O. Über die Chemiluminescenz des Aminophthalsäurehydrazids. *Z. Physik. Chem.* **1928**, *136*, 321.

(8) a) Su, Y.; Song, H.; Lv, Y. Recent advances in chemiluminescence for reactive oxygen species sensing and imaging analysis. *Microchem. J.* **2019**, *146*, 83; b) Khan, P.; Idrees, D.; Moxley, M. A.; Corbett, J. A.; Ahmad, F.; von Figura, G.; Sly, W. S.; Waheed, A.; Hassan, M. I. Luminol-Based Chemiluminescent Signals: Clinical and Non-clinical Application and Future Uses. *Appl. Biochem. Biotechnol.* **2014**, *173*, 333; c) Marquette, C. A.; Blum, L. J. Applications of the luminol chemiluminescent reaction in analytical chemistry. *Anal. Bioanal. Chem.* **2006**, *385*, 546.

(9) Griesbeck, A. G.; Díaz-Miara, Y.; Fichtler, R.; Jacobi von Wangelin, A.; Pérez-Ruiz, R.; Sampedro, D. Steric Enhancement of the Chemiluminescence of Luminols. *Chem. Eur. J.* **2015**, *21*, 9975.

(10) Brundrett, R. B.; White, E. H. Synthesis and Chemiluminescence of Derivatives of Luminol and Isoluminol. *J. Am. Chem. Soc.* **1974**, *96*, 7497-7502.

(11) Nishinaka, Y.; Aramaki, Y.; Yoshida, H.; Masuya, H.; Sugawara, T.; Ichimori, Y. A new sensitive chemiluminescence probe, L-012, for measuring the production of superoxide anion by cells. *Biochem. Biophys. Chem. Commun.* **1993**, *193*, 554.

(12) Karatani, H. Microenvironmental Effects of Water-Soluble Polymers on the Chemiluminescence of Luminol and Its Analogs. *Bull. Chem. Soc. Jpn.* **1987**, *60*, 2023-2029.

(13) a) Neumann, H.; Jacobi von Wangelin, A.; Klaus, S.; Strubing, D.; Gordes, D.; Beller, M. Anilines made easily: from aldehydes to tri-, tetra- and pentasubstituted anilines in two steps. *Angew. Chem. Int. Ed.* **2003**, *42*, 4503; b) Neumann, H.; Klaus, S.; Klawonn, M.; Strubing, D.; Hubner, S.; Gordes, D.; Jacobi von Wangelin, A.; Lalk, M.; Beller, M. A New Efficient Synthesis of Substituted Luminols Using Multicomponent Reactions. *Z. Naturforsch.* **2004**, *59b*, 431; c) Fichtler, R.; Neudorfl, J. M.; Jacobi von Wangelin, A. Practical three-component synthesis of crowded arenes with donor-acceptor substitution. *Org. Biomol. Chem.* **2011**, *9*, 7224.

(14) Pantelia, A.; Daskalaki, I.; Cuquerella, M. C.; Rotas, G.; Miranda, M. A.; Vougioukalakis, G. C. Synthesis and Chemiluminescent Properties of Amino-Acylated luminol Derivatives Bearing Phosphonium Cations. *Molecules* **2019**, *24*.

(15) Caswell, L. R.; Cavasos, G. Cyclic imides. 16. Hydroxy and methoxy derivatives of aminophthalimide and phthalhydrazide. *J. Heterocyclic Chem.* **1995**, *32*, 907.

(16) Ando, Y.; Niwa, K.; Yamada, N.; Irie, T.; Enomoto, T.; Kubota, H.; Ohmiya, Y.; Akiyama, H. Development of a quantitative bio/chemiluminescence spectrometer determining quantum yields: Re-examination of the aqueous luminol chemiluminescence standard. *Photochem. Photobiol.* **2007**, *83*, 1205.

(17) This value is stated as only 2x luminol Φ_{CL} in the literature (see ref. (10)). Yet, in spite of the CL being measured under different conditions (basicity, source of iron, measurement technology), the trend (enhanced luminescence in the 8-methyl derivative) is qualitatively confirmed.

(18) a) Yue, L.; Liu, Y.-T. Mechanistic Insight into pH-Dependent Luminol Chemiluminescence in Aqueous Solution. *J. Phys. Chem. B* **2020**, *124*, 7682; b) Giussani, A.; Farahani, P.; Martínez-Muñoz, D.; Lundberg, M.; Lindh, R.; Roca-Sanjuán, D. Molecular Basis of the Chemiluminescence Mechanism of Luminol. *Chem. Eur. J.* **2019**, *25*, 5202; c) Lind, J.; Merenyi, G.; Eriksen, T. E. Chemiluminescence

mechanism of cyclic hydrazides such as luminol in aqueous solutions. *J. Am. Chem. Soc.* **1983**, *105*, 7655; d) Merenyi, G.; Lind, J.; Eriksen, T. E. Luminol chemiluminescence: Chemistry, excitation, emitter. *J. Biolumin. Chemilumin.* **1990**, *5*, 53.

(19) Lee, J.; Seliger, H. H. Quantum yields of the luminol chemiluminescence reaction in aqueous and aprotic solvents. *Photochem. Photobiol.* **1972**, *15*, 227.

(20) a) Vacher, M.; Fdez. Galván, I.; Ding, B.-W.; Schramm, S.; Berraud-Pache, R.; Naumov, P.; Ferré, N.; Liu, Y.-J.; I. Navizet, I.; Roca-Sanjuán, D.; Baader, W. J.; Lindh, R. Chemi- and Bioluminescence of Cyclic Peroxides. *Chem. Rev.* **2018**, *118*, 6927; b) Yue, L.; Liu, Y.-T. Two Conical Intersections Control Luminol Chemiluminescence. *J. Chem. Theory Comput.* **2019**, *15*, 1798.

(21) Roca-Sanjuán, D.; Aquilante, F.; Lindh, R. Multiconfiguration second-order perturbation theory approach to strong electron correlation in chemistry and photochemistry. *WIREs Comput. Mol. Sci.* **2012**, *2*, 585.

(22) Stevani, C.; Silva, S.; Baader, W.; Studies on the Mechanism of the Excitation Step in Peroxyoxalate Chemiluminescence. *Eur. J. Org. Chem.* **2000**, 4037.

(23) Borrego-Sánchez, A.; Giussani, A.; Rubio, M.; Roca-Sanjuán, D. On the chemiluminescence emission of luminol: protic and aprotic solvents and encapsulation to improve the properties in aqueous solution. *Phys. Chem. Chem. Phys.* **2020**, *22*, 27617.

(24) Vacher, M.; Farahani, P.; Valentini, A.; Frutos, L. M.; Karlsson, H. O.; Fdez. Galván, I.; Lindh, R. How Do Methyl Groups Enhance the Triplet Chemiexcitation Yield of Dioxetane? *J. Phys. Chem. Lett.* **2017**, *8*, 3790.

(25) W.L.F. Armarego, C.L.L. Chai. Purification of Laboratory Chemicals (Sixth Edition), Butterworth-Heinemann, **2009**.

(26) CL of the compounds was also registered at different wavelengths ranging from 410 to 460 nm. We observed little if any variation in the results.

(27) a) Andersson, K.; Malmqvist, P. A.; Roos, B. O.; Sadlej, A. J.; Wolinski, K. Second-order perturbation theory with a CAS-SCF reference function. *J. Phys. Chem.* **1990**, *94*, 5483; b) Andersson, K.; Malmqvist, P.A.; Roos, B. O. Second-order perturbation theory with a complete active space self-consistent field reference function. *J. Chem. Phys.* **1992**, *96*, 1218.

(28) Frisch, M J.; Trucks, G. W.; Schlegel, H. B.; Scuseria, G. E.; Robb, M. A.; Cheeseman, J. R.; Scalmani, G.; Barone, V.; Petersson, G. A.; Nakatsuji, H.; Li, X.; Caricato, M.; Marenich, A.; Bloino, J.; Janesko, R.; Gomperts, R.; Menucci, B.; Hratchian, H. P.; Ortiz, J. V.; Izmaylov, A. F.; Sonnenberg, D.; Williams-Young, F.; Ding, F.; Lipparini, F.; Edigi, F.; Goings, J.; Peng, B.; Petrone, A.; Henderson, T.; Ranasinghe, D.; Zakrzewski, V. G.; Gao, J.; Rega, N.; Zheng, W.; Liang, W.; Hada, M.; Ehara, M.; Toyota, K.; Fukuda, R.; Hasegawa, M.; Ishida, T.; Nakajima, T.; Honda, Y.; Kitao, O.; Nakai, H.; Vreven, T.; Throssell, K.; Montgomery, Jr. J. A.; Peralta, J. E.; Ogliaro, F.

Bearpark, M.; Heyd, J. J.; Brothers, E.; Kudin, K. N.; Staroverov, V. N.; Keith, T.; Kobayashi, R.; Normand, J.; Raghavachari, K.; Rendell, A.; Burant, J. C.; Iyengar, S. S.; Tomasi, J.; Cossi, M.; Millam, J. M.; Klene, M.; Adamo, C.; Cammi, R.; Ochterski, J. W.; Martin, R. L.; Morokuma, K.; Farkas, O.; Foresman J. B.; Fox D. J. Gaussian 09, Revis. D.01, Gaussian, Inc., Wallingford CT, **2013**.

(29) Fdez. Galván, I.; Vacher, M.; Alavi, A.; Angeli, C.; Aquilante, F.; Autschbach, J.; Bao, J. J.; Bokarev, S. I.; Bogdanov, N. A.; Carlson, R. K.; Chibotaru, L. F.; Creutzberg, J.; N. Dattani, N.; Delcey, M. G.; Dong, S. S.; Dreuw, A.; Freitag, L.; Frutos, L. M.; Gagliardi, L.; Gendron, F.; Giussani, A.; González, L.; Grell, G.; Guo, M.; Hoyer, C. E.; Johansson, M.; Keller, S.; Knecht, S.; Kovačević, G.; Källman, E.; Li Manni, G.; Lundberg, M.; Ma, Y.; Mai, S.; Malhado, J. P.; Malmqvist, P. A.; Marquetand, P.; Mewes, S. A.; Norell, J.; Olivucci, M.; Oppel, M.; Phung, Q. M.; Pierloot, K.; Plasser, F.; Reiher, M.; Sand, A. M.; Schapiro, I.; Sharma, P.; Stein, C.J.; Sørensen, L. K.; Truhlar, D. G.; Ugandi, M.; Ungur, L.; Valentini, A.; Vancollie, S.; Veryazov, V.; Weser, O.; Wesolowski, T. A.; Widmark, P.-O.; Wouters, S.; Zech, A.; Zobel, J. P.; Lindh, R. OpenMolcas: From Source Code to Insight. *J. Chem. Theory Comput.* **2019**, *15*, 5925.

(30) Yanai, T.; Tew, D. P.; Handy, N. C. A new hybrid exchange-correlation functional using the Coulomb-attenuating method (CAM-B3LYP). *Chem. Phys. Lett.* **2004**, *393*, 51.

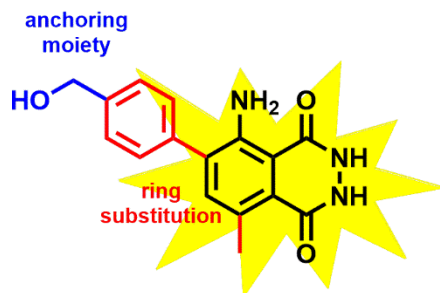
(31) a) Yue, L.; Roca-Sanjuán, D.; Lindh, R.; Ferré, N.; Liu, Y.-J. Can the Closed-Shell DFT Methods Describe the Thermolysis of 1,2-Dioxetane? *J. Chem. Theory Comput.* **2012**, *8*, 4359; b) Roca-Sanjuán, D.; Lundberg, M.; Mazziotti, D. A.; Lindh, R. Comment on "Density functional theory study of 1,2-dioxetane decomposition in condensed phase". *J. Comput. Chem.* **2012**, *33*, 2124.

(32) Pierloot, K.; Dumez, B.; Widmark, P.-O.; Roos, B. O. Density matrix averaged atomic natural orbital (ANO) basis sets for correlated molecular wave functions. *Theor. Chim. Acta* **1995**, *90*, 87.

(33) Roos, B. O.; Andersson, K.; Fülcher, M. P.; Malmqvist, P. A.; Serrano-Andrés, L.; Pierloot, K.; Merchán, M. Multiconfigurational perturbation theory: Applications in electronic spectroscopy. *Adv. Chem. Phys.* **1996**, *93*, 219.

(34) a) Giussani, A.; Worth, G. A. Similar chemical structures, dissimilar triplet quantum yields: A CASPT2 model rationalizing the trend of triplet quantum yields in nitroaromatic systems. *Phys. Chem. Chem. Phys.* **2019**, *21*, 10514; b) Giussani, A.; M. Merchán, Gobbo, J. P.; Borin, A. C. Relaxation Mechanisms of 5-Azacytosine. *J. Chem. Theory Comput.* **2014**, *10*, 3915.

(35) Tomasi, J.; Persico, M. Molecular Interactions in Solution: An Overview of Methods Based on Continuous Distributions of the Solvent. *Chem. Rev.* **1994**, *94*, 2027.



$$\Phi_{CL} = \begin{array}{l} 0.390 \text{ at pH}=12 \\ 0.058 \text{ at pH}=10 \\ 0.017 \text{ at pH}=8 \end{array}$$

- ✓ Modular synthesis
 - ✓ World record luminol
 - ✓ Chemiluminescence studies
 - ✓ Fluorescence studies
 - ✓ Quantum chemistry calculations
-

ELECTRONIC SUPPORTING INFORMATION

for

Building a functionalizable, potent chemiluminescent agent: A rational design study on 6,8-substituted luminol derivatives

by

Theodoros Mikroulis,^[a] M. Consuelo Cuquerella,^[b] Angelo Giussani,^[c] Anna Pantelia,^[a] Gemma M. Rodríguez-Muñiz,^[b] Georgios Rotas,^[a] Daniel Roca-Sanjuán,^{*,[c]} Miguel A. Miranda,^{*,[b]} and Georgios C. Vougioukalakis,^{*,[a]}

[a] Laboratory of Organic Chemistry, Department of Chemistry, National and Kapodistrian University of Athens, Panepistimiopolis, 15771 Athens, Greece, E-mail: vougiouk@chem.uoa.gr

[b] Instituto de Tecnología Química UPV-CSIC, Universitat Politècnica de València, Camino de Vera s / n, 46022 València, Spain, Email: mmiranda@qim.upv.es

[c] Instituto de Ciencia Molecular, Universitat de València, P.O. Box 22085, 46071 València, Spain, Email: daniel.roca@uv.es

Table of contents

- S3: Figure S1.** ¹H-NMR (200 MHz, DMSO-*d*₆) spectrum of **1**.
- S4: Figure S2.** ¹H-NMR (200 MHz, CDCl₃) spectrum of **2**.
- S5: Figure S3.** ¹H (200 MHz, up) and ¹³C (50 MHz, down) NMR (CDCl₃) spectra of **4**.
- S6: Figure S4.** ¹H (400 MHz, up) and ¹³C (101 MHz, down) NMR (CDCl₃) spectra of **6a**.
- S7: Figure S5.** 2D (¹H, ¹³C) HMBC NMR (CDCl₃) correlation of **6a**
- S8: Figure S6.** ¹H (200 MHz, up) and ¹³C (50 MHz, down) NMR (CDCl₃) spectra of **6b**
- S9: Figure S7.** ¹H (200 MHz, up) and ¹³C (50 MHz, down) NMR (CDCl₃) spectra of **7a**.
- S10: Figure S8.** ¹H (200 MHz, up) and ¹³C (50 MHz, down) NMR (CDCl₃) spectra of **7b**.
- S11: Figure S9.** ¹H (200 MHz, up) and ¹³C (50 MHz, down) NMR (CDCl₃) spectra of **5a**.
- S12: Figure S10.** ¹H (200 MHz, up) and ¹³C (50 MHz, down) NMR (CDCl₃) spectra of **5b**.
- S13: Figure S11.** ¹H (200 MHz, up) and ¹³C (50 MHz, down) NMR (CDCl₃) spectra of **5c**.
- S14: Figure S12.** ¹H (200 MHz, up) and ¹³C (50 MHz, down) NMR (CDCl₃) spectra of **5d**.
- S15: Figure S13.** ¹H (400 MHz, up) and ¹³C (100 MHz, down) NMR (CDCl₃) spectra of **5e**.
- S16: Figure S14.** 2D (¹H,¹³C)-HMBC NMR (CDCl₃) correlation of **5e**. Down: magnification.
- S17: Figure S15.** ¹H (200 MHz, up) and ¹³C (50 MHz, down) NMR (CDCl₃) spectra of **5f**.
- S18: Figure S16.** ¹H (400 MHz, up) and ¹³C (100 MHz, down) NMR (CDCl₃) spectra of **5g**.
- S19: Figure S17.** ¹H (200 MHz, up) and ¹³C (50 MHz, down) NMR (CDCl₃) spectra of **5h**
- S20: Figure S18.** ¹H (400 MHz, up) and ¹³C (100 MHz, down) NMR (CDCl₃) spectra of **5i**.
- S21: Figure S19.** ¹H NMR (200 MHz, DMSO-*d*₆) spectrum of **8a**
- S22: Figure S20.** ¹H (400 MHz, up) and ¹³C (100 MHz, down) NMR (DMSO-*d*₆) spectra of **8b**.
- S23: Figure S21.** ¹H (200 MHz, up) and ¹³C (50 MHz, down) NMR (DMSO-*d*₆) spectra of **8c**.
- S24: Figure S22.** ¹H (400 MHz, up) and ¹³C (100 MHz, down) NMR (DMSO-*d*₆) spectra of **8d**.
- S25: Figure S23.** ¹H (400 MHz, up) and ¹³C (100 MHz, down) NMR (DMSO-*d*₆) spectra of **8e**.
- S26: Figure S24.** ¹H (400 MHz, up) and ¹³C (100 MHz, down) NMR (DMSO-*d*₆) spectra of **8f**.
- S27: Figure S25.** ¹H (400 MHz, up) and ¹³C (101 MHz, down) NMR (DMSO-*d*₆) spectra of **8g**.
- S28: Figure S26.** ¹H (400 MHz, up) and ¹³C (101 MHz, down) NMR (DMSO-*d*₆) spectra of **8h**.

- S29:** **Figure S27.** ^1H (400 MHz, MeOD- d_4 , top), ^1H (400 MHz, DMSO- d_6 , middle), and ^{13}C (100 MHz, DMSO- d_6 , bottom) NMR spectra of **8i**.
- S30:** **Figure S28.** ^1H (200 MHz, up) and ^{13}C (50 MHz, down) NMR (DMSO- d_6) spectra of **9a**.
- S31:** **Figure S29.** ^1H (400 MHz, up) and ^{13}C (101 MHz, down) NMR (CDCl_3) spectra of **9b**.
- S32:** **Figure S30.** ^1H (200 MHz, up) and ^{13}C (50 MHz, down) NMR (CDCl_3) spectra of **9c**.
- S33:** **Figure S31.** ^1H (400 MHz, up) and ^{13}C (101 MHz, down) NMR (CDCl_3) spectra of **9d**.
- S34:** **Figure S32.** ^1H (400 MHz, up) and ^{13}C (101 MHz, down) NMR (CDCl_3) spectra of **9e**.
- S35:** **Figure S33.** ^1H (400 MHz, up) and ^{13}C (101 MHz, down) NMR (CDCl_3) spectra of **9f**.
- S36:** **Figure S34.** ^1H (400 MHz, up) and ^{13}C (101 MHz, down) NMR (CDCl_3) spectra of **9g**.
- S37:** **Figure S35.** ^1H (400 MHz, up) and ^{13}C (101 MHz, down) NMR (CDCl_3) spectra of **9h**.
- S38:** **Figure S36.** Hydrolysis of the phthalic acid anhydrides yielding the corresponding phthalates **9a-h** in aqueous alkaline media monitored by UV spectroscopy.
- S39:** **Figure S37.** Normalized fluorescence spectra corresponding to phthalates **9a-e**, **9h** and **3AP** in basic aqueous solution.
- S39:** **Figure S38.** Typical chemiluminescence kinetics displayed by luminol (LH_2 , A), and its derivatives **8a** (B) and derivative **8i** (C) in aqueous solutions at different pH: pH= 8, pH= 10 and pH= 12.
- S41:** **Figure S39.** Typical chemiluminescence kinetics displayed by luminol (LH_2), and its derivatives **8a** and **8i** in aqueous solutions at pH=8.
- S41:** **Table S1.** Energy barrier between **CP⁻²** and **TS** (ΔE^\ddagger , in eV) of luminol derivatives **8** computed in the gas phase, DMSO solution, and water solution.

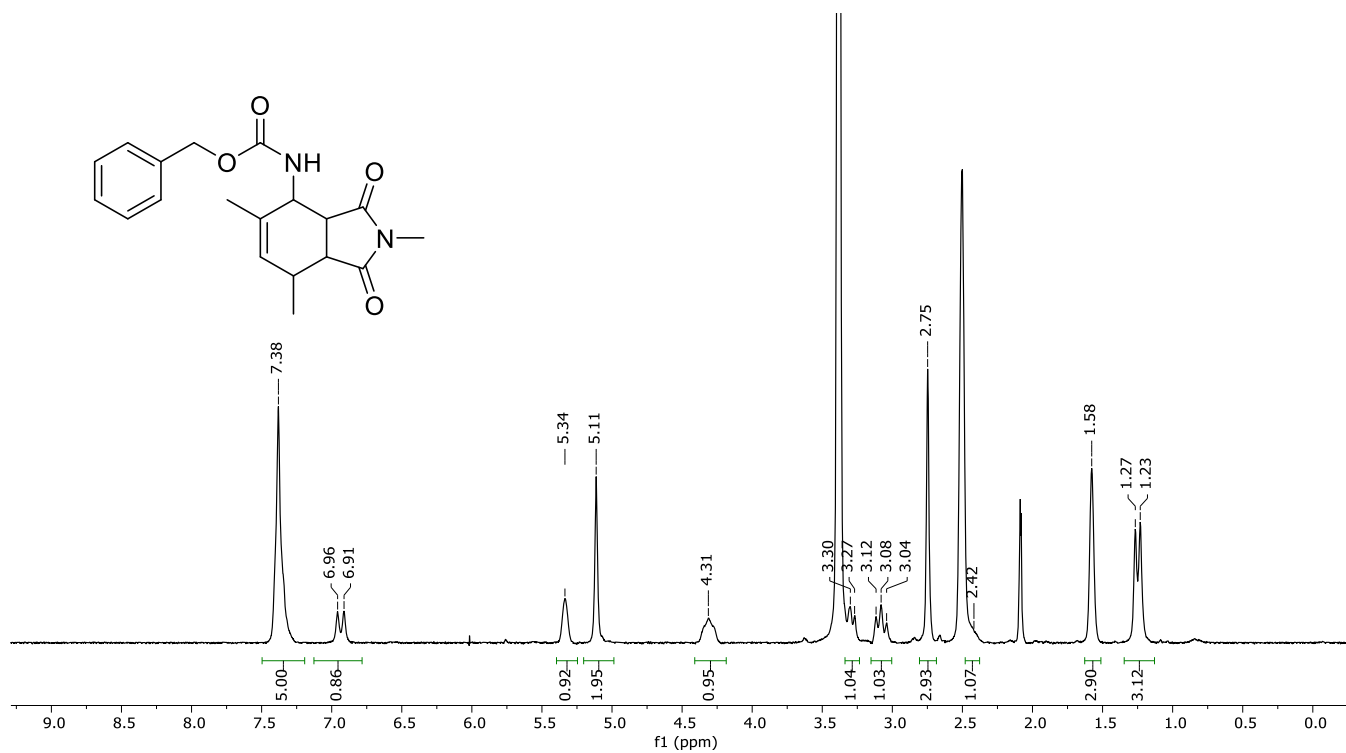
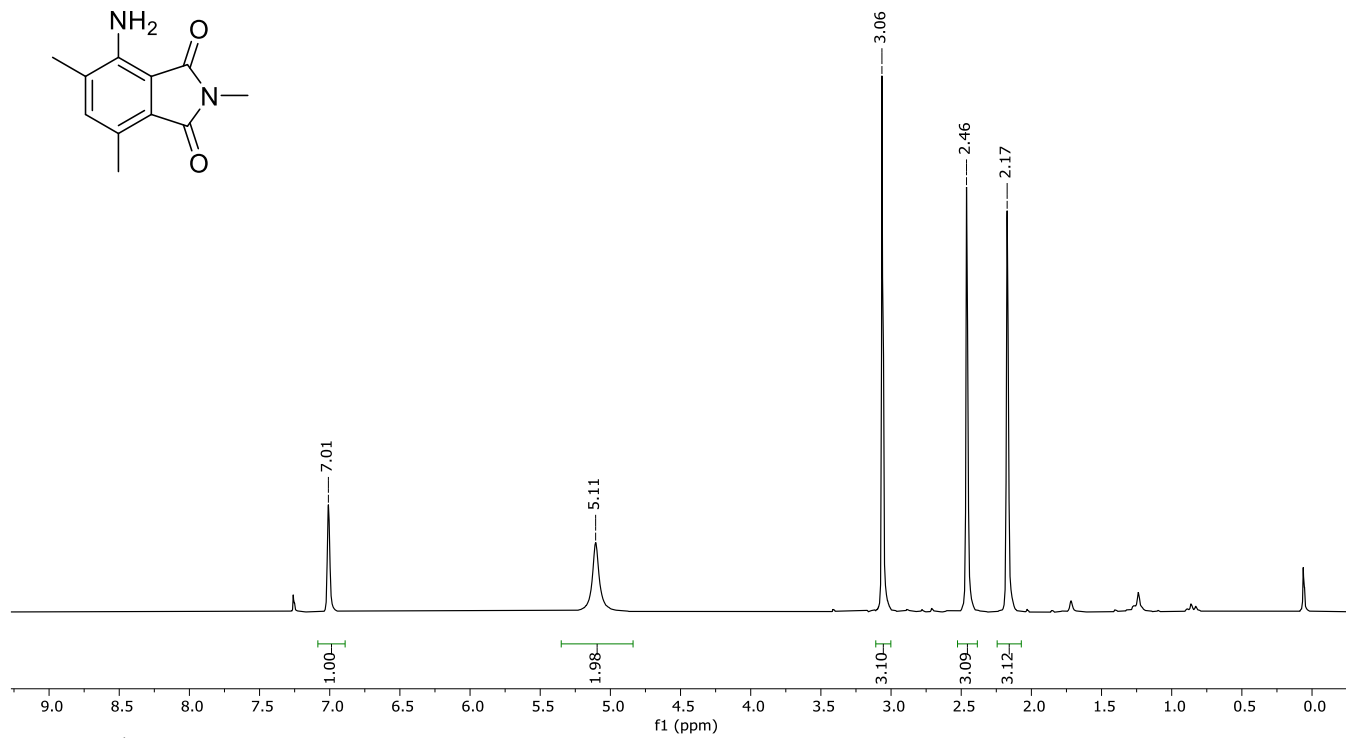
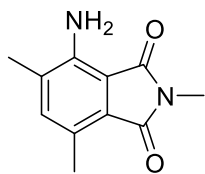


Figure S3. ¹H-NMR (200 MHz, DMSO-d₆) spectrum of 1.



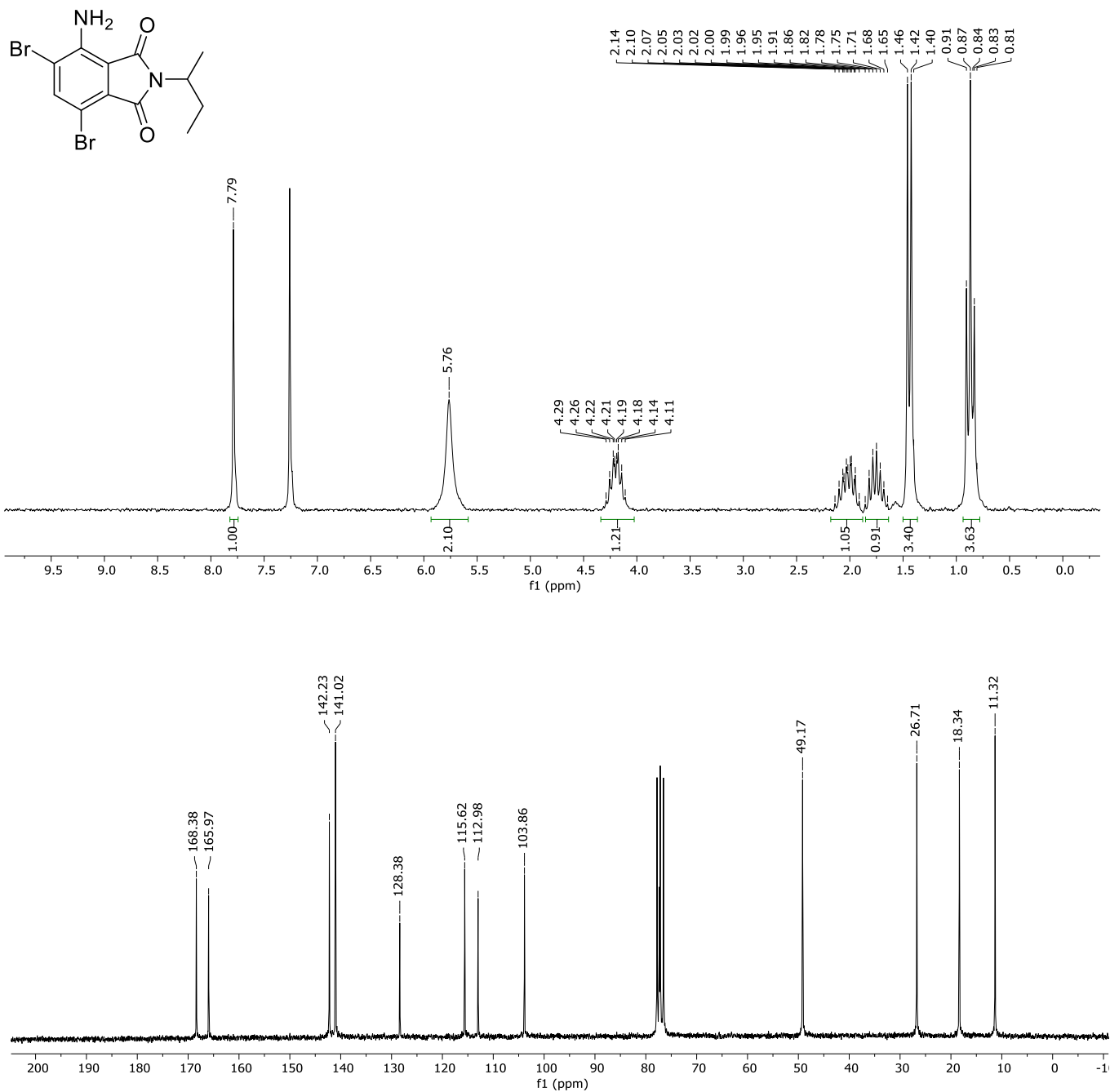


Figure S3. ¹H (200 MHz, up) and ¹³C (50 MHz, down) NMR (CDCl₃) spectra of 4.

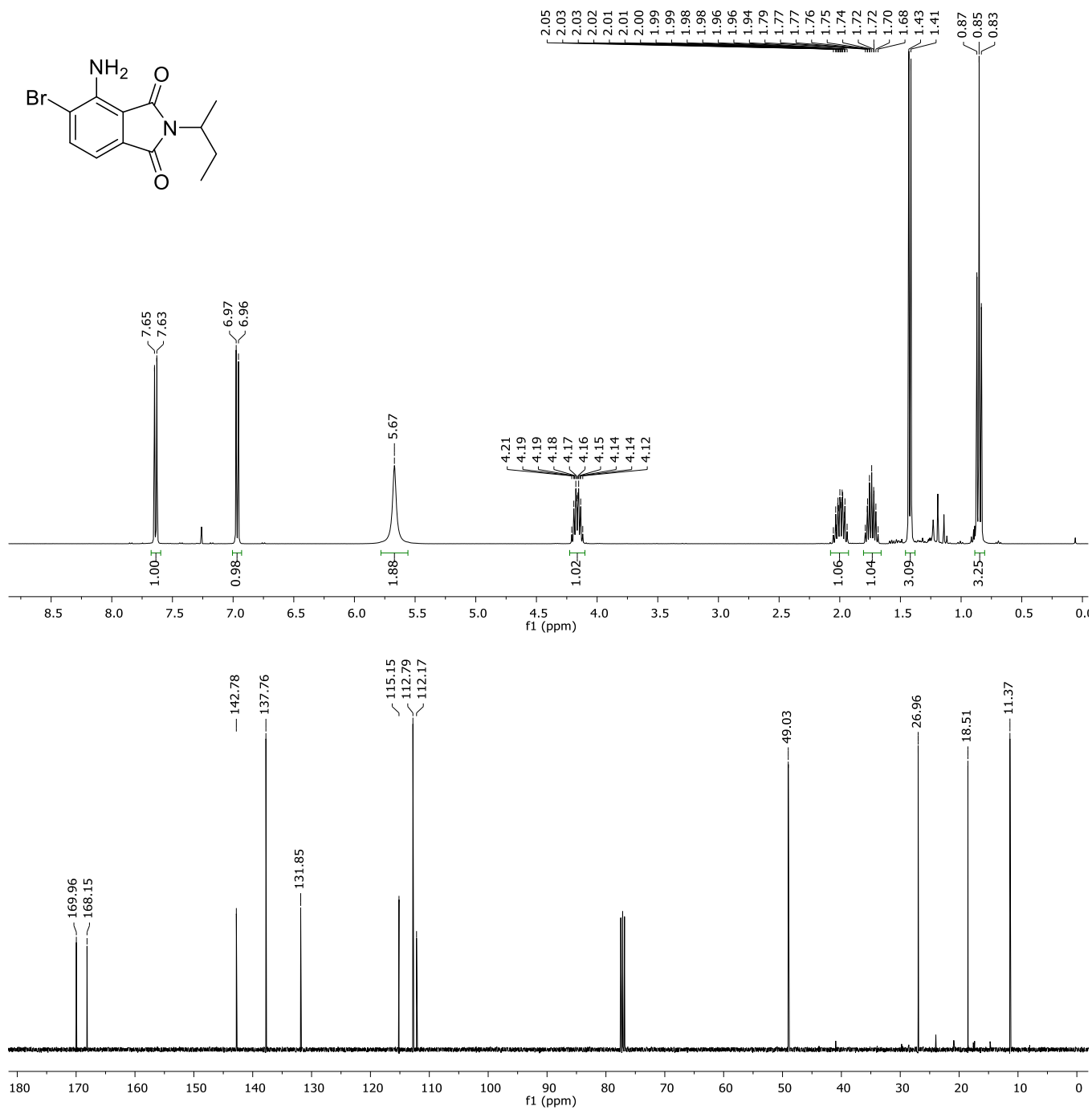


Figure S4. ¹H (400 MHz, up) and ¹³C (101 MHz, down) NMR (CDCl₃) spectra of 6a.

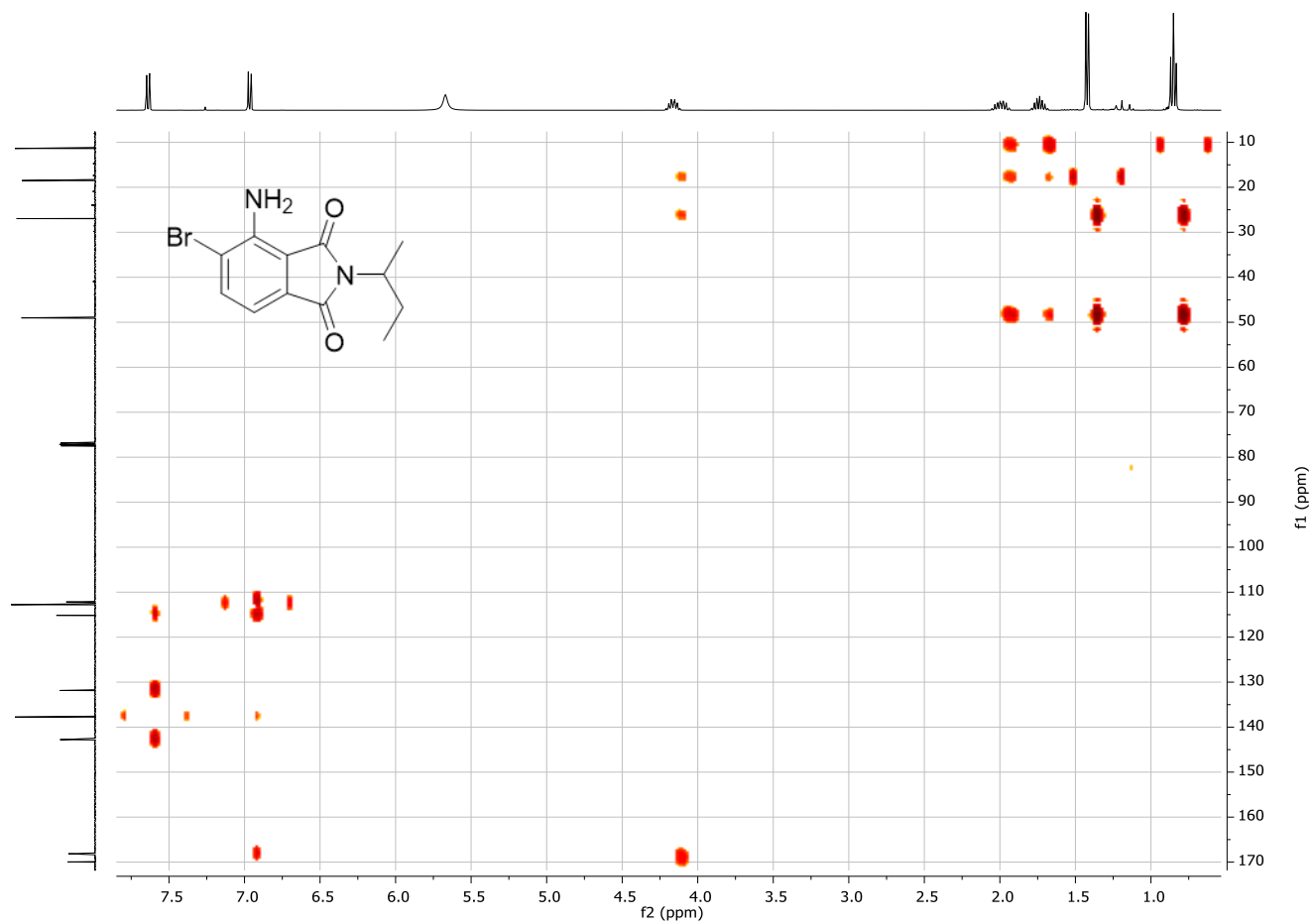


Figure S5. 2D (^1H , ^{13}C) HMBC NMR (CDCl_3) correlation of **6a**.

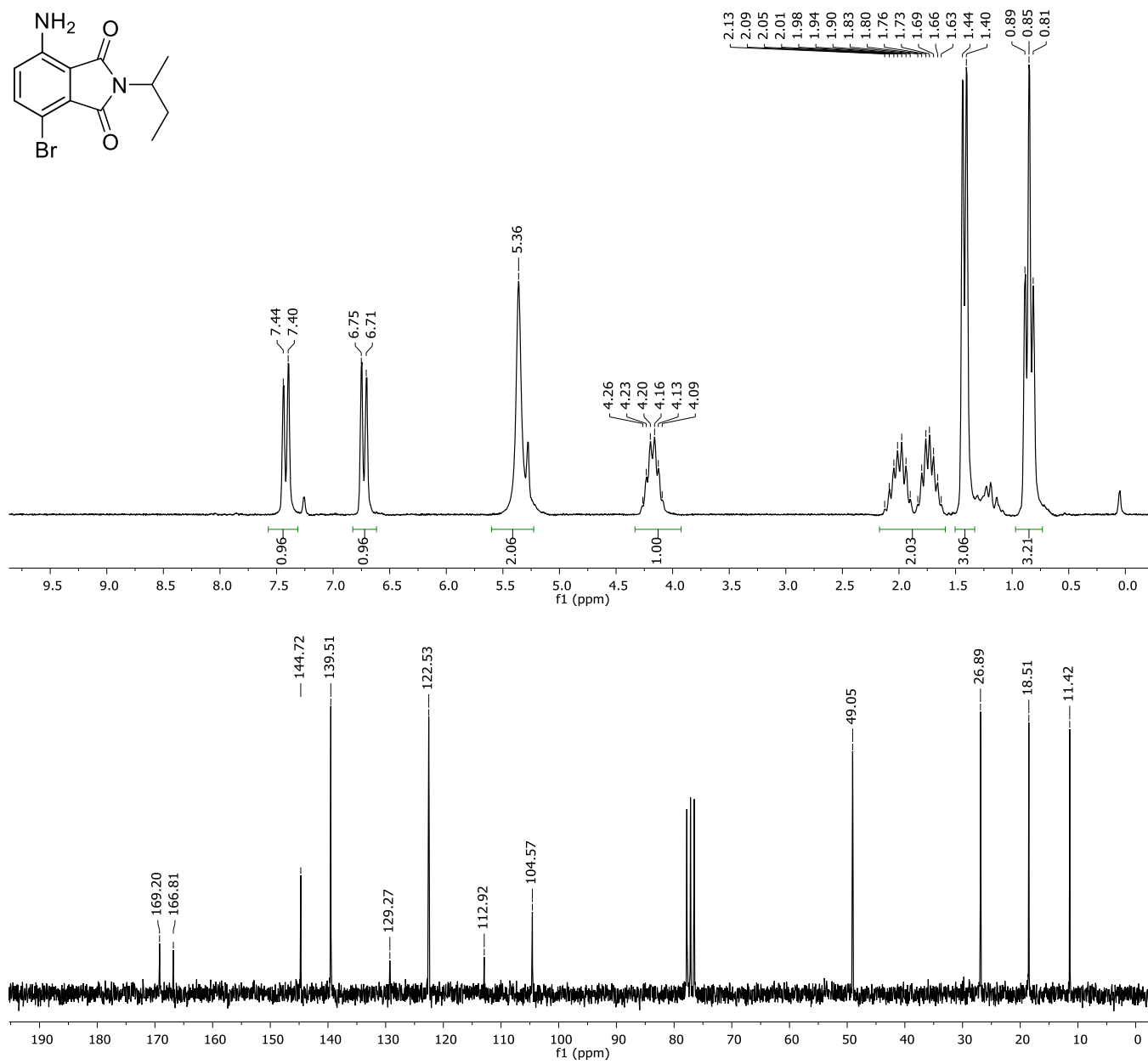
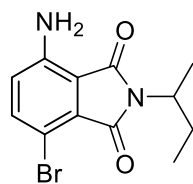


Figure S6. ¹H (200 MHz, up) and ¹³C (50 MHz, down) NMR (CDCl₃) spectra of **6b**.

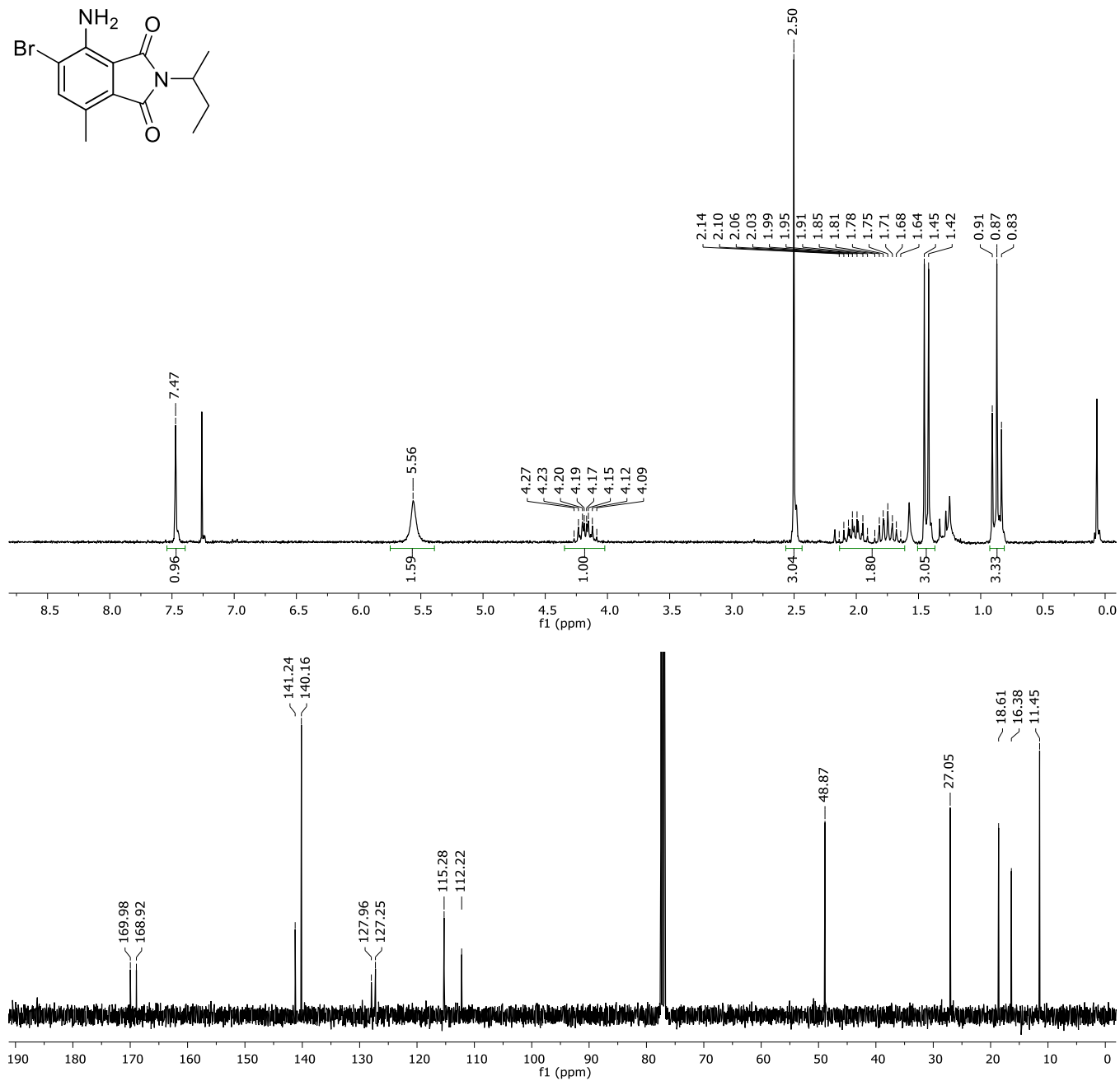
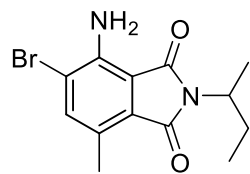


Figure S7. ¹H (200 MHz, up) and ¹³C (50 MHz, down) NMR (CDCl₃) spectra of 7a.

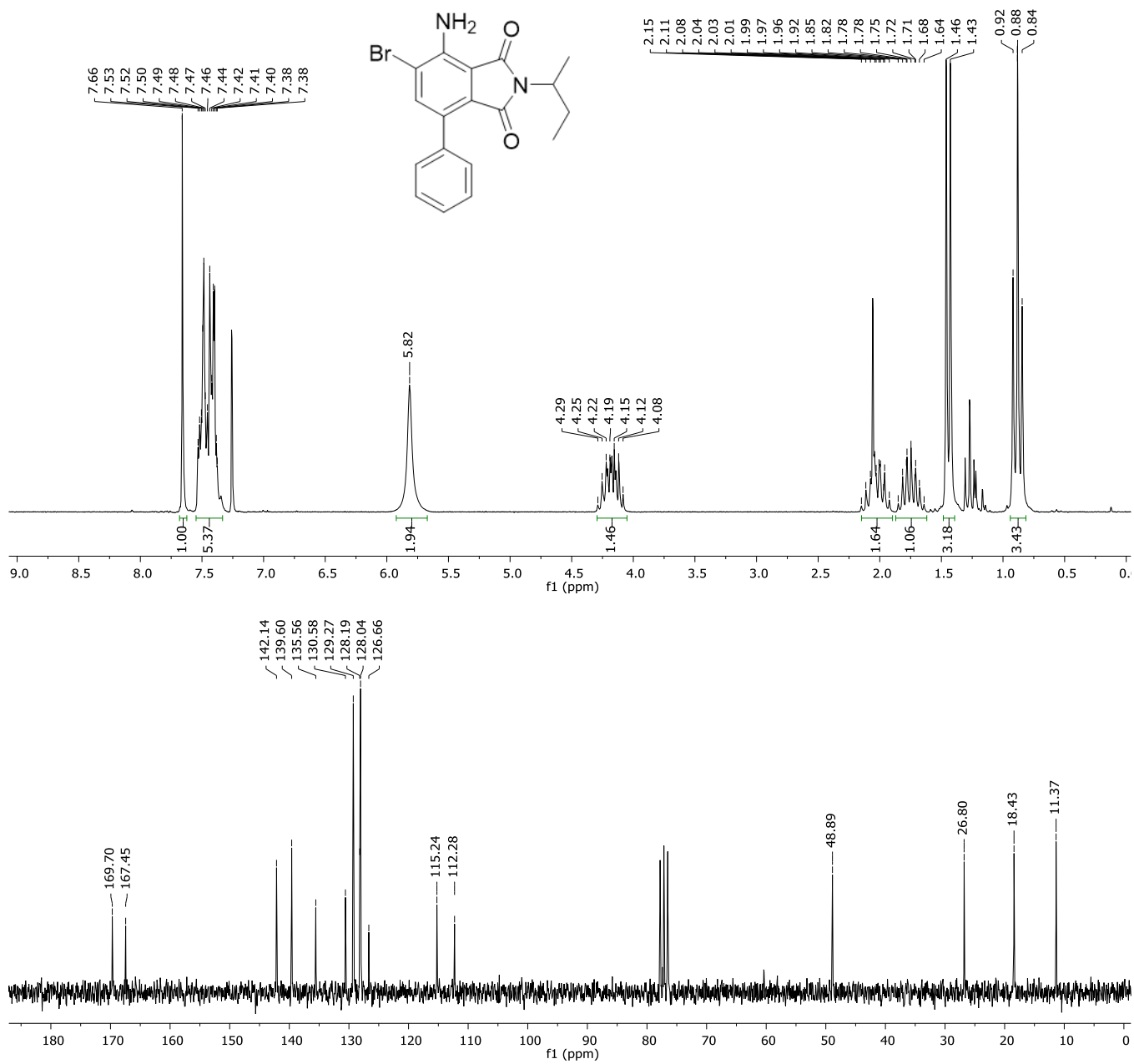


Figure S8. ¹H (200 MHz, up) and ¹³C (50 MHz, down) NMR (CDCl₃) spectra of **7b**.

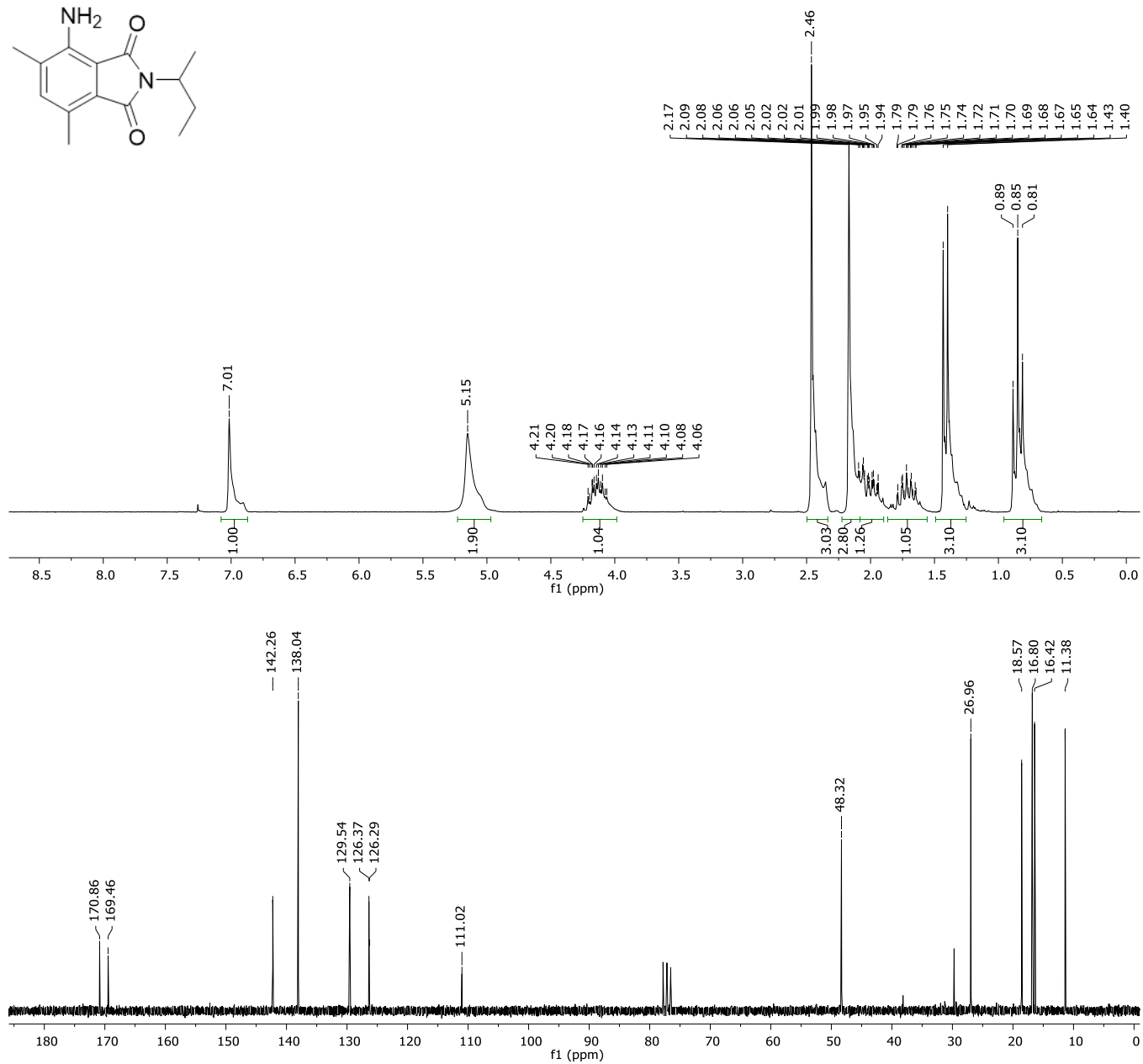
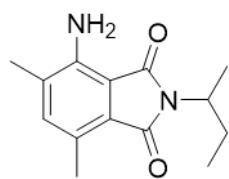


Figure S9. ¹H (200 MHz, up) and ¹³C (50 MHz, down) NMR (CDCl₃) spectra of **5a**.

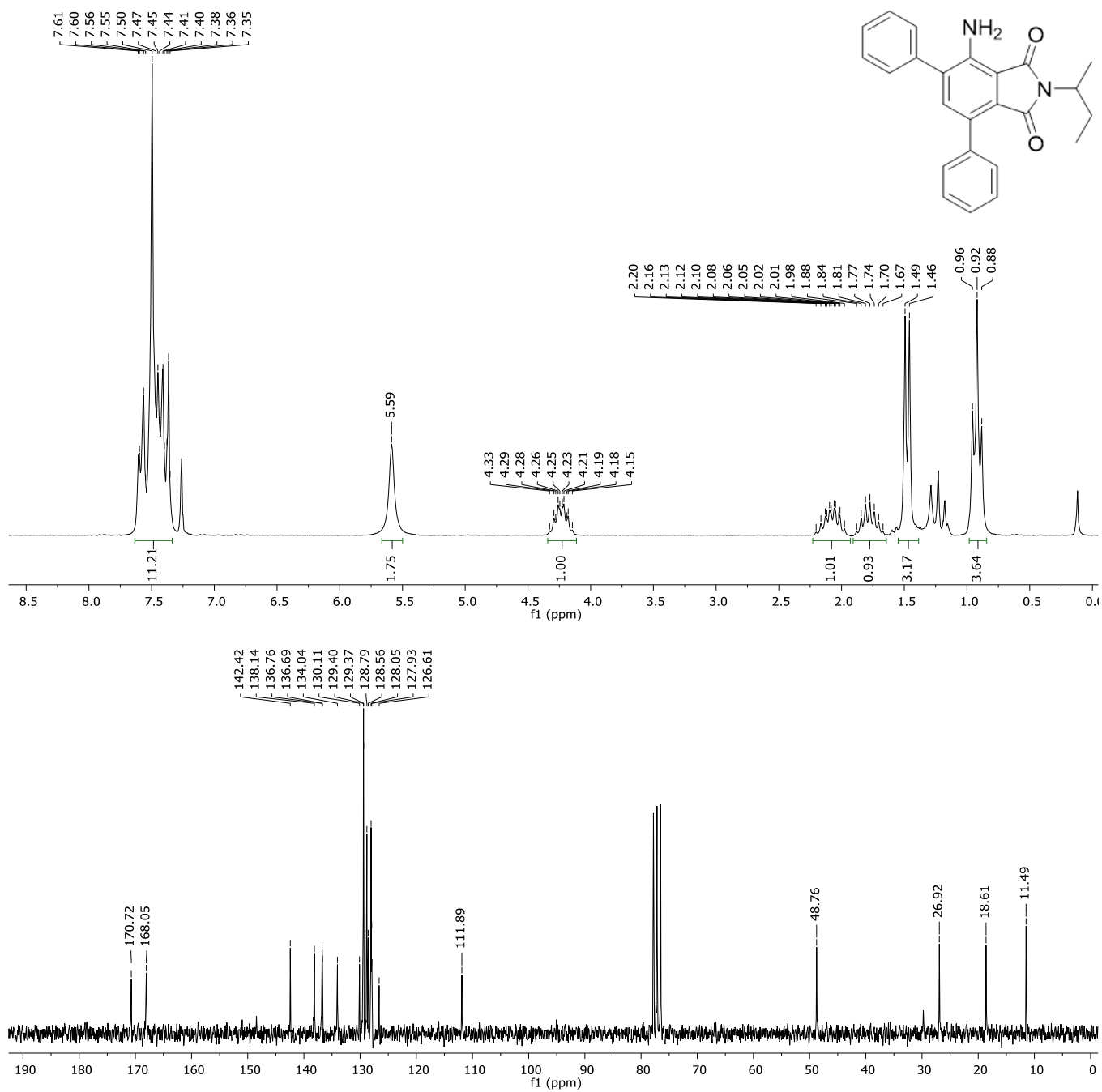


Figure S10. ¹H (200 MHz, up) and ¹³C (50 MHz, down) NMR (CDCl₃) spectra of **5b**.

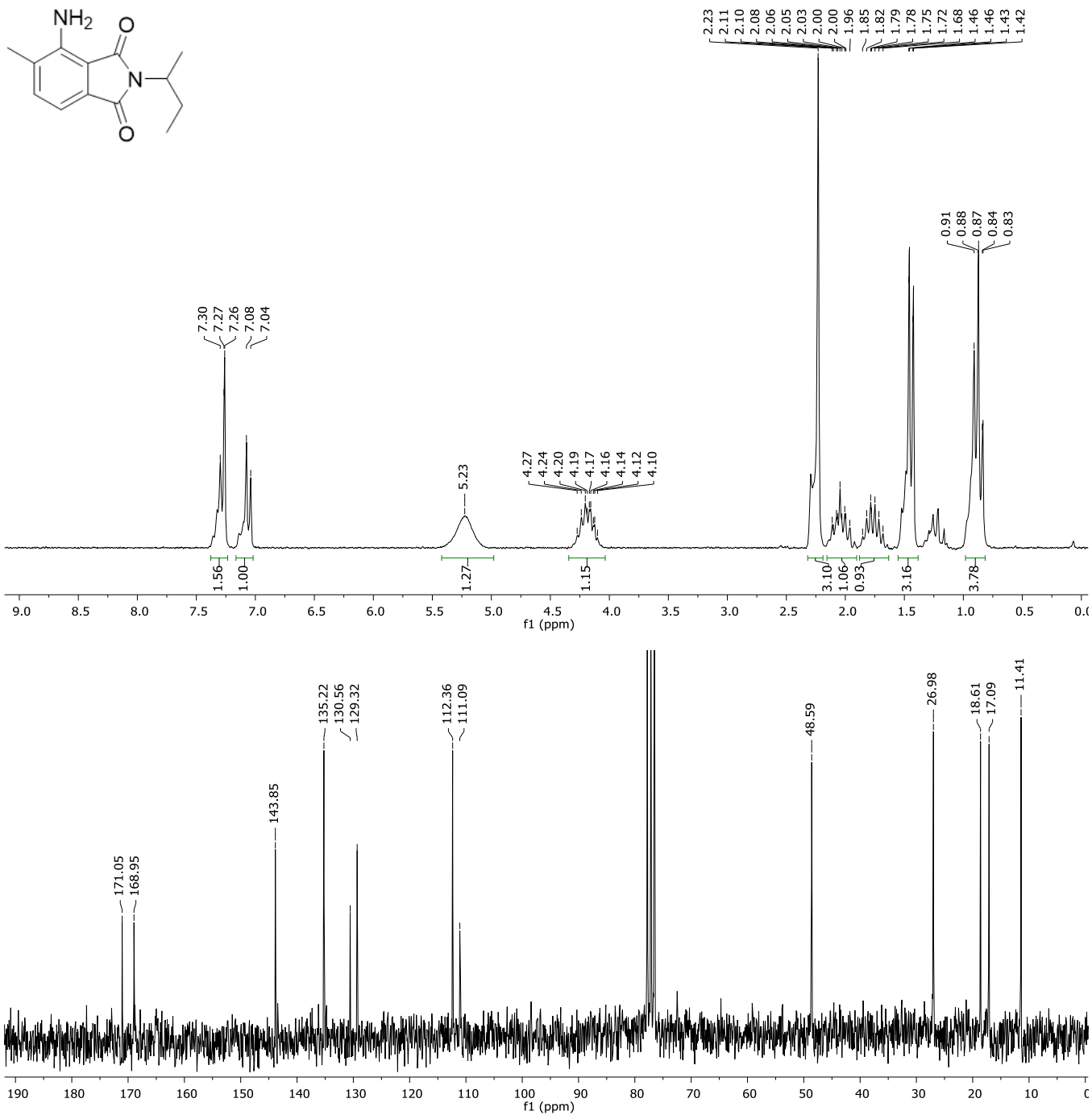


Figure S11. ¹H (200 MHz, up) and ¹³C (50 MHz, down) NMR (CDCl₃) spectra of 5c.

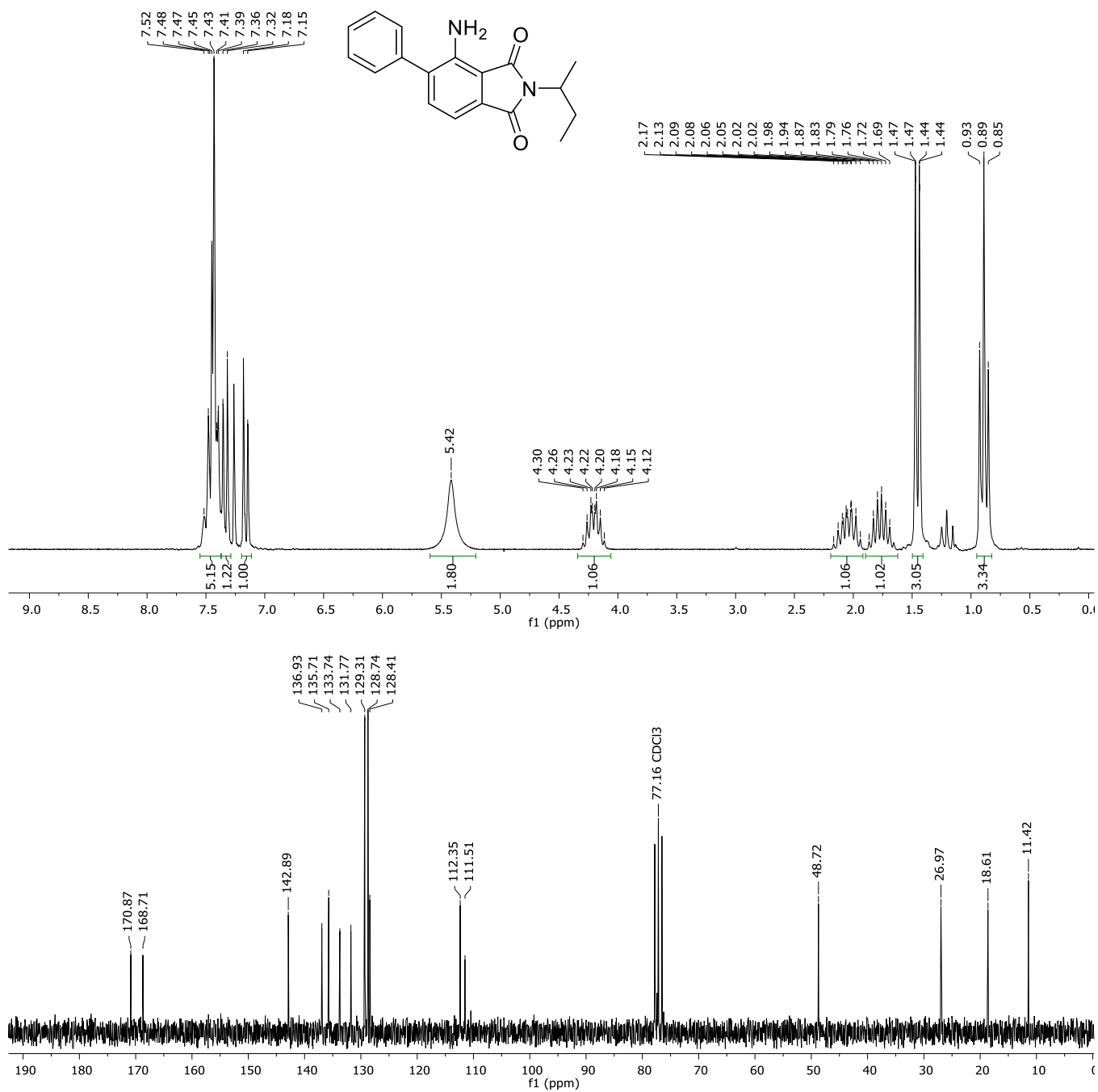


Figure S12. ¹H (200 MHz, up) and ¹³C (50 MHz, down) NMR (CDCl₃) spectra of 5d.

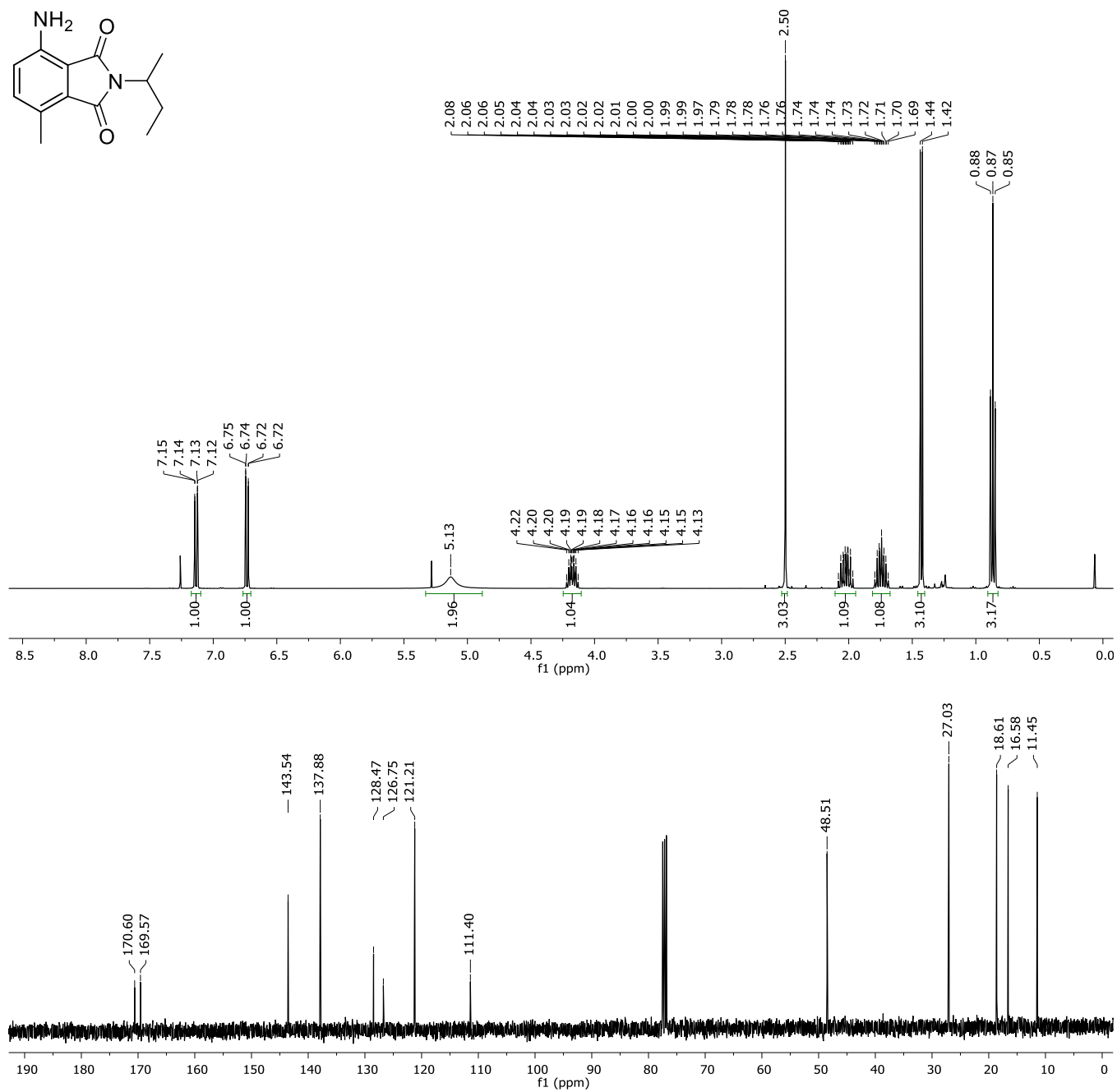
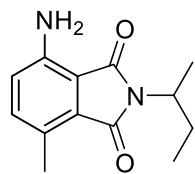


Figure S13. ¹H (400 MHz, up) and ¹³C (100 MHz, down) NMR (CDCl₃) spectra of **5e**.

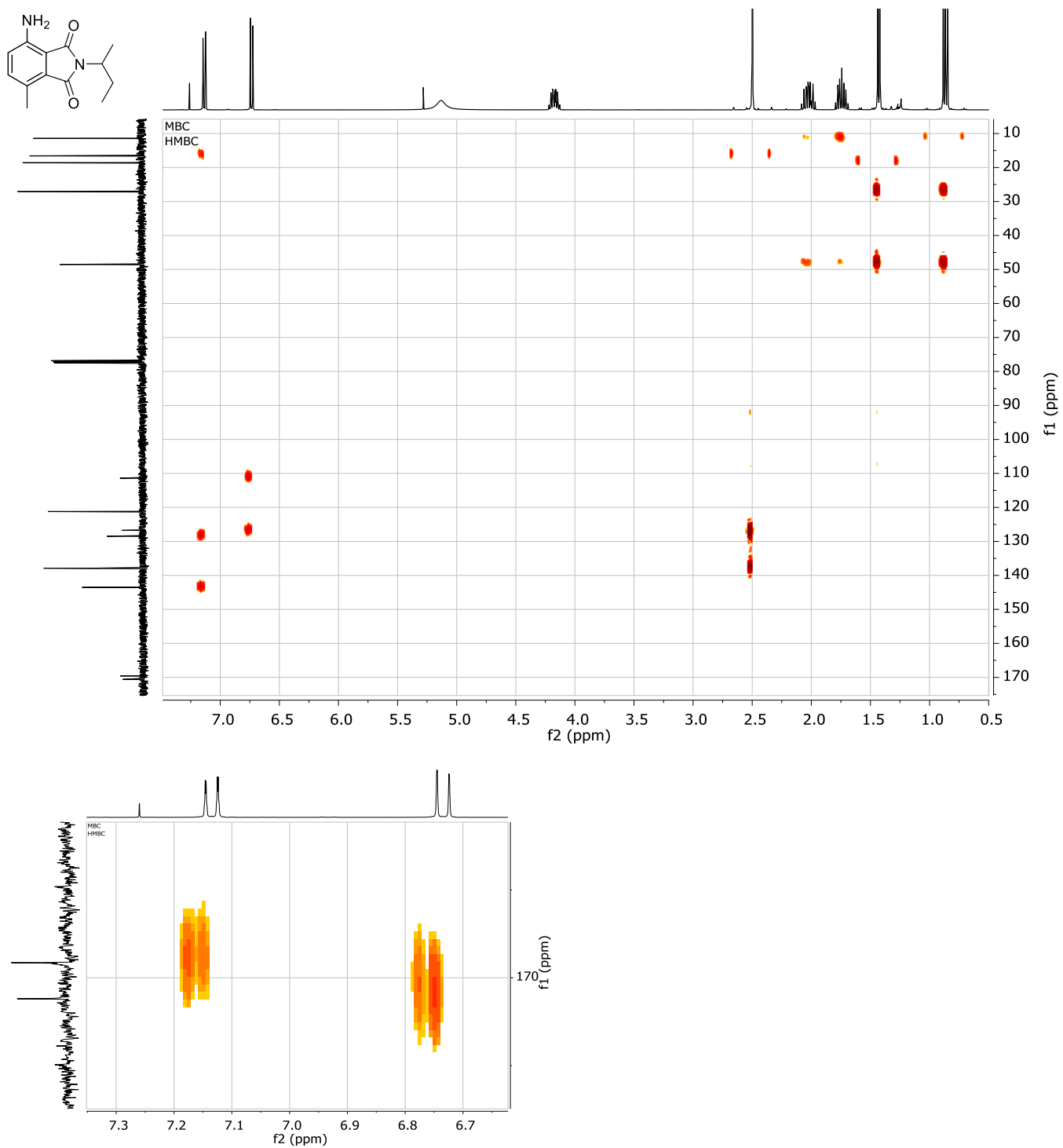


Figure S14. 2D (¹H, ¹³C)-HMBC NMR (CDCl₃) correlation of 5e. Down: magnification.

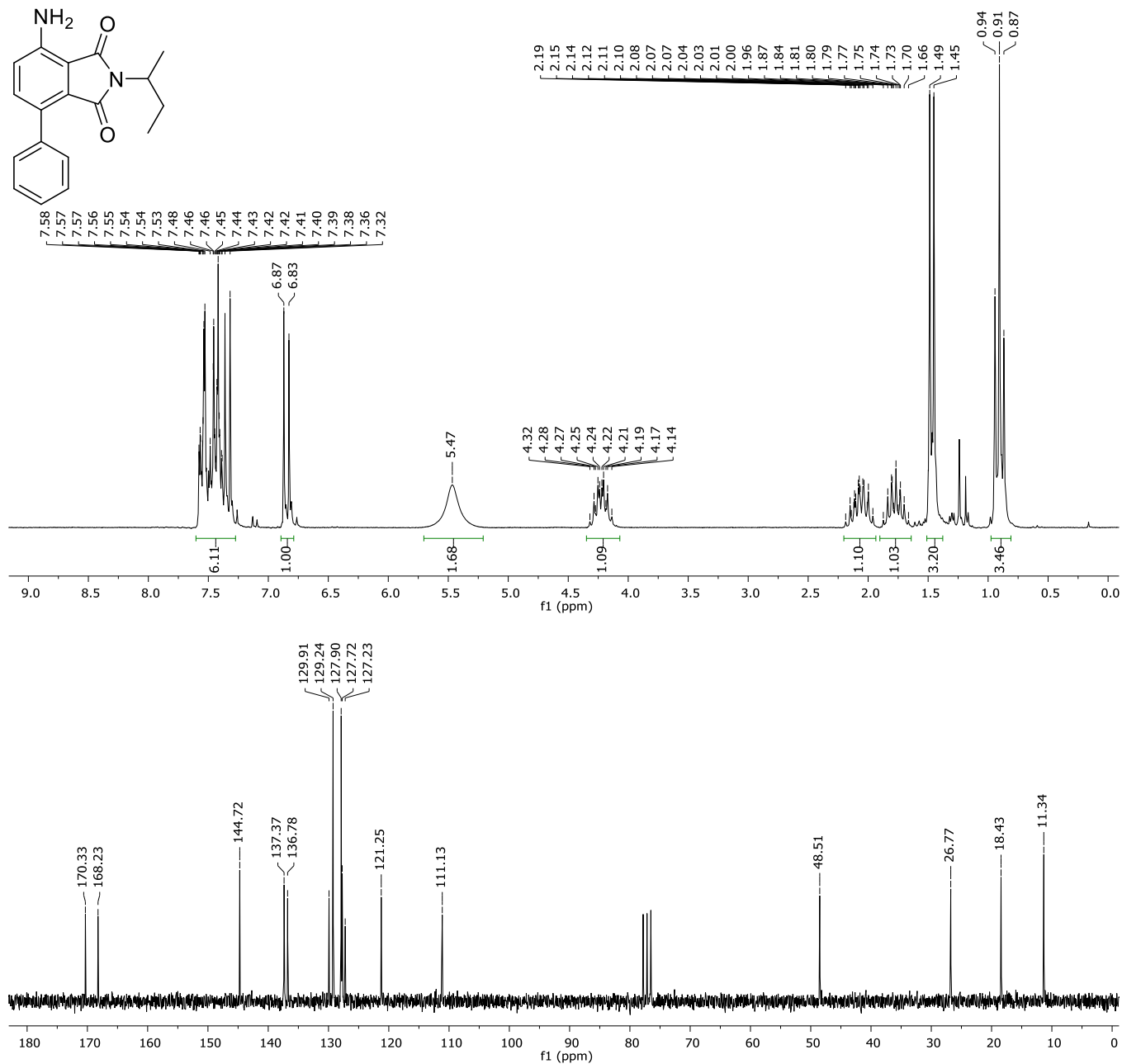


Figure S15. ¹H (200 MHz, up) and ¹³C (50 MHz, down) NMR (CDCl₃) spectra of **5f**.

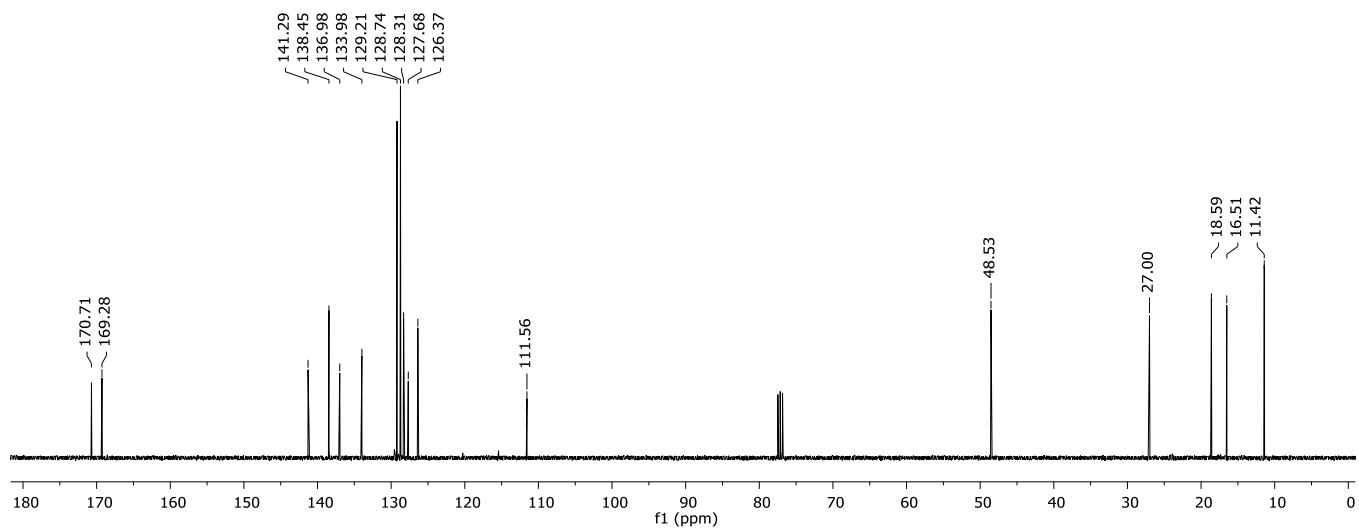
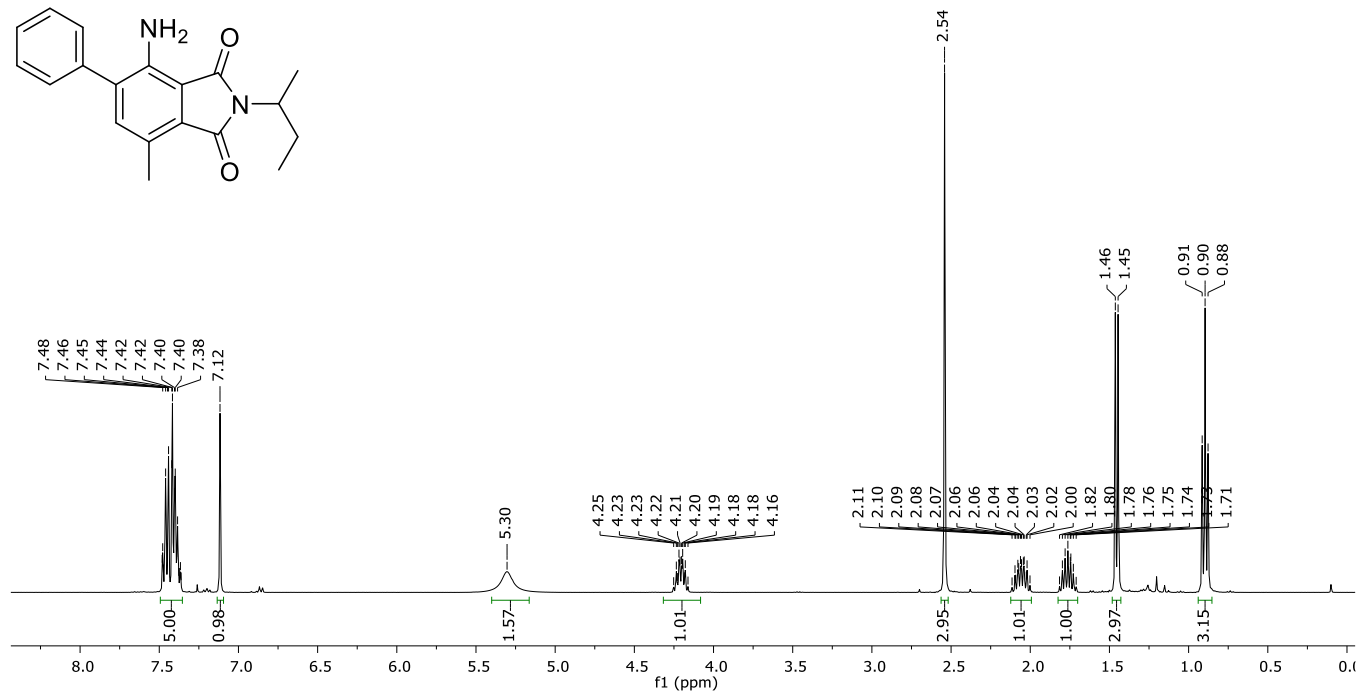
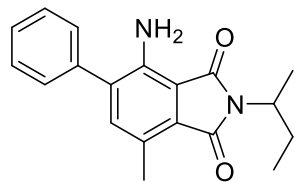


Figure S16. ¹H (400 MHz, up) and ¹³C (100 MHz, down) NMR (CDCl₃) spectra of **5g**.

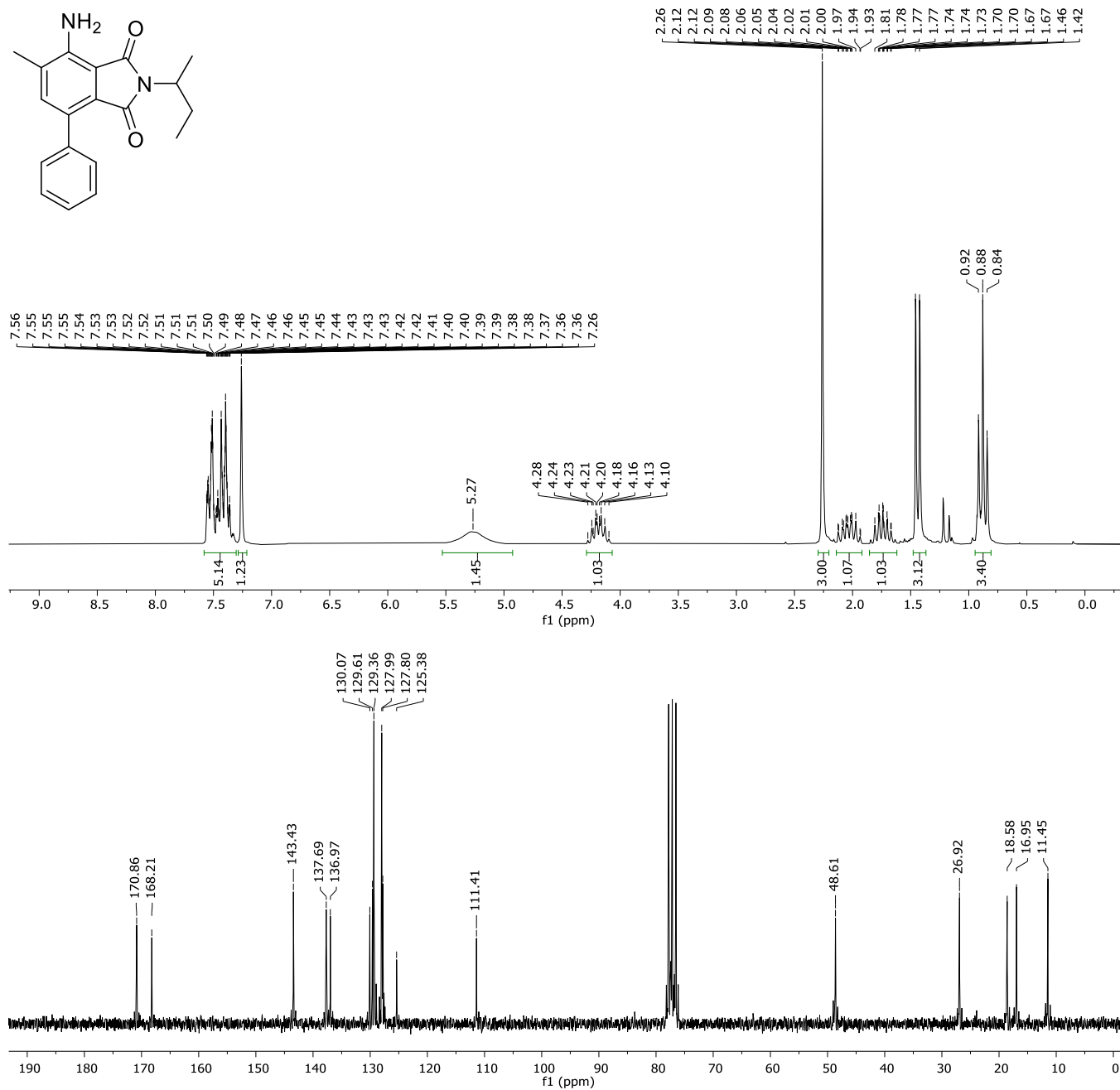


Figure S17. ¹H (200 MHz, up) and ¹³C (50 MHz, down) NMR (CDCl₃) spectra of 5h.

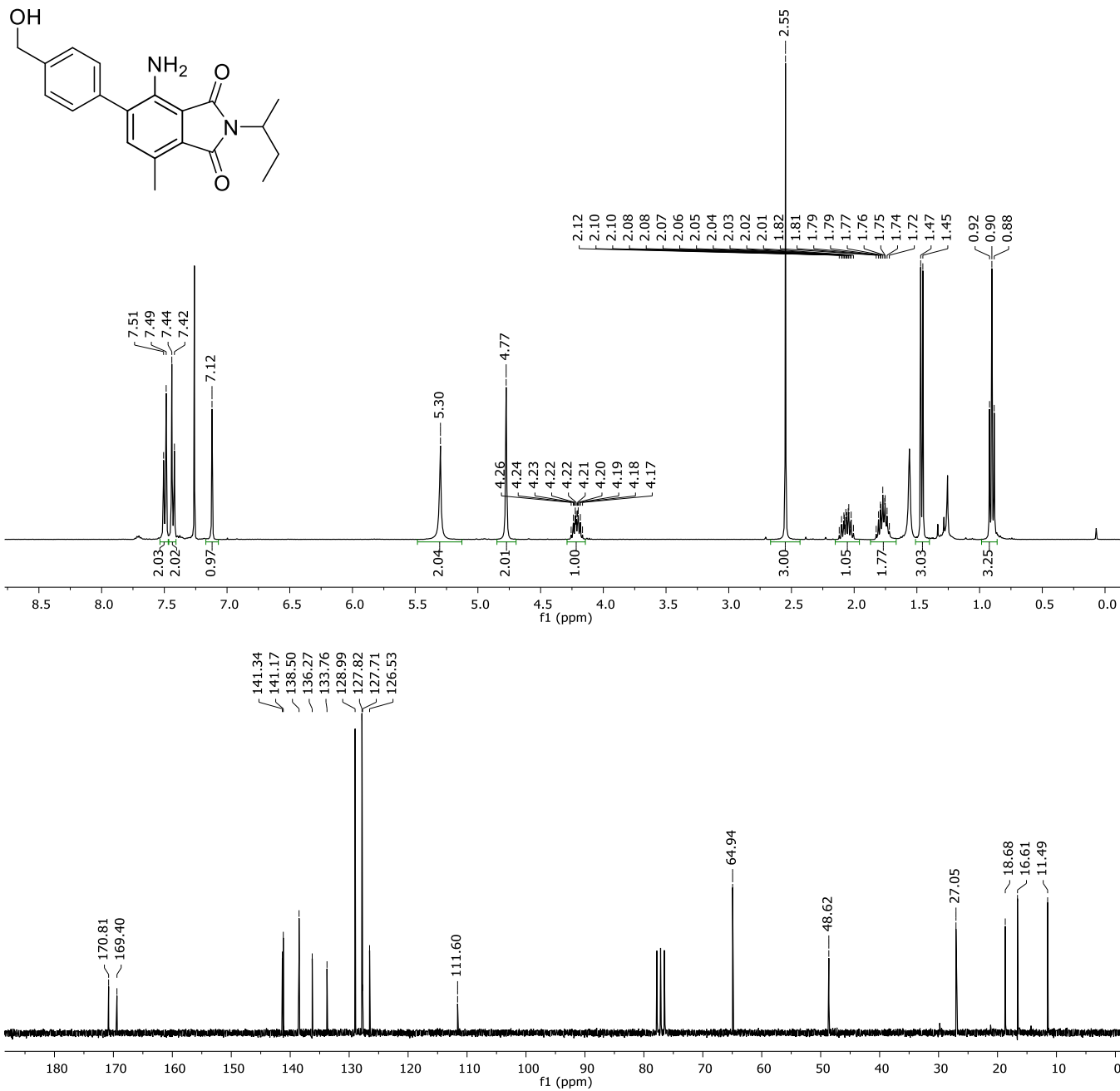


Figure S18. ¹H (400 MHz, up) and ¹³C (100 MHz, down) NMR (CDCl₃) spectra of **5i**.

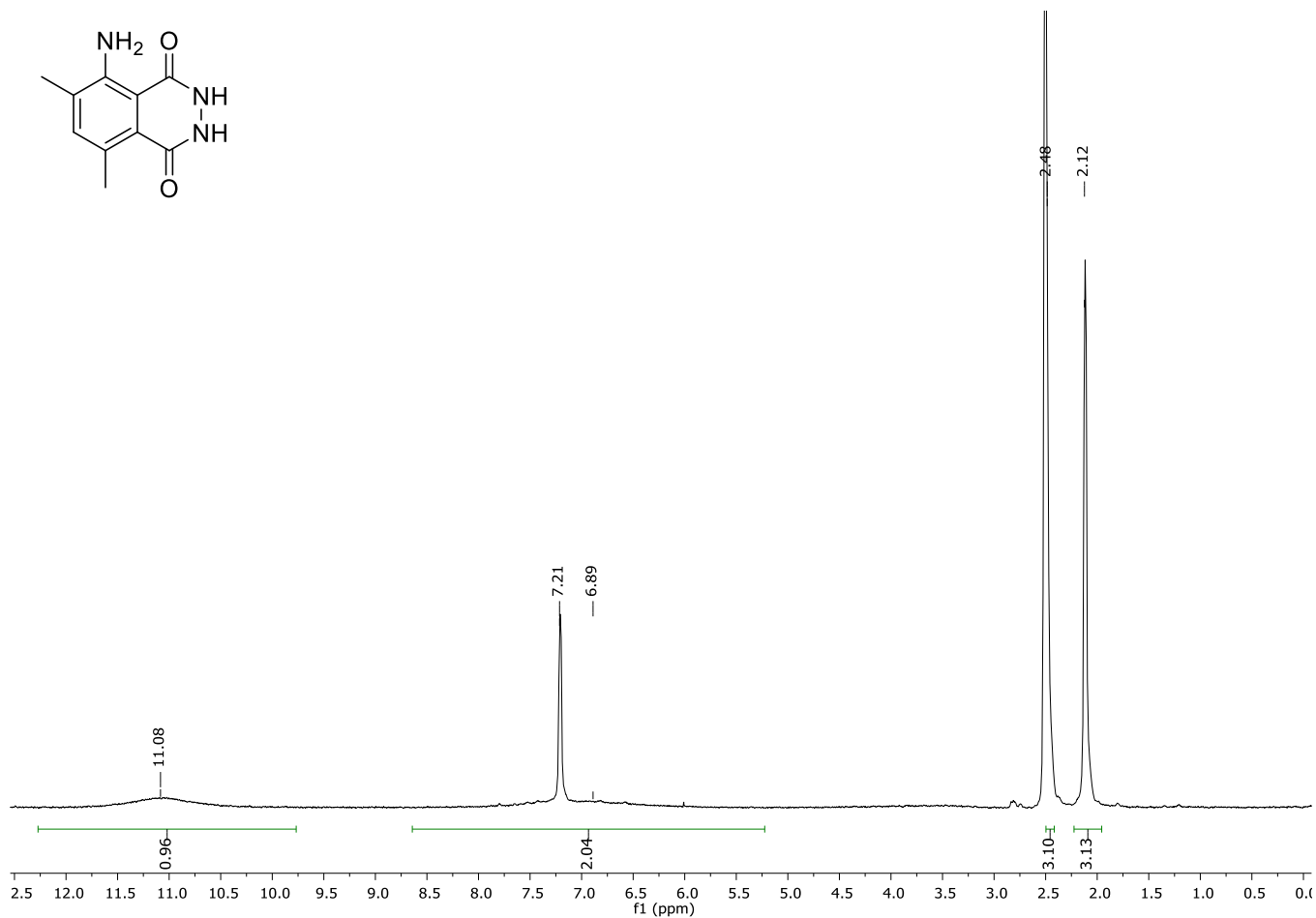
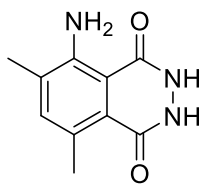


Figure S19. ¹H NMR (200 MHz, DMSO-d₆) spectrum of 8a

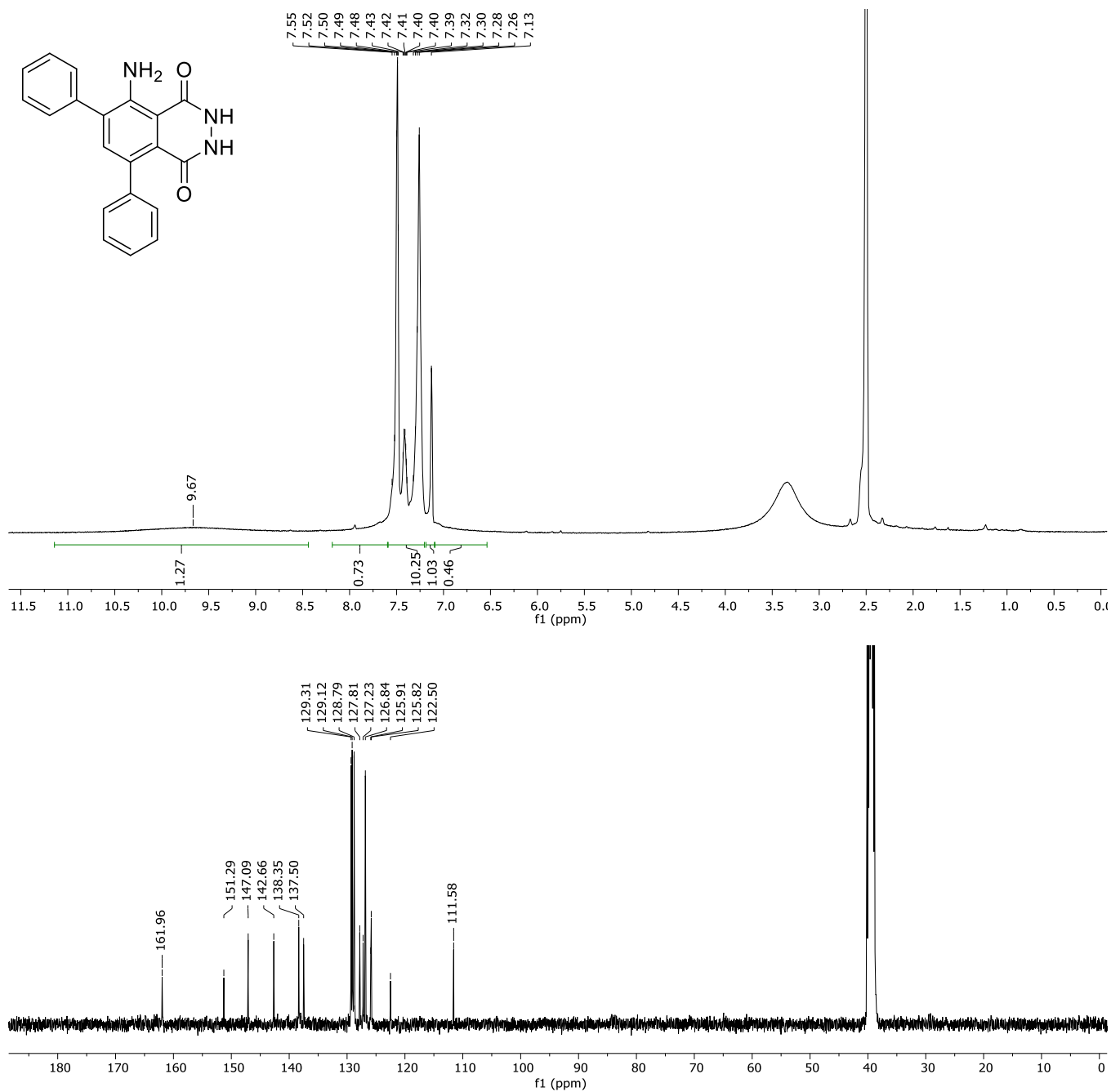


Figure S20. ¹H (400 MHz, up) and ¹³C (100 MHz, down) NMR (DMSO-d₆) spectra of **8b**.

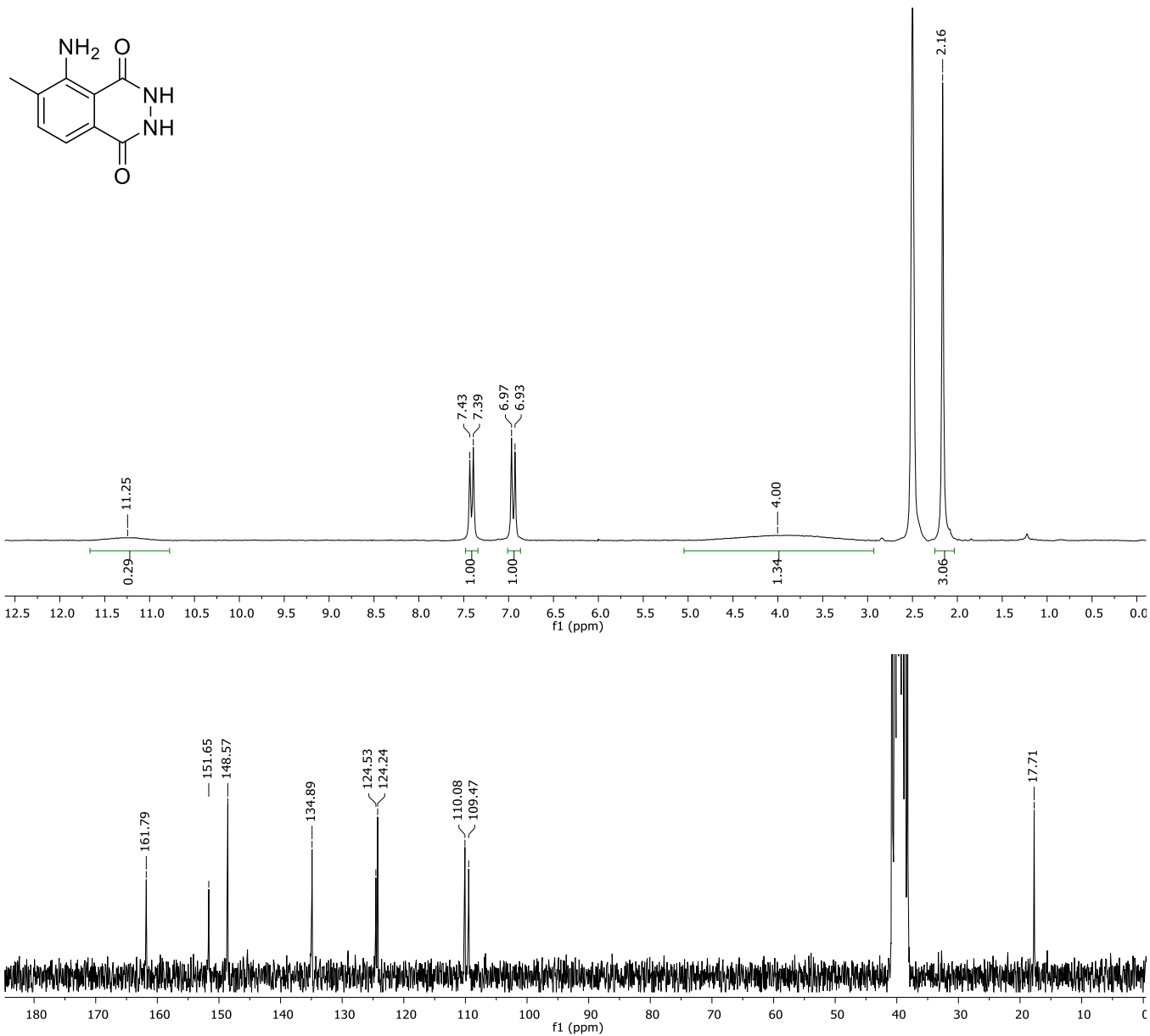


Figure S21. ^1H (200 MHz, up) and ^{13}C (50 MHz, down) NMR (DMSO-d_6) spectra of **8c**.

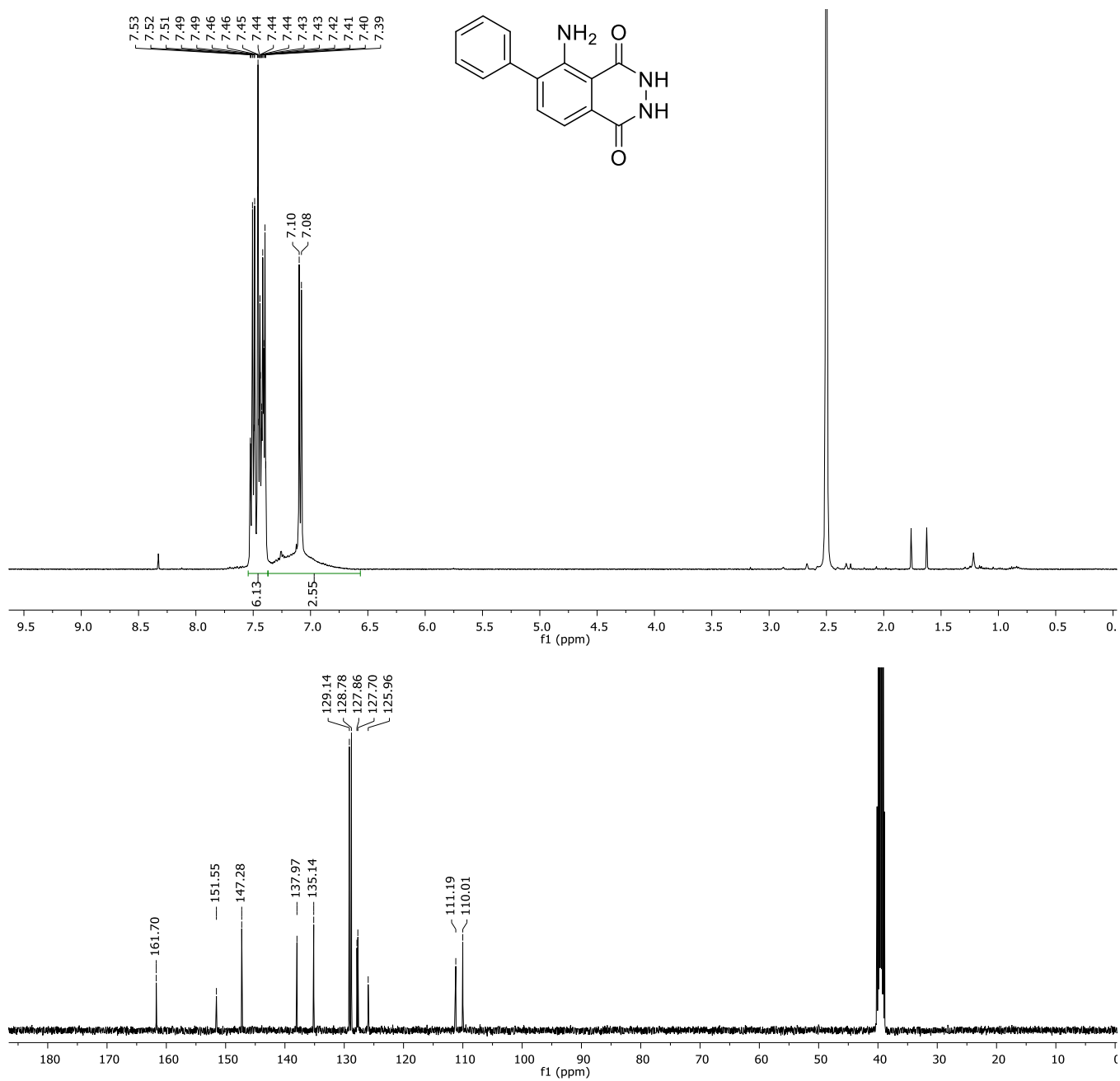


Figure S22. ¹H (400 MHz, up) and ¹³C (100 MHz, down) NMR (DMSO-d₆) spectra of 8d.

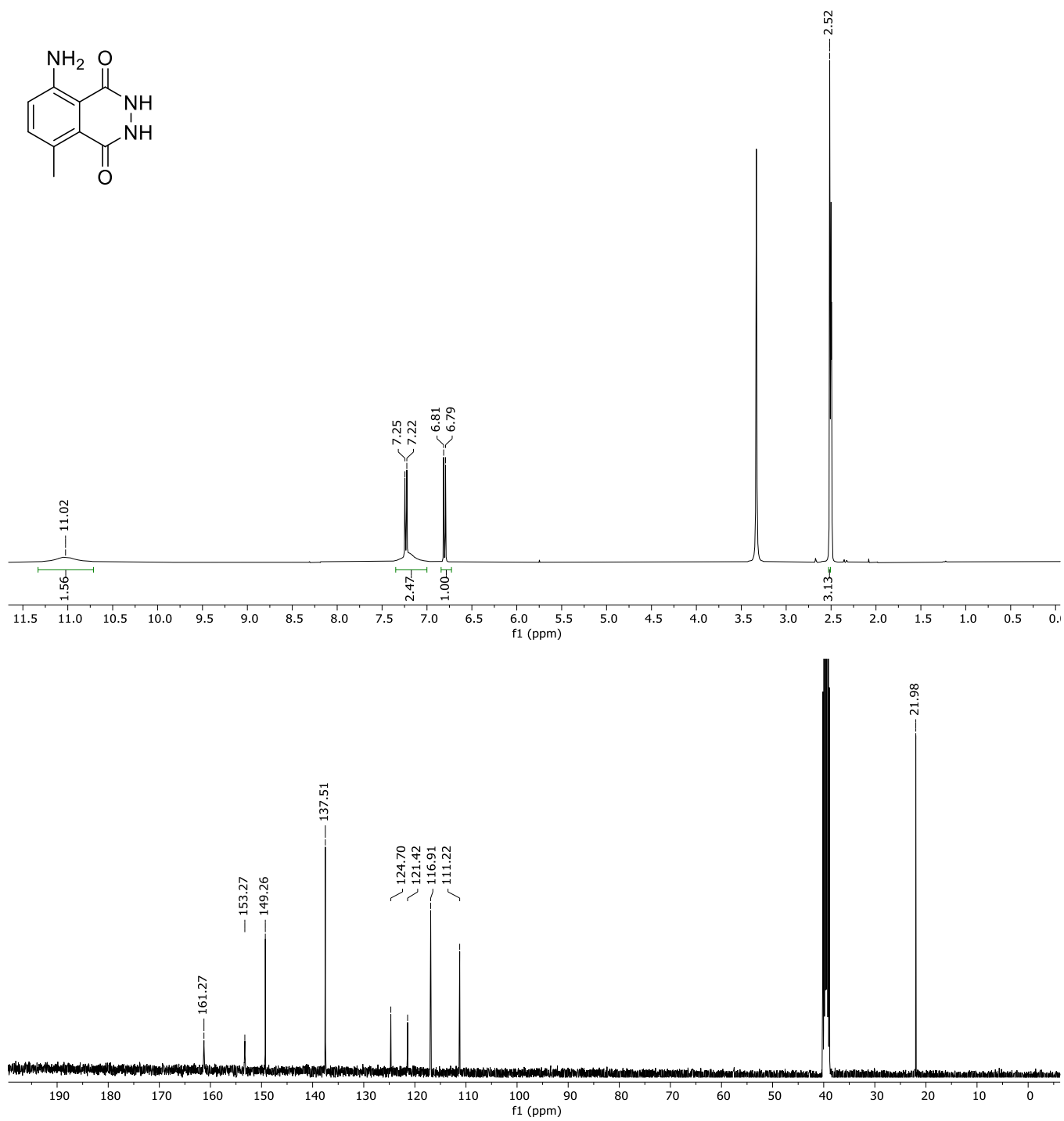


Figure S23. ¹H (400 MHz, up) and ¹³C (100 MHz, down) NMR (DMSO-d₆) spectra of **8e**.

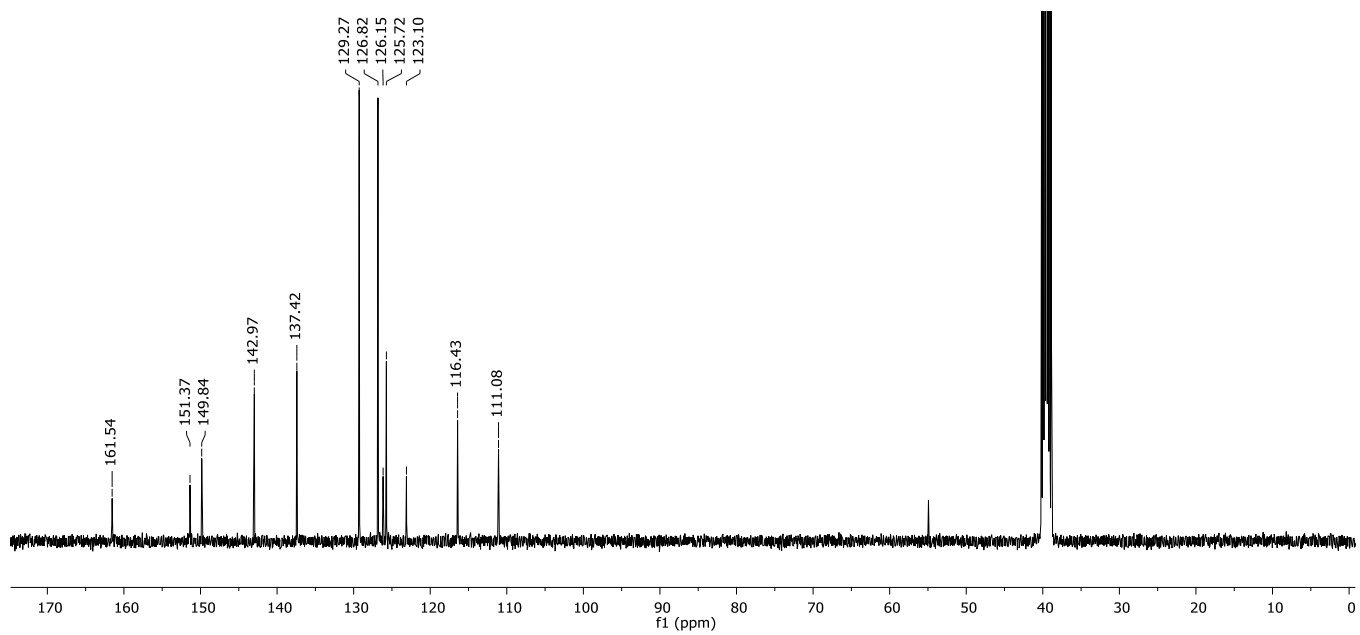
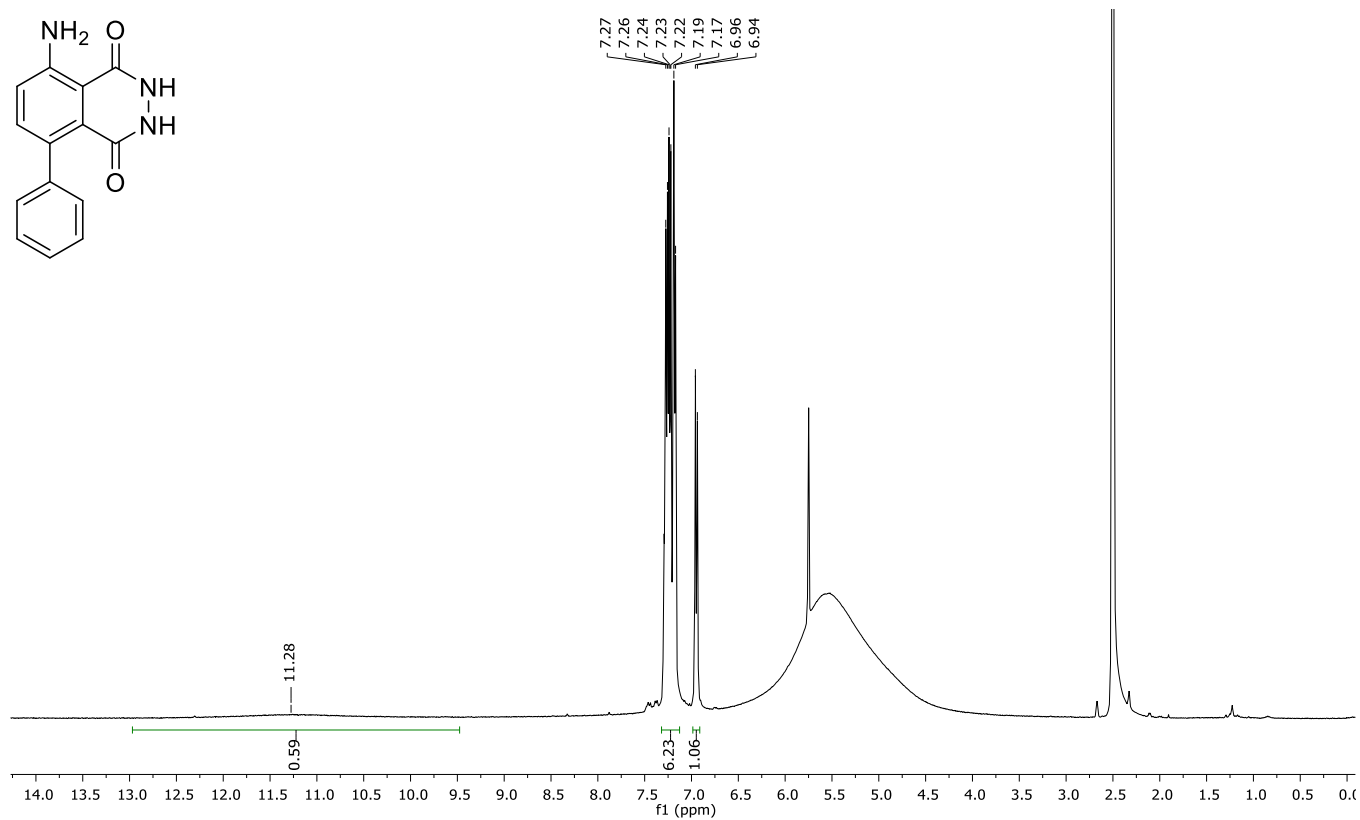
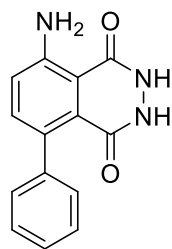


Figure S24. ^1H (400 MHz, up) and ^{13}C (100 MHz, down) NMR (DMSO-d_6) spectra of **8f**.

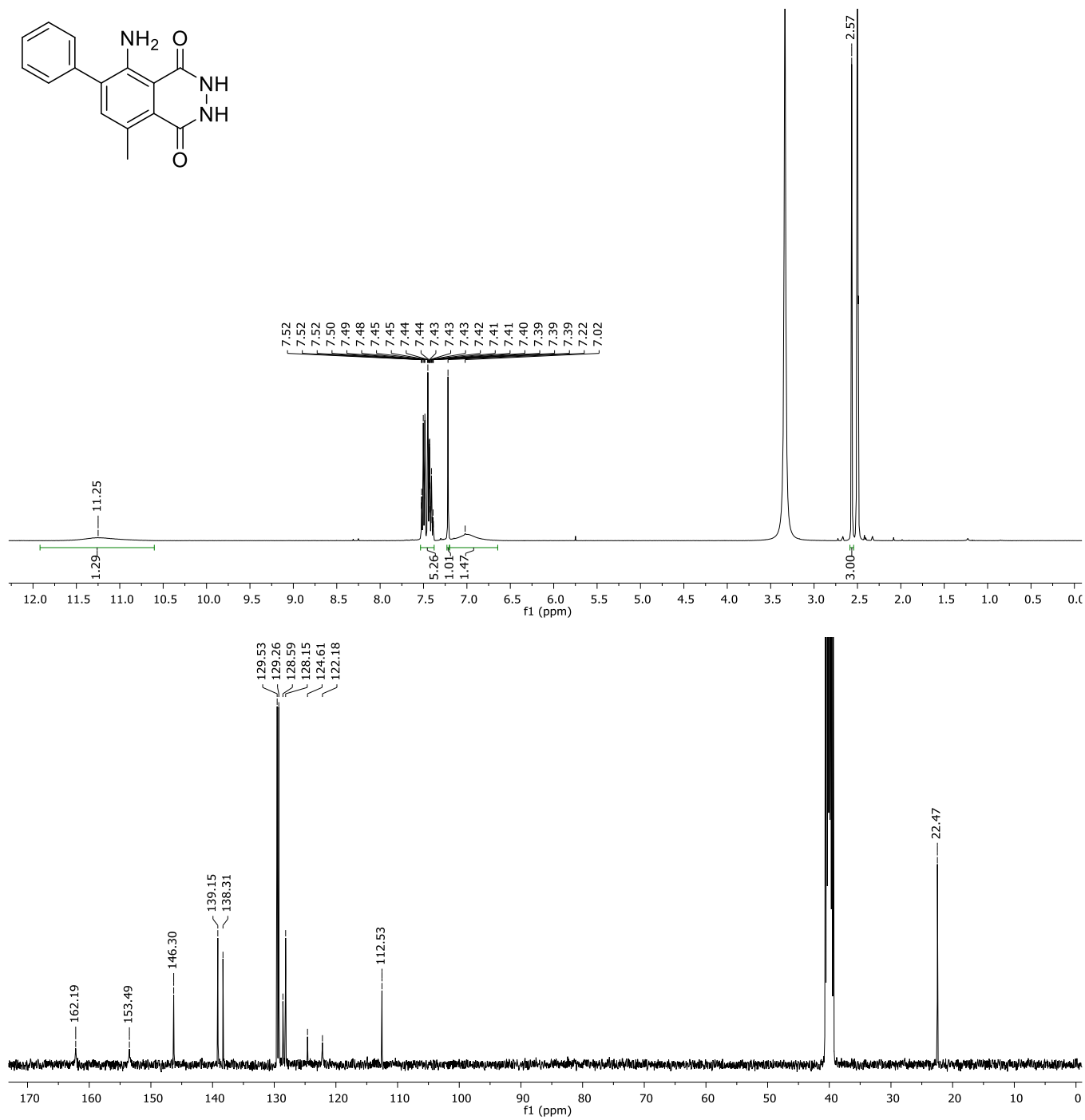


Figure S25. ¹H (400 MHz, up) and ¹³C (101 MHz, down) NMR (DMSO-d₆) spectra of **8g**.

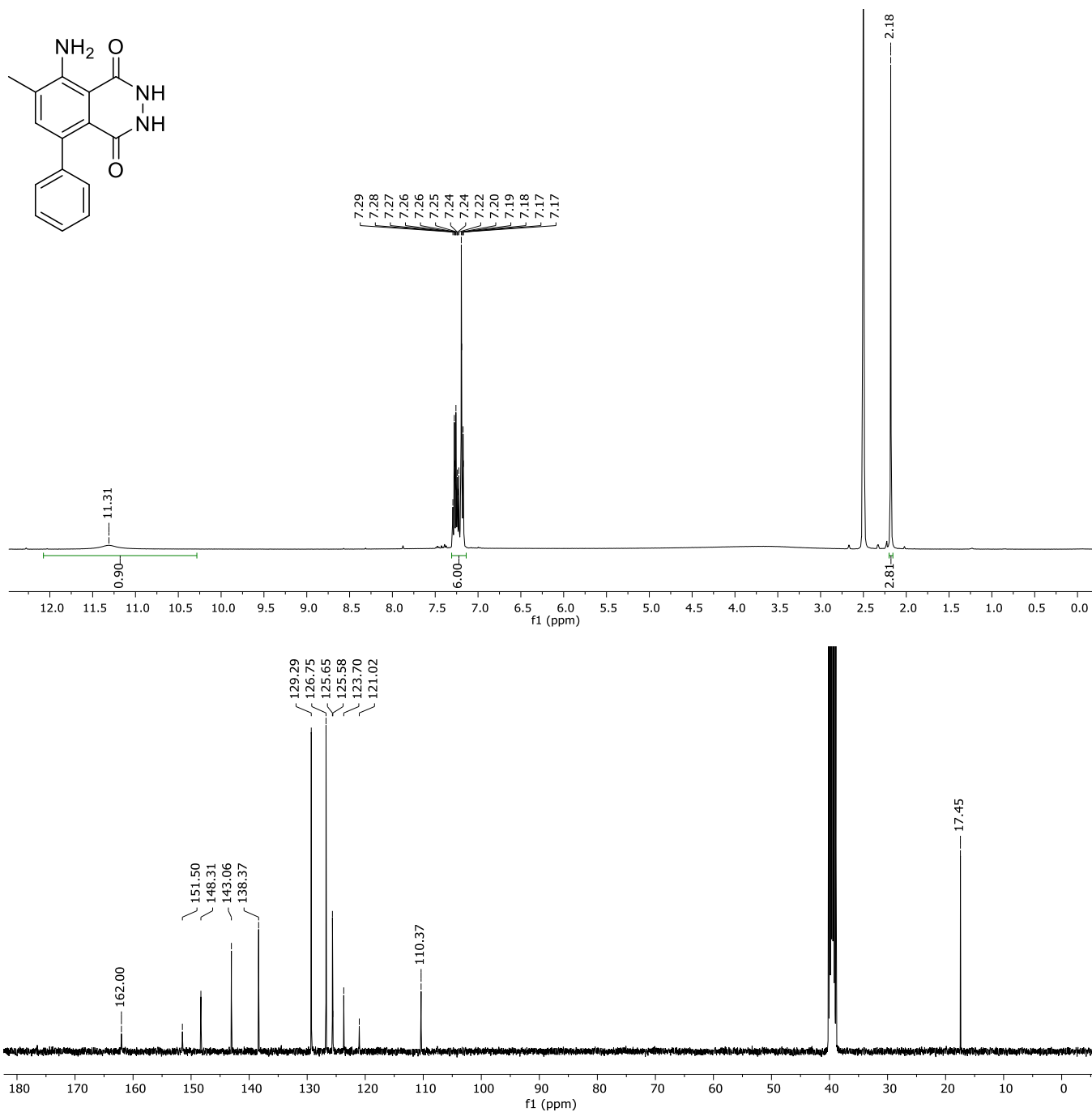


Figure S26. ¹H (400 MHz, up) and ¹³C (101 MHz, down) NMR (DMSO-d₆) spectra of 8h.

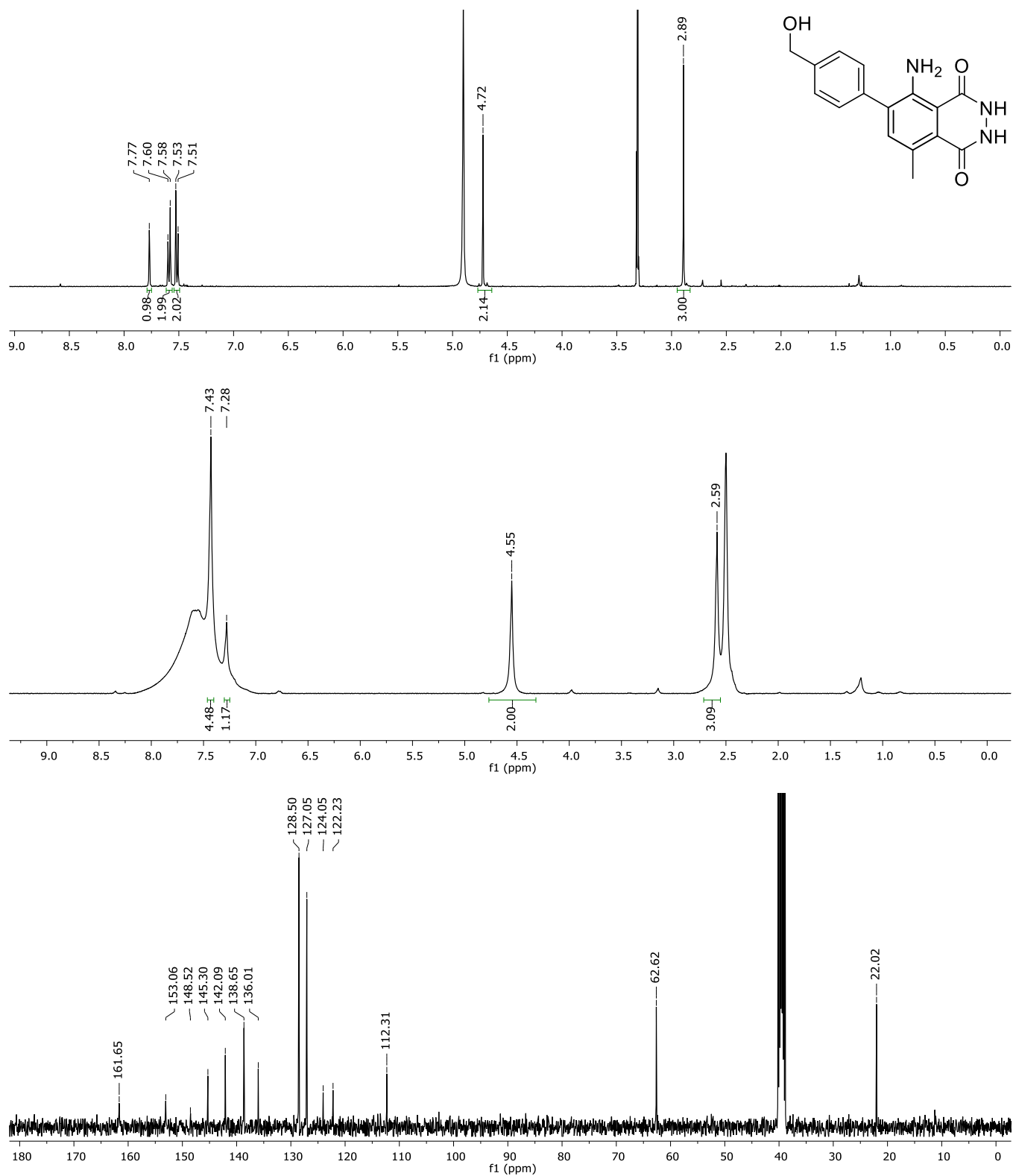


Figure S27. ^1H (400 MHz, $\text{MeOD-}d_4$, top), ^1H (400 MHz, $\text{DMSO-}d_6$, middle), and ^{13}C (100 MHz, $\text{DMSO-}d_6$, bottom) NMR spectra of **8i**.

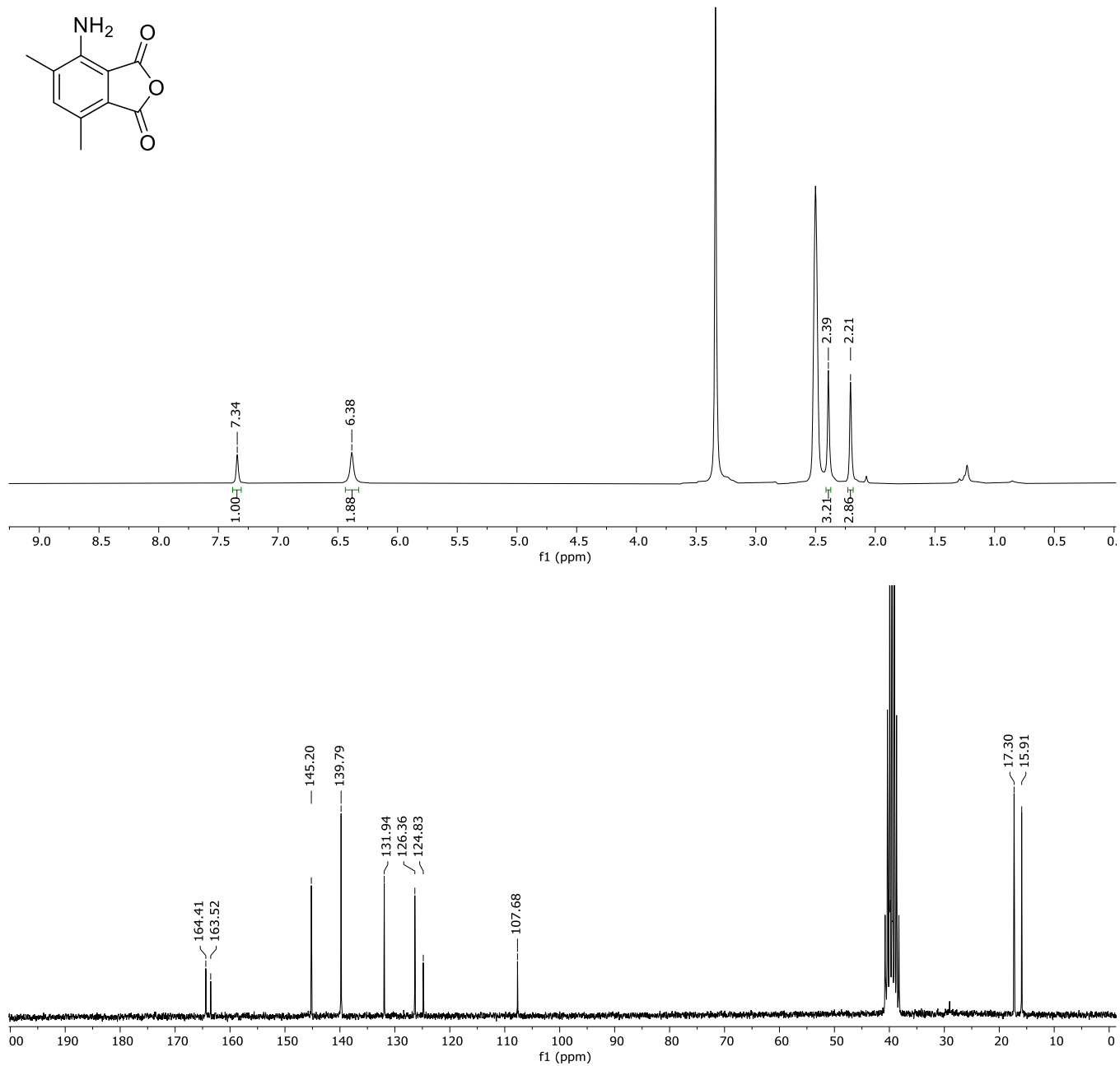


Figure S28. ¹H (200 MHz, up) and ¹³C (50 MHz, down) NMR (DMSO-d₆) spectra of **9a**.

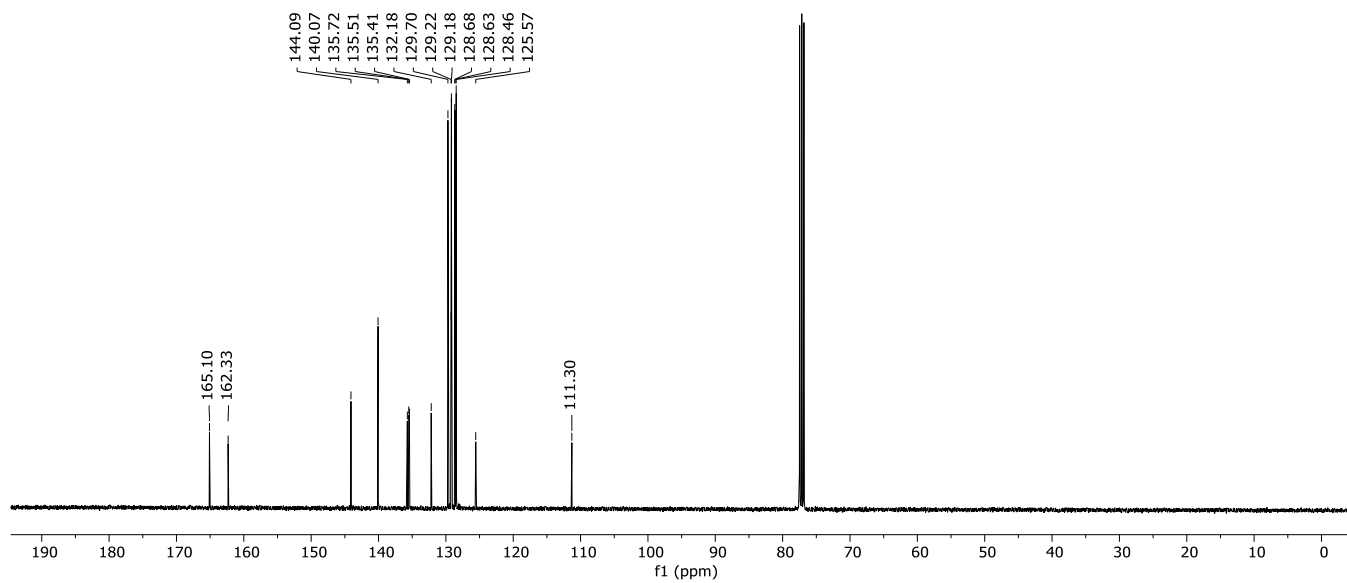
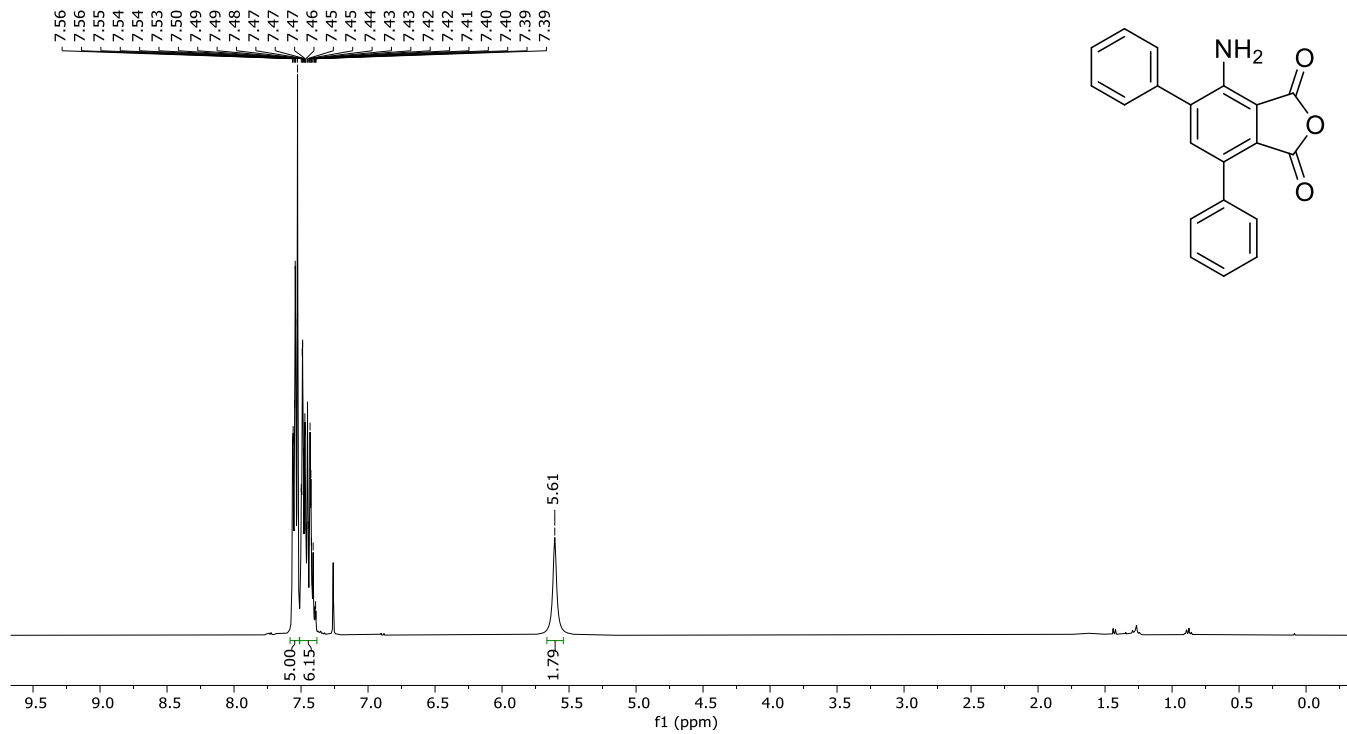


Figure S29. ¹H (400 MHz, up) and ¹³C (101 MHz, down) NMR (CDCl₃) spectra of 9b.

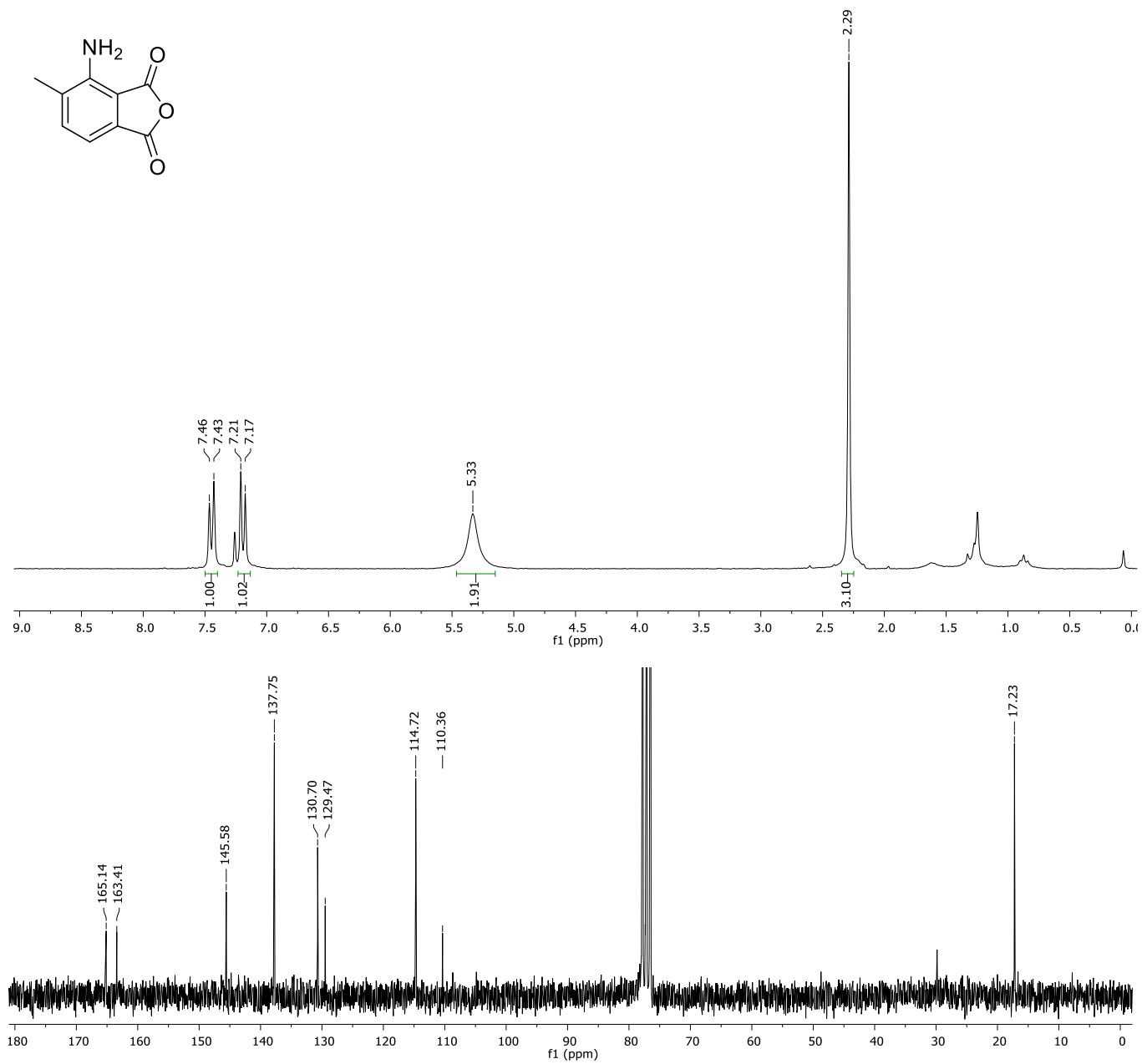


Figure S30. ¹H (200 MHz, up) and ¹³C (50 MHz, down) NMR (CDCl₃) spectra of 9c.

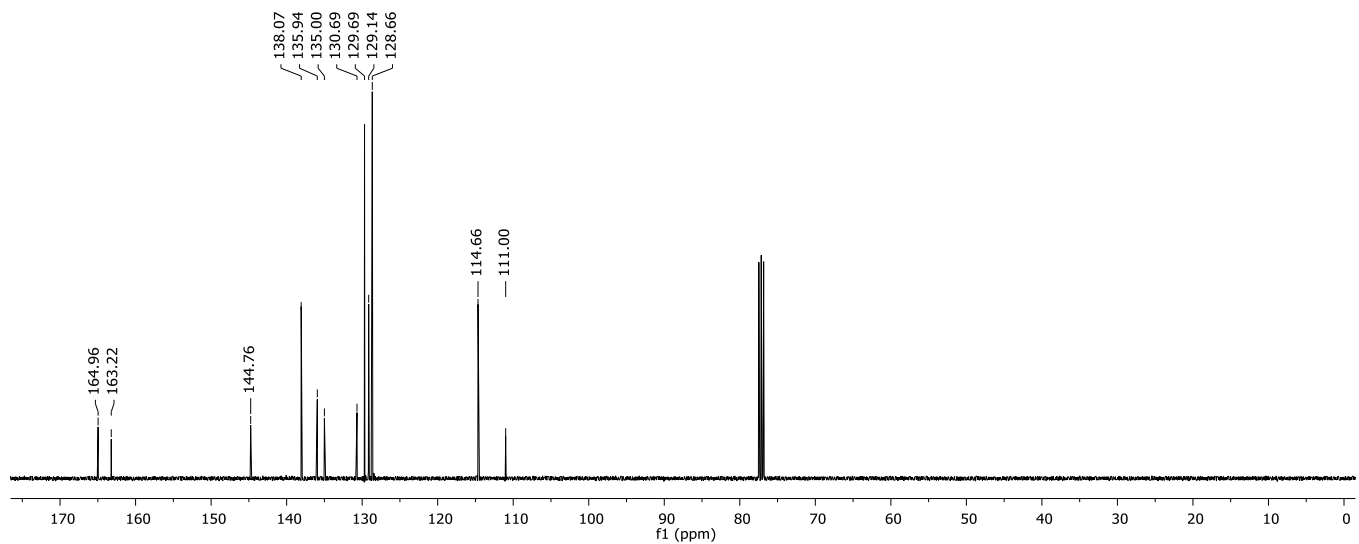
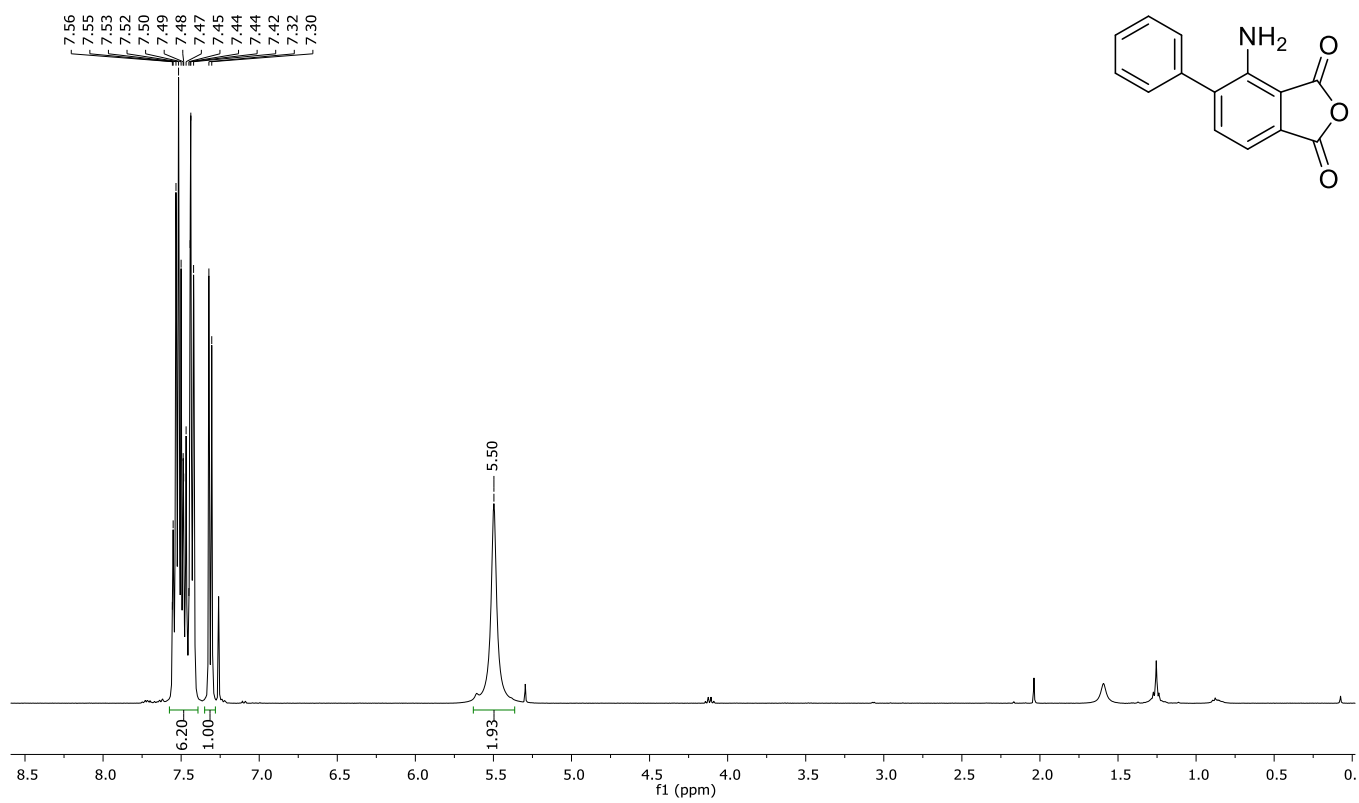


Figure S31. ¹H (400 MHz, up) and ¹³C (101 MHz, down) NMR (CDCl₃) spectra of 9d.

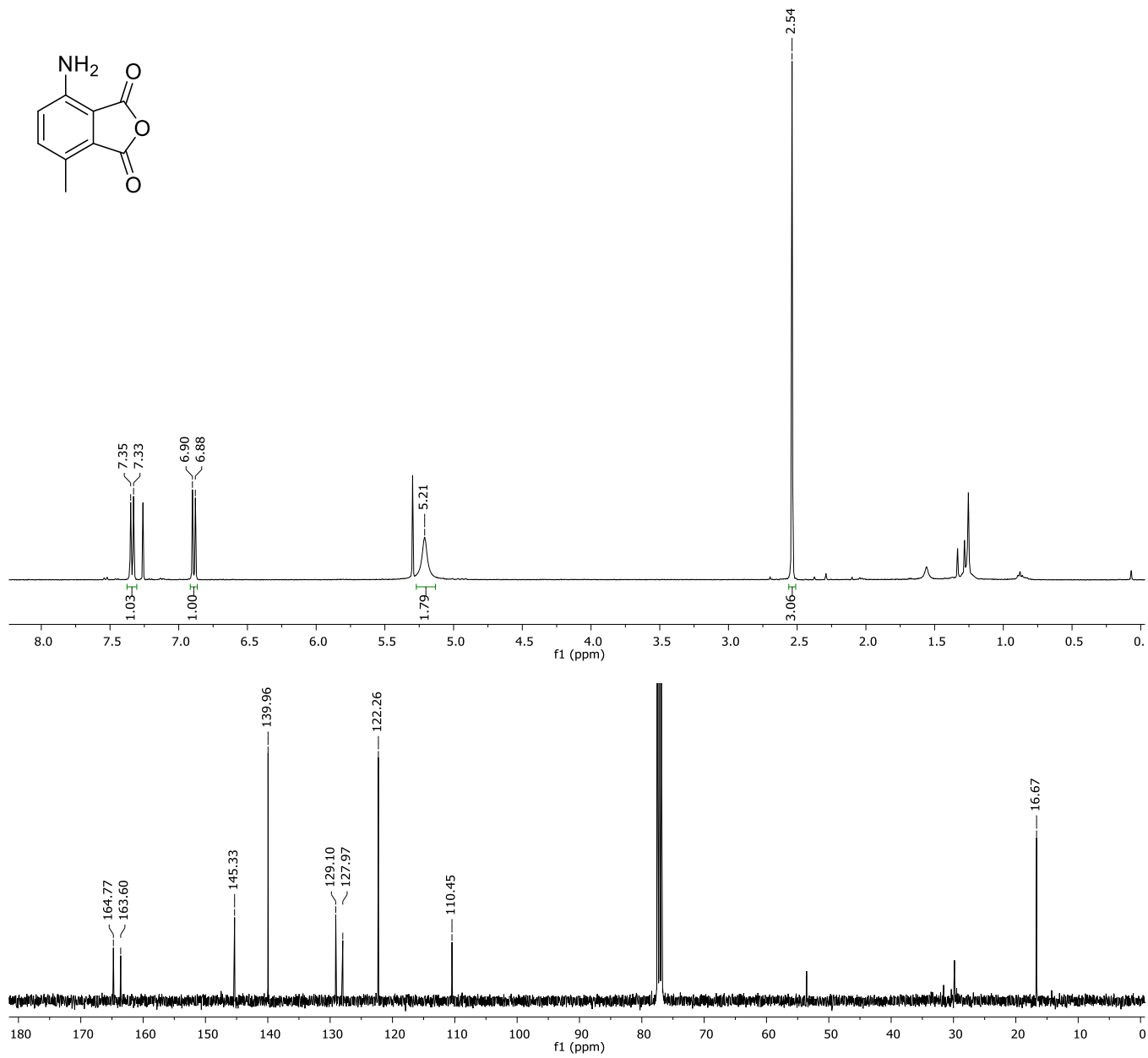


Figure S32. ^1H (400 MHz, up) and ^{13}C (101 MHz, down) NMR (CDCl_3) spectra of 9e.

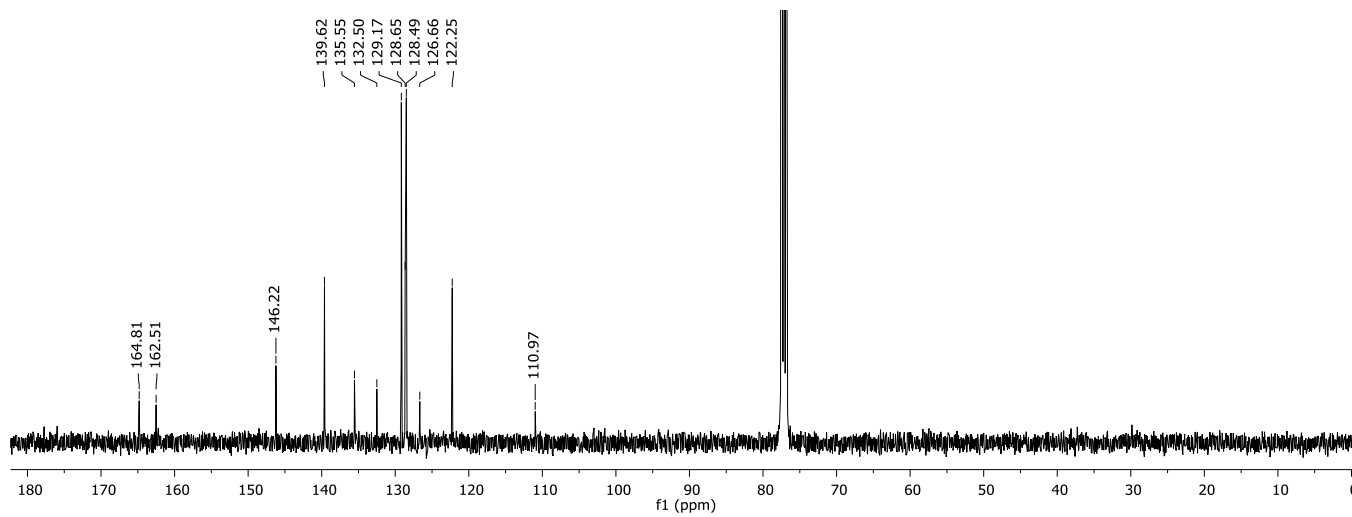
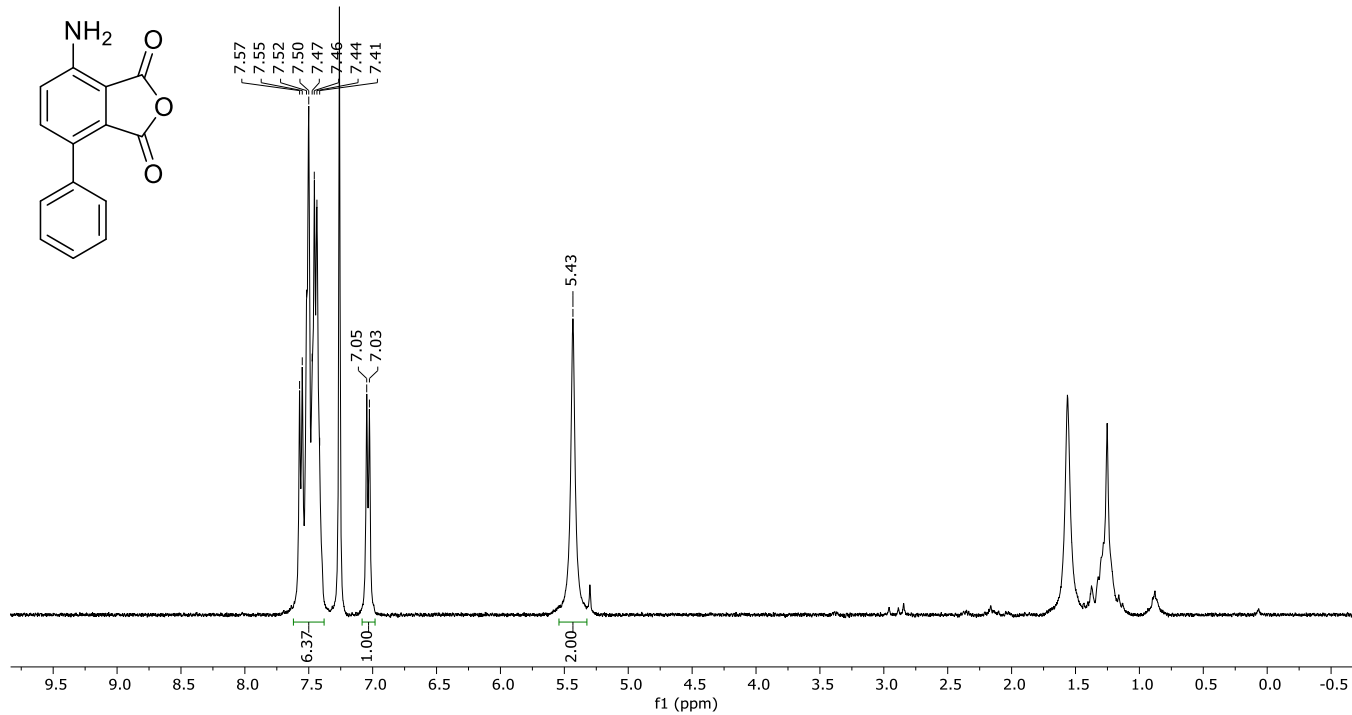


Figure S33. ¹H (400 MHz, up) and ¹³C (101 MHz, down) NMR (CDCl₃) spectra of **9f**.

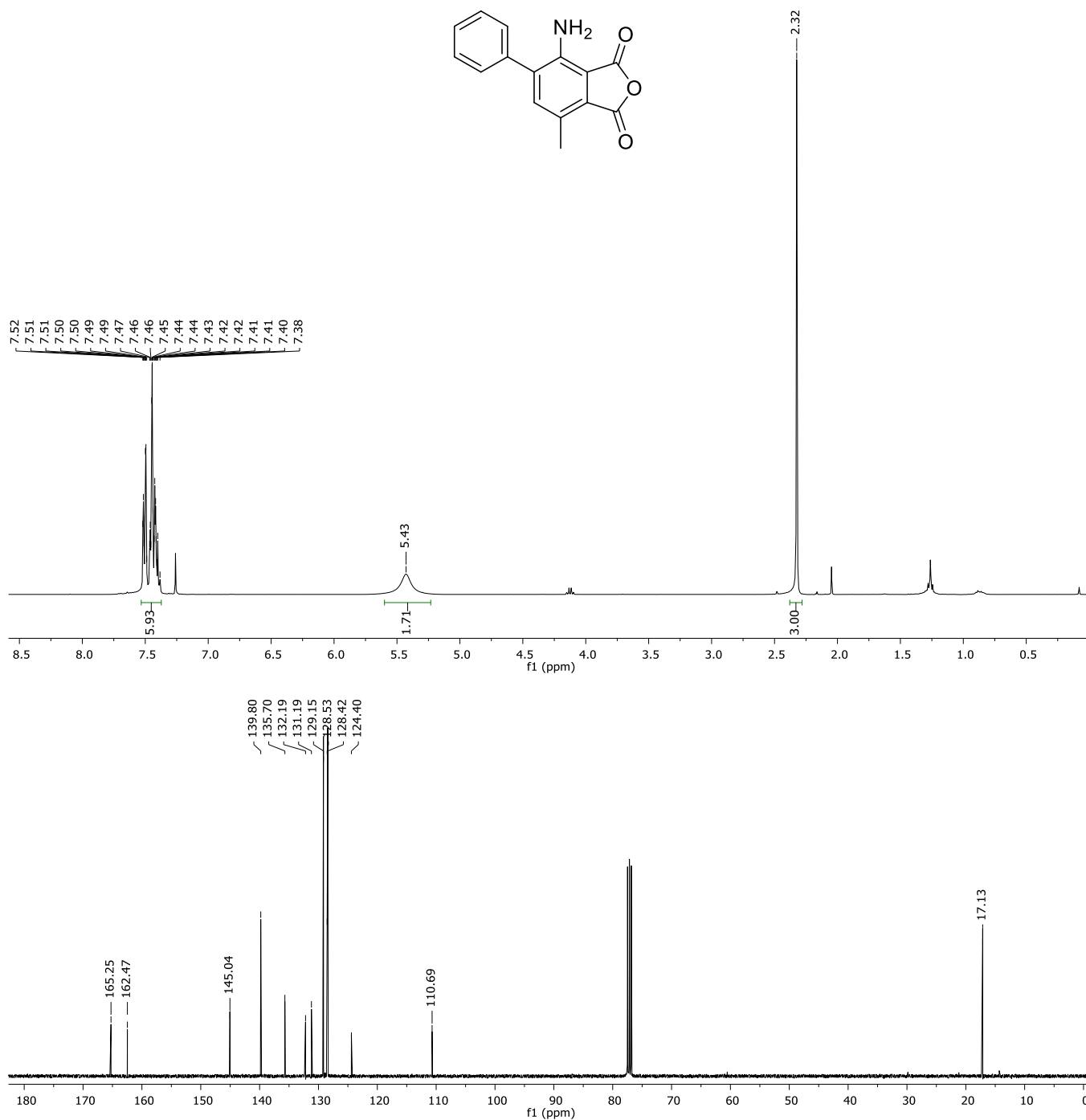


Figure S34. ¹H (400 MHz, up) and ¹³C (101 MHz, down) NMR (CDCl₃) spectra of 9g.

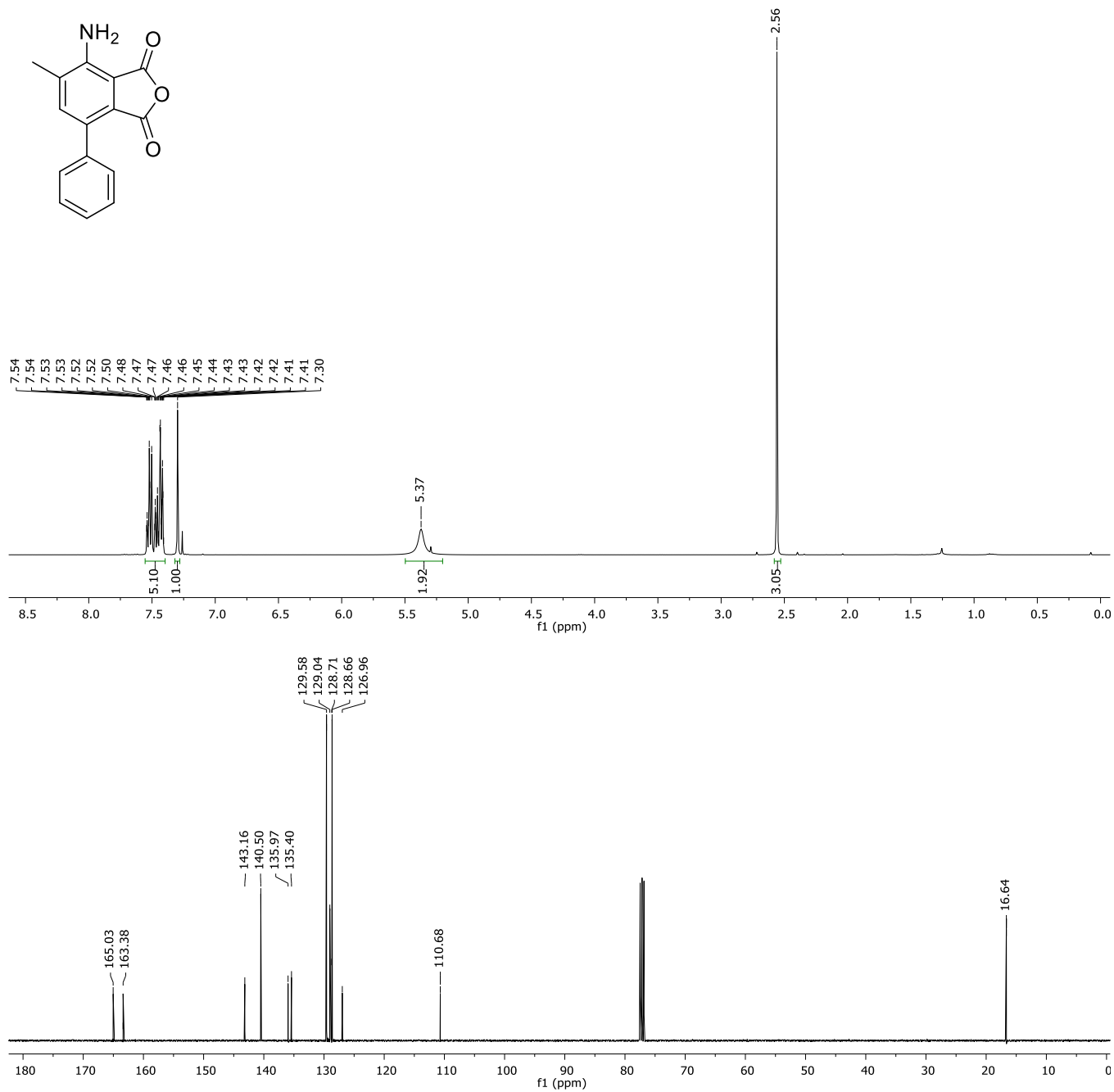


Figure S35. ¹H (400 MHz, up) and ¹³C (101 MHz, down) NMR (CDCl₃) spectra of 9h.

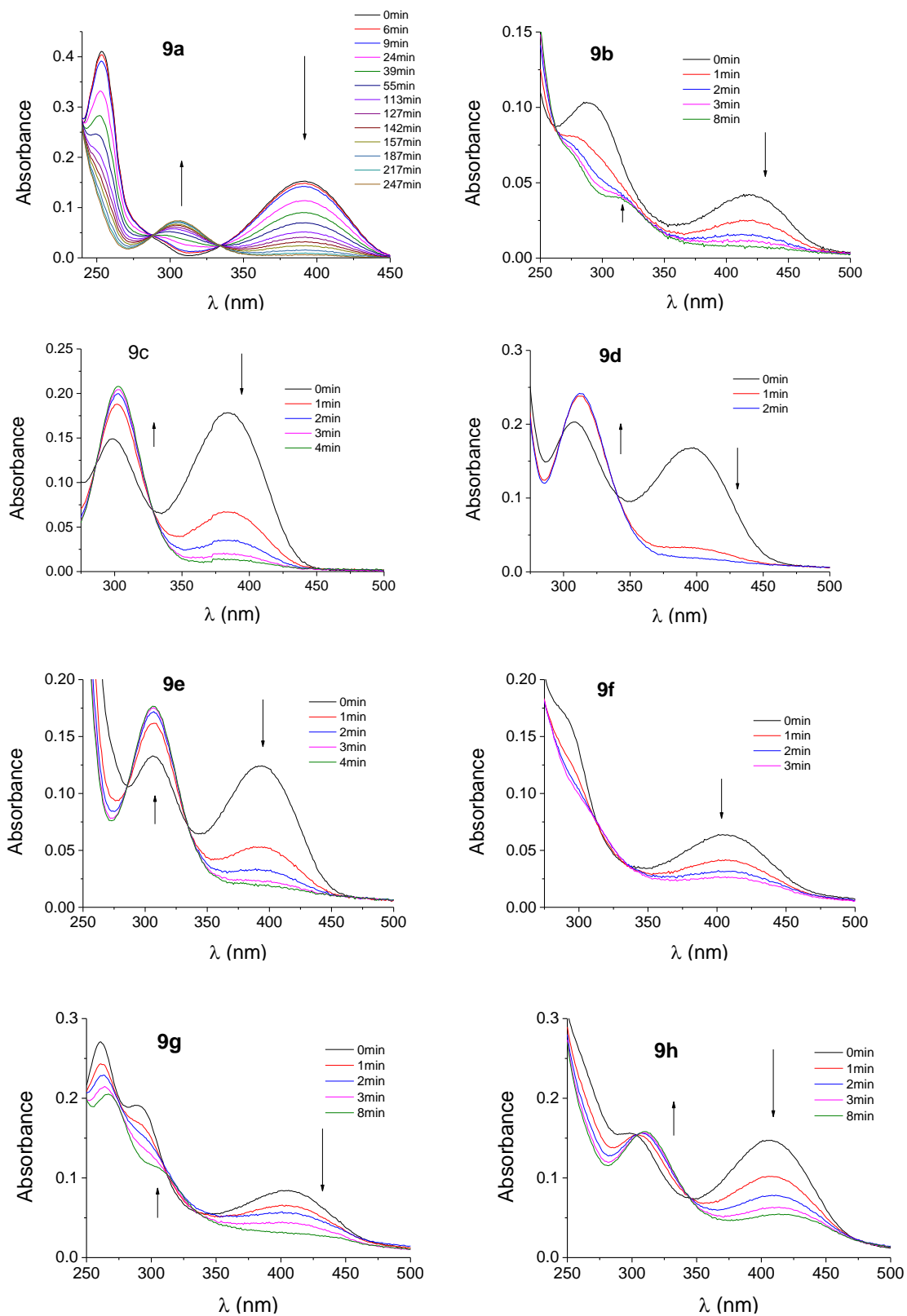


Figure S36. Hydrolysis of the phthalic acid anhydrides yielding the corresponding phthalates **9a-h** in aqueous alkaline media monitored by UV spectroscopy.

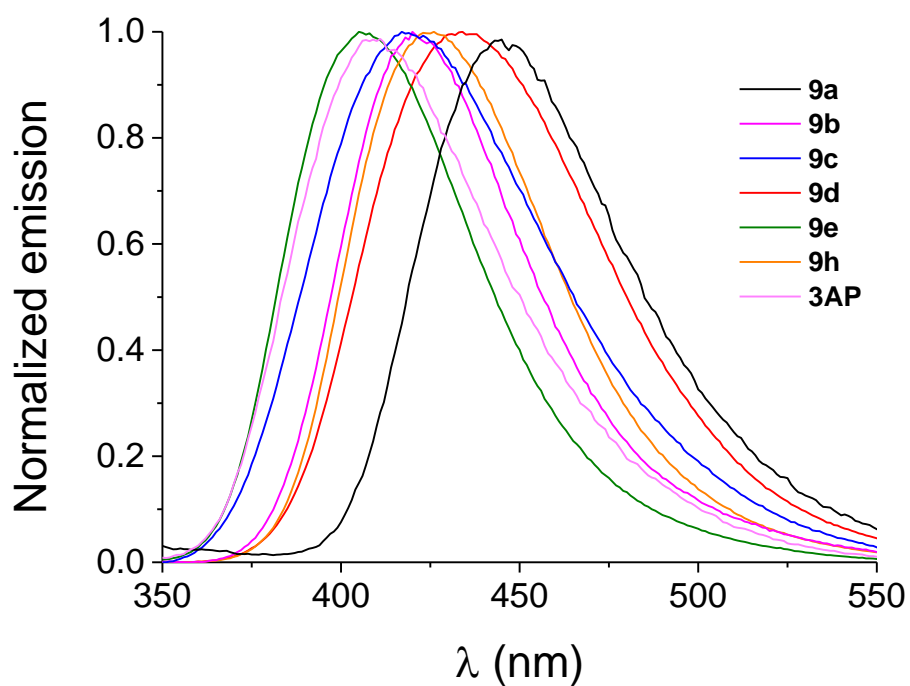
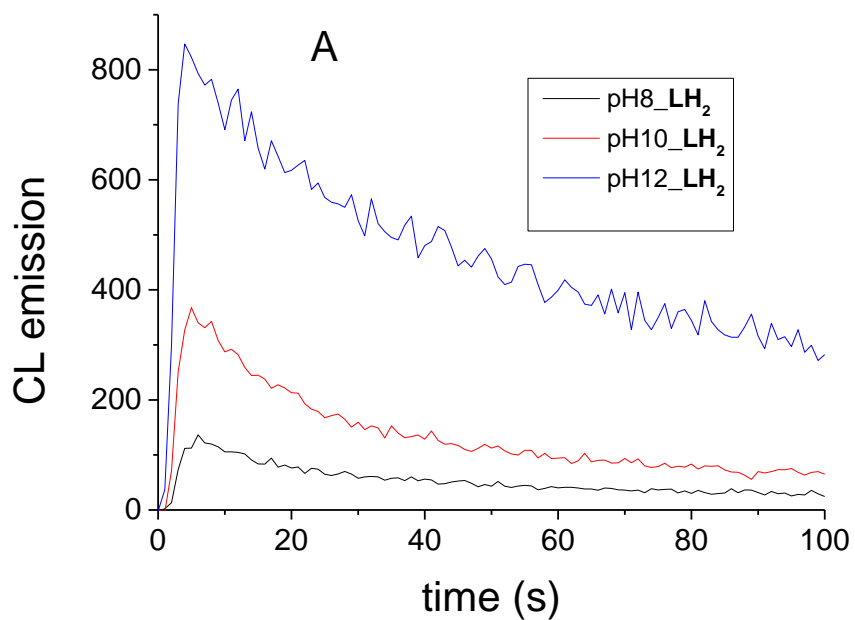


Figure S37. Normalized fluorescence spectra corresponding to phthalates **9a-e**, **9h** and **3AP** in basic aqueous solution (pH 10, $\lambda_{\text{exc}} = 310$ nm, $A(310 \text{ nm}) = 0.1$ for each sample).



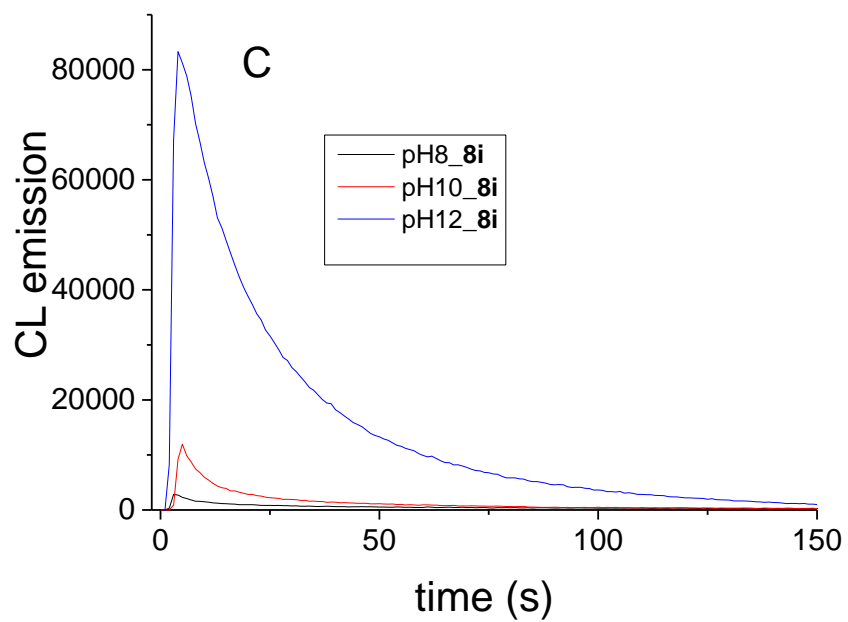
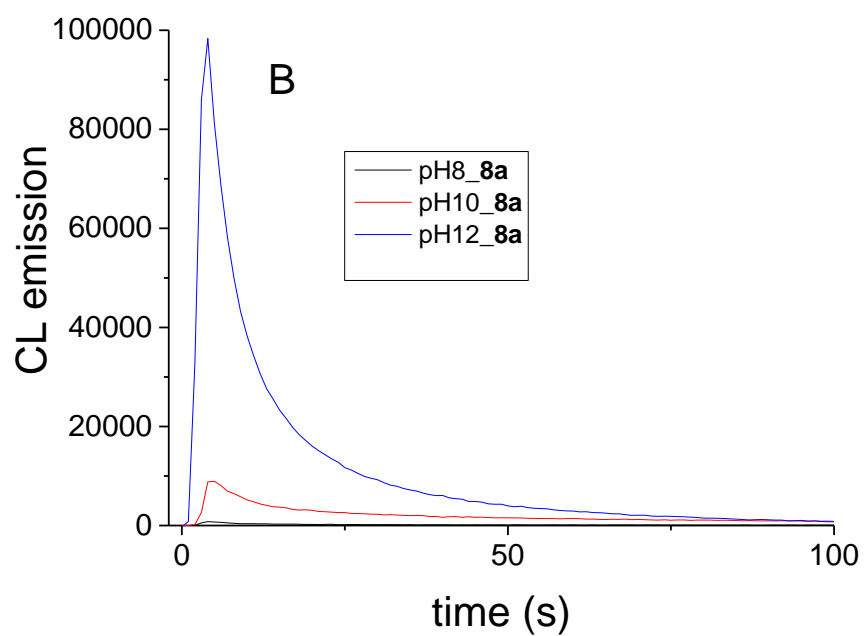


Figure S38. Typical chemiluminescence kinetics displayed by luminol (LH_2 , A) and its derivatives **8a** (B) and **8i** (C) in aqueous solutions at different pH: pH= 8, pH= 10 and pH= 12.

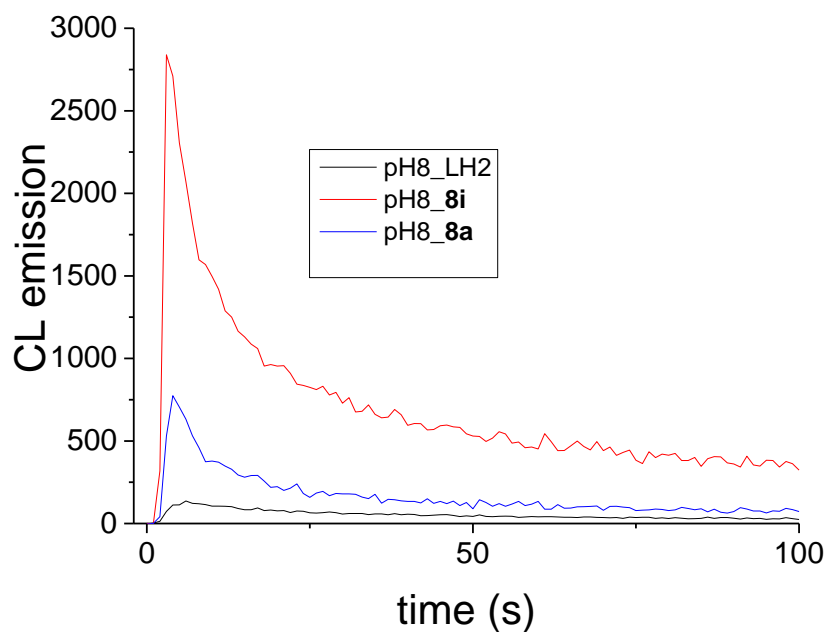


Figure S39. Typical chemiluminescence kinetics displayed by luminol (LH₂), and its derivatives **8a** and **8i** in aqueous solutions at pH=8.

Table S1. Energy barrier between CP² and TS (ΔE^\ddagger , in eV) of luminol derivatives **8** computed in the gas phase, DMSO solution, and water solution.

Compound	Gas phase	DMSO	water
Luminol	0.17	0.14	0.14
8c	0.18	0.14	0.14
8d	0.24	0.17	0.16
8f	0.22	0.22	0.22
8h	0.23	0.23	0.23
8b	0.26	0.24	0.24
8e	0.2	0.17	0.17
8a	0.22	0.18	0.18
8g	0.26	0.2	0.2